1972

Study of power-jet dynamics in fluid amplifiers

R. C. Sekhar
Lehigh University

STUDY OF POWER-JET DYNAMICS IN FLUID AMPLIFIERS

by
R.C. Sekhar

ABSTRACT

The problem of a submerged, incompressible, two-dimensional jet issuing into a semi-infinite field and pivotally oscillated at the point of entry was studied analytically and experimentally. The experimentally observed velocity of the propogating disturbances is much less than the velocity of the jet itself. The ratio decreases for decreasing Strouhal numbers for a given Reynolds number of the flow. In the linear region near the nozzle the amplitude grows a little faster than linearly in most cases.

An idealized inviscid analysis agrees qualitatively with these results except that a much faster growth rate is predicted. Initial results of a theory which introduces viscosity via an assumed model for the velocity decay and entrainment of the jet suggest that these added effects suppress the growth rate. A better model for the velocity and entrainment of the jet was deduced, including wall effects in the third dimension, which may lead toward a more definitive analysis.

STUDY OF POWER-JET DYNAMICS IN FLUID AMPLIFIERS

by

R.C. Sekhar

A Thesis

Presented to the Graduate Committee

of Lehigh University

in Candidacy for the Degree of

Master of Science

in

Mechanical Engineering

Lehigh University

1972

This thesis is accepted and approved in partial fulfillment of the requirements for the degree of Master of Science.

6 Sept 1972
(date)

Forbes T. Brown
Professor in Charge

R. Lambdin
Chairman of Department

ACKNOWLEDGEMENTS

The author wishes to express his sincere gratitude to Dr. Forbes T. Brown for valuable guidance which made this study, involving new concepts, a very educative experience for the author. The author expresses his sincerest thanks to Prof. J.V. Epps whose enthusiasm and help, especially in the use of his photographic and video equipment, made possible the efficient recording of experimental data.

TABLE OF CONTENTS

	Page
ABSTRACT	1
NOMENCLATURE	2
1. INTRODUCTION	4
2. EXPERIMENT	6
2.1. Main Apparatus	6
2.2. Auxilliary Apparatus	7
2.3. Recording Techniques	9
2.4. Experimental Procedure	12
3. ANALYSIS	17
3.1. Introduction	17
3.2. The Inviscid Pivoting Jet	21
3.3. The Exponential-viscous Pivoting Jet	36
3.4. The Viscous drag on a Jet between two Plates	41
4. CONCLUSION	48
FIGURES 1-61	49
LIST OF REFERENCES	104
APPENDIX	105
VITA	113

LIST OF FIGURES

1 The Experimental Apparatus

2 The Main Apparatus

3 Drive Mechanism

4 Auxilliary Apparatus

5 End view of Nozzle

6 Side view of Nozzle

7 The Semi-infinite Field

8 Phase Velocity vs Distance
Re = 53·5

9 Phase Velocity vs Distance
Re = 92

10 Phase Velocity vs Distance
Re = 154

11 Phase Velocity vs Distance
Re = 158

12 Phase Velocity vs Distance
Re = 193

13 Phase Velocity vs Distance
Re = 193

14 Phase Velocity vs Distance
Re = 43·5 , St = 0·082

15 Phase Velocity vs Distance
Re = 43·5 , St = 0·154

16 Phase Velocity vs Distance
Re = 43·5 , St = 0·475

17 Phase Velocity vs Distance
Re = 116 , St = 0·082

18 Phase Velocity vs Distance
Re = 116 , St = 0·192

19 Phase Velocity vs Distance
Re = 116 , St = 0·305

20 Phase Velocity vs Distance
Re = 177 , St = 0.042

21 Phase Velocity vs Distance
Re = 196 , St = 0.013

22 Phase Velocity vs Distance
Re = 196 , St = 0.038

23 Phase Velocity vs Distance
Re = 223 , St = 0.014

24 Phase Velocity vs Distance
Re = 223 , St = 0.034

25 Phase Velocity vs Distance
Re = 267 , St = 0.028

26 Amplitude Growth
Re = 43.5

27 Amplitude Growth
Re = 116

28 Amplitude Growth
Re = 177

29 Amplitude Growth
Re = 196

30 Amplitude Growth
Re = 196

31 Amplitude Growth
Re = 223

32 Amplitude Growth
Re = 267

33 Centerline Velocity vs Distance
Re = 43.5

34 Centerline Velocity vs Distance
Re = 116

35 Centerline Velocity vs Distance
Re = 177

36 Centerline Velocity vs Distance
Re = 196

37 Centerline Velocity vs Distance
Re = 223

38 Centerline Velocity vs Distance
Re = 217

39 Appearance of Jet

40 Exponential Theory Phase Velocities

41 The Fluid Field

42 Right Wave

43 Left Wave

44 Superposed Left and Right Wave

45 Fourier Components

46 The Fourier Wave

47 Transverse Velocities at instant zero seconds

48 Transverse Velocities near origin

49 Transverse Velocities at instant 1/4 time period

50 Transverse Velocities near origin

51 Total Wave

52 Total Wave

53 Total Wave

54 Total Wave

55 Phase Velocity vs Distance from Inviscid Pivoting Jet Theory

56 The Exponential-viscous Jet

57 Double Parabolic Profile

58 Single Parabolic Profile

59 Complete Slug Profile

60 Wave Patterns

61 Wave Patterns

ABSTRACT

The problem of a submerged, incompressible, two-dimensional jet issuing into a semi-infinite field and pivotally oscillated at the point of entry was studied analytically and experimentally. The experimentally observed velocity of the propogating disturbances is much less than the velocity of the jet itself. The ratio decreases for decreasing Strouhal numbers for a given Reynolds number of the flow. In the linear region near the nozzle the amplitude grows a little faster than linearly in most cases.

An idealized inviscid analysis agrees qualitatively with these results except that a much faster growth rate is predicted. Initial results of a theory which introduces viscosity via an assumed model for the velocity decay and entrainment of the jet suggest that these added effects suppress the growth rate. A better model for the velocity and entrainment of the jet was deduced, including wall effects in the third dimension, which may lead toward a more definitive analysis.

NOMENCLATURE

a = width of nozzle

b = amplitude growth exponent of exponential wave

f = real part of transverse velocity, v_j

g = imaginary part of transverse velocity, v_j

K = total number of Fourier components

k = wave number for the exponential wave

k_o = π/x_m

L = total number of discrete locations on the x-axis

p = pressure at any point in the field

t = time elapsed

U = non-dimensional effective slug velocity of jet-stream

u = particle velocity in the +ve x direction

$u_{c.l.}$ = centerline velocity of the jet stream

V = Equivalent slug jet-stream velocity

V_o = Equivalent slug jet-stream velocity at x = 0

v = particle velocity in the +ve y direction

v_j = transverse velocity of jet segment in the +ve y direction

v_p = phase velocity of wave

v_{pc} = phase velocity of the crossovers

v_{pp} = phase velocity of the peaks

v_s = velocity of particle along any path s in the field of fluid

W = w/a

W_o = dimensionless width of the jet at x = 0

w = equivalent width of slurlike jet stream

w_o = equivalent width of jet stream at x = 0

χ = x/a

x = distance from the origin along x-axis

x_i = distance where jet properties are assumed to change from viscous to inviscid

x_m = termination distance of the Fourier wave

x_r = relaxation length for jet velocity decay

y = distance from the origin along y-axis

α = $1/x_r$

η_j = displacement of a jet segment from the x-axis

ν = kinematic viscosity of fluid at the temperature

ρ = density of the fluid

ϕ = potential function of the fluid flow

ϕ_o = magnitude of the potential function of the exponential wave at x = 0

ω = oscillation frequency of the nozzle in radians/sec.

1. INTRODUCTION

This study is aimed at a better understanding of the basic dynamic behaviour of fluidic amplifiers leading to better design and more accurate modelling in systems analysis. Dynamic behaviour of fluidic amplifiers have thus far been studied from a macroscopic point of view. This has led to empirical design of amplifiers while their modelling parameters are decided from actual tests. Extrapolation of such test results to other geometries is exceedingly difficult due to the lack of an adequate theory based on the physics of the situation existing inside the amplifier. As opposed to electronic devices of the same nature, fluidic amplifiers pose considerable difficulty in the accurate, yet general, prediction of their dynamic behaviour. The heart of the dynamics involves the interaction between the power jet, with lateral forces, and the surrounding fluid. The essence of this problem is closely represented by the dynamics of a pivotally oscillating submerged incompressible fluid jet emanating into a two-dimensional semi-infinite fluid field. This thesis deals, analytically and experimentally with this representation.

The apparatus used for experimentation is intended, with the addition of downstream surfaces not yet built, to resemble a prototype proportional fluidic amplifier.

The experimental apparatus has a jet (the power jet of a fluidic amplifier) which enters a field of fluid confined in between two parallel walls at the top and bottom. When pivotally oscillated this jet simulates a fluidic amplifier with periodic excitation of its control ports. Experimentation on this apparatus was carried out with various velocities of the jet stream, characterized by Reynolds number, and various oscillation frequencies characterized by Strouhal number. Observations of the phase velocities and the growth of amplitude of the resulting wave pattern propogating away from the nozzle were visualized with a dark dye. Correlation of these results with specific flow conditions and a well established theory would describe the dynamics of the jet adequately.

Theoretical analysis of this situation has been in the general direction of describing the linear behaviour of this pivotally oscillating jet and its interaction with the surrounding fluid in terms of superposed fluid flow patterns, in effect satisfying all the existing boundary conditions of the given physical set-up. Analytical models describing the linearized behaviour without viscosity, and with a crude representation of viscosity, are described.

The results of the present thesis is expected to be of semi-quantitative usefulness in the design of fluidic amplifiers and circuits. Extensions including the effects of downstream walls, etc., could result in more quantitative knowledge.

2. EXPERIMENT

2.1. Main Apparatus

The experimental model tries to simulate closely a practical amplifier in which the power jet oscillates from one extreme angle to the other as a sinusoidal function in time. The experimental apparatus, a photograph of which is shown in Fig. 1, in this study achieves this oscillation by rotating the power jet nozzle sinusoidally in time. The main apparatus (Fig. 2) utilizes a crank mechanism (Fig. 3) to oscillate the shaft on which the nozzle is mounted through the desired angles of $\pm 1°$, $\pm 2°$, $\pm 3°$. The frequency of oscillation is varied by changing the speed of the motor which drives the crank. Water enters as a jet through the nozzle into a semi-infinite space between two plexiglass plates separated quarter of an inch, and overflows from this bath at the extreme end* Vibration isolation of the crank mechanism which oscillates the nozzle and the drive motor from the semi-infinite bath is achieved by mounting them on different tables. The semi-infinite bath itself is mounted on vibration pads to damp out vibrations from the room. The sliding nozzle plexiglass interface is damped well with vaseline to further cut out high frequency vibration components from the motor.

*Detailed drawings and explanation of the main working apparatus are available in J.C. Bell's M.S. Thesis (1).

2.2. Auxiliary Apparatus

Figure 4 shows the schematic sketch of the set-up. Water is used as the working medium. The water is degassed by evacuating a stainless steel tank and slowly sucking in the water from a sump placed on the floor. This water drips into the evacuated tank from the top and on its way to the bottom of the tank is effectively degassed. This same tank is next pressurized with compressed air and held at a constant pressure of approximately 1 atmosphere gage with the help of a pressure regulator (M.B. Products, Inc., 0-30 p.s.i. downstream pressure, three to four times upstream pressure). This pressure is large enough to drive the water into the apparatus at any desired flow rate.

Flow rates of water into the main apparatus are adjusted with the help of two valves. One serves as a flow control and the other as an On-Off device. A drain tube is located between these two valves, facilitating draining the apparatus when the tank is under pressure. The overflowing liquid is collected in a small catch-basin and drained down to the sump from which it is later sucked into the degassing tank. Such a set-up can use more expensive liquids which would have to be recycled for economy.

Flow visualization is achieved by using "Crystal Violet" dye (J.T. Baker Chem. Co., Phillipsburg, N.J.). This dye trace takes on a very deep violet coloration and a very dilute solution was sufficiently dark. A greater

concentration of the crystals would cause the dye to sink slowly in water. This fact was tested periodically, separately, in a beaker, to check if the dye sank too rapidly due to increased concentration from evaporation.

The dye as it exited from the nozzle of aspect ratio 2 formed a thin vertical sheet of colored matter (see Fig. 5). This causes the dye particles which are closer to the top and bottom plates to slow down due to the viscosity, while at the middle the dye particles move faster. Towards the end of the wave where the dye trace gets more nearly perpendicular to the center line, as seen in Fig. 60, the sheet of dye deforms with the middle portion travelling faster. This shows up as a dye trace with a leading edge and a diffused trail. Measurements were taken on the leading edge of this fuzzy dye trace since this represents the motion midway between the plates. Certain additional accessories were added on to the apparatus to overcome some difficulties. A bicycle wheel, 24 inch diameter was fixed on to the motor spindle to eliminate the salient-pole ripple in the torque of the motor at very low speeds. A cap could be mounted on the dye injecting tube to flatten out the dye trace for visualization of the velocity profile of the jet in the plane of the semi-infinite bath. (See Fig. 7). A spirit level was used to ensure that the bath was level to avoid gravity effects.

A cylindrical lens was placed above the field of

observation of the wave to accentuate the apparent deflection of the jet. This aided measurement of the location of the peaks and crossovers of the wave near the origin where its actual amplitude was quite small. A grid pasted below the wave was used as reference and so distortion of the image did not matter. However, this was used only with the T.V. recorder (see next section) in which the magnification and resolution were poor.

2.3. Recording Techniques

Four recording methods were used:

1. A T.V. recording unit was used to record the motion of the wave and was later played back for measurement.
2. A movie camera was used to film the motion of the wave and later, measure a blown up projection of the film.
3. Still photographs of the wave to determine the right lighting, exposure, etc.
4. A prolonged exposure of the same film while a stroboscope shed light at fixed intervals on the moving wave.

Of these the most successful was the movie camera. A Bolex 16 mm movie camera with lens f=25 was used. At times, for greater resolution and magnification, a Nikon Micro-lens (f=55mm) which could go as close as $1\frac{1}{2}$ ft. was used on the Bolex movie camera. The speed of the movie was fixed at 32 frames/sec. which gave an exposure of 1/200 sec. The exposure could be further adjusted by opening wider or

narrower the slit of the revolving shutter in the camera. A lightmeter was used to decide on the various settings and after a trial shot at these settings the one which gave the clearest picture was used.

The background of the wave formation was marked with two lines parallel to the direction of flow of the jet. These served as a reference while aligning a grid on the blown up projection. A dot on the axis-center of the oscillating nozzle also was a reference.

Frame-by-frame viewing of the film was very convenient with a special projector (Perceptoscope, Perceptual Development Labs, Texas). The position of the wave every third of a second was viewed. The locations of the cross-over intersection with the centerline (see Fig. 41) and the locations of the peaks were thus recorded. The position of the centerline was found from a run of the non-oscillating jet at the mid position, nearly parallel to the reference line on the grid below. Velocities on the center line of the straight jet (non-oscillating nozzle) were arrived at by photographing the movement of a streak of dye pinched into the clear field of fluid. The leading tip of this streak travelled at the center line velocity.

The T.V. recording unit gave good preliminary readings which helped to shed light in the direction of improvement in photography techniques. However, its resolution was poor, and keeping track of the frames in a video recorder

was awkward. However, contrast was quite good even under poor lighting (one photoflood lamp of 100 w.). The magnification achieved was poorer than with the film projection. The main advantage of this method was its low running cost.

The stroboscope method required the use of a special dye. Since this involved multiple exposure of the same film, everything except the dye line had to be dark while the different positions of the light dye trace would be exposed on the same film. The powerful strobe used was adequate for light but a dye which would show up white in a black background was difficult to obtain. The method was further complicated by the fact that the dye had to be soluble in water; any colloid would settle in the apparatus calling for impractically frequent cleaning. Flourscein as dye with an ultraviolet filter on the strobe proved a failure since the dispersed dye gave the whole field of fluid a flourescent glow thus effecting very poor contrast. This method was abandoned.

Still photographs were taken on Tri-X film (400 A.S.A.) and developed in Diafine which increases the speed three-fold. A very clear contrast was achieved. Movies were taken on a 4-x reversal film (A.S.A. 320) under tungsten light. Lighting was always from 45° below the vertical. The camera was always held above the field of view on a rigid stand which stood seperately on the floor.

2.4. Experimental Procedure

The basic idea in the experimental readings was to cover as wide a range of Strouhal numbers as possible. Low Strouhal numbers could be reached only for higher velocities of efflux of the jet since the rpm of the motor had a practical lower limit. Also, very low Strouhal numbers could not be observed very well on a projection. The higher limit on the Strouhal number was due to the fact that the jet came to a virtual stop very close to the nozzle for the necessary low velocities. Non linear effects were predominant in the region and hence were not of interest.

This meant readings had to be taken at different velocities of efflux of the jet. Thus the readings were classified according to the Reynolds numbers of the flow.

$$\text{Reynolds No.} = \frac{V_o\ a}{\nu}$$

a = width of nozzle = 1/8 ins.

V_o = Velocity of efflux of jet
= Volume Rate of flow/Area of nozzle.

ν = Kinematic viscosity of the liquid at the temperature.

Each of these readings would have different Strouhal numbers.

$$\text{Strouhal number} = \frac{\omega\ a}{V_o}$$

ω = Frequency of oscillation of the nozzle in rad/s.

As a basis for the experimental readings use was made of the exponentially growing wave theory which predicts the ratio of phase velocity to the center line velocity for given Strouhal numbers (see Fig. 40). The range of Strouhal numbers as given there run from .0001 to 10. Experimental readings were for .01 to .475.

The steps followed in the experimental procedure were as follows:

Preparation

1) Detach oscillating mechanism and tilt the apparatus sloping upwards downstream of the jet.

2) Open inlet valve and allow liquid to fill in slowly. The upward slope eliminates air bubbles to collect in the bath while filling.

3) Level the bath using a spirit level so that the region near the nozzle is perfectly horizontal.

4) Set inlet valve at a particular flow rate. An approximate judgement is gotten by looking at the velocity of a squirt of dye issuing through the nozzle.

5) Open dye valve so that a thin line of dye is seen.

6) Set camera above field of view.

7) Adjust the nozzle position so that the dye flows parallel to the grid in the bottom which is pasted square to the wall of the bath.

8) Clamp oscillating mechanism crank to the nozzle shaft

so that the nozzle is fixed in the mid position.

9) Measure flow rate by collecting the overflow liquid for a period of time.

Setting Reynolds Number

10) If a desired value of the Reynolds number is not achieved, adjust flow rate with the valve and check again after about 10 minutes during which time the overflow rate attains its steady-state value.

Setting Strouhal Number

11) Switch motor on and adjust speed to a low value. For low speeds of about 5 cycles per minute of the nozzle, the bicycle wheel is hooked on to the motor shaft to absorb the salient-pole ripple on the shaft of the motor.

12) Measure frequency of oscillation and record Strouhal number.

Recording

13) Photograph the dye trace while the nozzle is not oscillating and is positioned in its mid position. This gives a reference center line for later alignment of the projection.

14) Start the oscillation of the nozzle and record the wave formation of the dye line.

15) Use smaller angles of oscillation if the wave becomes non-linear at too short a distance. This is done by using the $\pm 2°$ and $\pm 1°$ positions on the crank. (Fig. 3).

Changing Strouhal Number

16) Change the frequency of oscillation by increasing the speed of the motor. Remove the bicycle wheel for higher speeds. Note the Strouhal number.

17) Record as before. Generally three Strouhal numbers have been obtained for each Reynolds number.

Recording Center line velocity of Jet

18) Stop oscillation. Bring nozzle to the mid position by positioning the crank.

19) Stop dye flow till the field gets clear.

20) Pinch the dye introducing tube so that a small streak of dye issues out and flows with a neatly formed head. This can be gotten from practice. Do not squeeze too fast since the velocity may be altered.

21) Record this streak of dye as it flows past.

End

22) Check Reynolds number again. If widely different, repeat experiment.

This procedure was followed for various Reynolds numbers and all the data stored in video tape or film.

Reading the Data: The tape or film was run and each sequence carefully viewed. The movement of the crossover intersections of the wave with the center line was measured for every interval of time (generally 1/3 sec.). The interval of time was made certain by calibrating the record with an electric clock. Similarly, the movement of the peaks

(the point of tangency on a line parallel to the center line) was also recorded.

The velocities were computed by finding the distance moved after each interval of time. Significant randomness resulted from the fluid motion itself and partly from the recording technique. This was smoothed somewhat by finding the velocities as the slope of a distance vs time curve.

The growth curve was also recorded by marking of the peaks of the wave on a white paper directly from the projection. (Figs. 26 to 32).

The center line velocity of the straight jet was recorded just as above by following the streak of dye.

3. ANALYSIS

3.1. Introduction

The range of the experiment described earlier has been limited because of practical considerations. A theory which presumably applies over a larger range could be checked with these experimental results at least over the small range. This check is necessary because the theory involves several assumptions.

The motion of the jet oscillating in the semi-infinite fluid field is described as being the sum of three components. The primary component is a rightward-travelling (away from the nozzle) exponentially growing wave (see Fig. 42). The second component is a leftward-travelling exponentially growing (in the negative x direction) wave (see Fig. 43). The third component is the residue which is represented by a sum of Fourier sub-components and herein is called the Fourier wave (though it does not have particularly wave-like features). The oscillating jet is supposed to exist in an infinitisimally narrow strip along the x-axis and the fluid away from the x-axis is referred to as the field. All three components which make up the final wave pattern neglect the effects of viscosity in the field. This field is two dimensional, incompressible and irrotational (potential flow) bounded only by a wall along the y-axis (i.e. u=0 at x=0). (See Fig. 41). The other directions extend to infinity and so the width of the jet is presumed

infinitely narrow (despite growth in its width towards the right). Another boundary condition which specifies the motion of the jet exists all along the x-axis which results from the characteristics of the jet. In the analysis only the first quadrant ($x \geq 0$, $y \geq 0$) need be considered so long as the mirror image of this motion in the first quadrant is recognized to exist in the fourth quadrant. Also, all along the x-axis, the existence of the jet means a discontinuity in the pressure between the first and fourth quadrant. The absolute deflection of the jet from the x-axis is considered to be very small as viewed from the fluid motions in the field.

The undeflected jet itself is described by a finite width and effective slug velocity, both of which can vary with position because of viscosity. These parameters are presumed to be independent of lateral motion of the jet. However, interpretation of these measures into the field boundary conditions at the pressure discontinuity ($y=0$) is as though the jet deflection and width were zero. Moreover, there exists at the origin a singular point that has

$$u=0,\ v=0, \text{at } x=0,\ y=0.$$

which means

$$v_j \text{ at } \begin{matrix} x=0 \\ \text{and } y=0 \end{matrix} = 0$$

Along the x-axis, the wave motion should satisfy an equation which involves the stream velocity and transverse velocity at every point along the line. This equation,

obtained by F.T. Brown, resulted from a consideration of the interaction between the jet and the field. Referring to Fig. 41 we write the momentum equation in differential form for a segment of the jet stream of width w. This segment moves longitudinally with a velocity V and laterally with a transverse velocity v_j, and at any instant is at a displacement of η_j from the x-axis. Thus if Δp is the differential pressure acting in the positive y direction on the segment, then

$$\Delta_p = \frac{D}{Dt}\left[\rho w \frac{D}{Dt}(\eta_j)\right] \qquad (1)$$

where $\frac{D}{Dt}$ is the material time derivative $\left(\frac{\delta}{\delta t} + V\frac{\delta}{\delta x}\right)$.

Using the spatial derivatives and noting that

$$\frac{\delta w}{\delta t} = 0$$

and

$$\frac{\delta V}{\delta t} = 0$$

we obtain,

$$\Delta p = \rho\left[V\frac{\delta w}{\delta x}\left(v_j + V\frac{\delta \eta_j}{\delta x}\right) + w\left(\frac{\delta v_j}{\delta t} + 2.V.\frac{\delta v_j}{\delta x} + V.\frac{\delta V}{\delta x}.\frac{\delta \eta_j}{\delta x} + V^2.\frac{\delta^2 \eta_j}{\delta x^2}\right)\right]$$

Observing that η_j and v_j vary sinusoidally in time we write,

$$v_j\, e^{j\omega t} = \frac{\partial \eta_j}{\partial t} = j\omega \eta_j\, e^{j\omega t}$$

or

$$\eta_j = \frac{1}{j\omega} \cdot v_j$$

Substituting this in the previous equation and simplifying we obtain,

$$\Delta p = \rho\, j\omega w \left[\left(1 + \frac{V}{j\omega} \cdot \frac{1}{w} \frac{dw}{dx}\right) v_j \right.$$

$$+ \left(\frac{2V}{j\omega} - \frac{V^2}{\omega^2} \frac{1}{w} \frac{dw}{dx} - \frac{V}{\omega^2} \frac{dV}{dx} \right) \frac{\partial v_j}{\partial x}$$

$$\left. - \left(\frac{V^2}{\omega^2} \frac{\partial^2 v_j}{\partial x^2} \right) \right] \qquad (3)$$

We consider the fourth quadrant to be a mirror image of the first quadrant. Hence if a particle in the first quadrant lying just above the jet experiences a pressure p, the corresponding particle lying just below the jet and at the same location from the origin, experiences a pressure -p. Thus the differential pressure at the location acting on the jet itself is $\Delta p = -2p$. For any path s in the field,

$$\frac{dp}{ds} = -\rho \frac{\partial v_s}{\partial t}$$

Since everything oscillates sinusoidally,

$$\frac{dp}{ds} = -\rho\, j\omega v_s\, e^{j\omega t} = -\rho\, j\omega \frac{\partial \phi}{\partial s}\, e^{j\omega t}$$

Integrating between any two points in the field,

$$(p_2 - p_1)\, e^{j\omega t} = -\rho j\omega(\phi_2 - \phi_1)\, e^{j\omega t} \tag{4}$$

where p_2 and p_1 are magnitudes of the pressures at any two points in the field and ϕ_2 and ϕ_1 are the values of the corresponding potential function (2).

If we choose to call pressure at infinity in the field zero (some datum level) then the pressure at any point in the field is,

$$(p_2 - 0) = -\rho j\omega(\phi_2 - \phi_\infty) \tag{5}$$

In particular we consider the points in the field just adjacent to the x-axis.

Thus,

$$\Delta p = 2\rho j\omega(\phi_x - \phi_\infty) \tag{6}$$

where ϕ_x is the potential function at x for y = 0 in the first quadrant, giving

$$\frac{2(\phi_x - \phi_\infty)}{w} = \left[\left(1 - j\frac{V}{\omega}\frac{1}{w}\frac{dw}{dx}\right) v_j + \left(-j\frac{2V}{\omega} - \frac{V^2}{\omega^2}\frac{1}{w}\frac{dw}{dx} - \frac{V}{\omega^2}\frac{dV}{dx}\right)\frac{\delta v_j}{\delta x} - \left(\frac{V^2}{\omega^2}\right)\frac{\delta^2 v_j}{\delta x^2} \right] \tag{7}$$

This equation, which has to be satisfied at every $x>0$ is called the coupled boundary equation.

3.2. The Inviscid Pivoting Jet

For inviscid jets with no entrainment and no velocity decay with x, $\frac{dw}{dx}$ and $\frac{dV}{dx}$ are zero, so the coupled boundary equation (eqn. 7) simplifies to

$$\frac{2}{w}(\phi_x - \phi_\infty) = \left[v_j - j \cdot \frac{2V}{\omega}\frac{\delta v_j}{\delta x} - \frac{V^2}{\omega^2}\frac{\delta^2 v_j}{\delta x^2}\right] \qquad (8)$$

The other boundary conditions of this problem are the same as discussed in section 3.1 namely,

$$u \text{ at } x=0 = 0 \qquad (9)$$

$$v_j \text{ at } x=0 \text{ and } y=0 = 0 \qquad (10)$$

As described before, three component fluid flows were summed to produce the effective wave satisfying all boundary conditions. The rightward travelling wave, derived by F.T. Brown (2) has the potential function,

$$\phi = \phi_o \, e^{(bx-ky)} \, e^{j(\omega t-kx-by)} \qquad (11)$$

which satisfies the jet interface boundary condition (at y=0) but does not satisfy the wall boundary condition (at x=0) or the requirement at the origin that $\eta_j = 0$. This wave grows exponentially in amplitude (e^{bx}) and travels at a constant phase velocity ω/k. The flow extends from

$x = -\infty$ to $x = +\infty$ (see Fig. 42).

Such a field causes transverse velocities at y=0 given by

$$v_j = \phi_o \, (-k - jb) e^{bx} e^{j(\omega t-kx)} \qquad (12)$$

and particle velocities in the field given by

$$v = v_j \, e^{-ky} \, e^{-jby}$$

$$u = jv$$

The values for the quantities b and k are found from the following equations.

$$bw = \frac{(2-a)^2}{a^2} \quad \frac{a+1}{a-1} \tag{13}$$

$$St = \frac{\omega w}{V} = \frac{(2-a)^3}{a^2(a-1)} \tag{14}$$

where $$a \equiv \sqrt{1+(b/k)^2} \tag{15}$$

The ratio of the phase velocity of the wave to the stream velocity of the jet is

$$v_p/V = 2-a \tag{16}$$

A table of values for v_p/V, b and k for a corresponding Strouhal number is listed in Fig. 40.

The wall boundary condition (Eqn. 9) was next satisfied by superposing on this rightward travelling wave a leftward travelling wave (Fig. 43) growing exponentially in the negative x-direction (and decaying in the +ve direction). This wave is described by

$$\phi = \phi_o \, e^{(-bx-ky)} \, e^{j(\omega t+kx-by)} \tag{17}$$

The values of b, k and ϕ_o are the same as in the rightward wave. This causes particles in the field and along the y-axis to be acted upon by the two travelling waves in an equal and opposite fashion (see Fig. 44) so that,

$$\left(u \text{ at } x=0 \text{ from right wave} + u \text{ at } x=0 \text{ from left wave}\right) = 0$$

This leftward wave does not satisfy the jet-interface

boundary condition and so the sum of the two components also do not satisfy the boundary condition. Moreover the velocity contribution at the origin by these two waves do not cancel and we are left with a non-zero velocity v_j at the origin. The third component of flow should force $v_j = 0$ at the origin and make the sum of the three components satisfy the jet interface boundary condition. The third flow component was assumed to have a potential function in the form of a truncated cosine Fourier series. The necessary truncation implies an approximation. Such an even function will preserve the wall boundary condition (Eqn. 9). Thus the Fourier wave is described by

$$\phi_{Fourier} = \sum_{m=1}^{K} - \frac{a_m}{k_o m} \cdot e^{-k_o m y} \cos k_o m x \cdot e^{j\omega t} \qquad (18)$$

This function was chosen so that its fundamental component has a wavelength equal to twice the distance x_m (see Fig. 45) i.e.

$$k_o = \frac{\pi}{x_m} \qquad (19)$$

For distances greater than x_m from the origin the Fourier function repeats itself periodically as shown in Fig. 46. Thus the solution for $x > x_m$ is not generally physically meaningful. In particular we want the contribution of the Fourier function to tend to zero for distances approaching x_m. This is so because we are interested in solutions where energy propogates rightwards only. Although

the leftward travelling component which we mentioned earlier does indicate leftward propogating energy, this does not imply that the overall energy is propogating to the left.

The boundary conditions specified so far do not preclude solutions which have leftward travelling energy; indeed, the boundary conditions are not complete. For example, v_j at any finite x could be included as an additional boundary condition and the component solutions (which are added on to the rightward wave) found. The result would be an undesired standing wave pattern. Such solutions were seemingly unavoidable with other formulations of the solution, and caused a few headaches.

The breakdown of the solution into the three components is designed specifically to overcome this problem. The rightward travelling wave in effect constitutes a right-end boundary condition. The other two component solutions are added to achieve the boundary conditions at x=0. The effects of these additional components should not therefore change the situation to the right. This was made certain in the case of the leftward travelling wave (Eqn. 17) where the transverse velocities and their x-derivatives decay exponentially to zero for large x. Thus a criterion of success is whether the contribution of the Fourier function to the velocities and their x-derivatives also decays for large x and is very small for $x = x_m$. This situation

resulted, fortunately. (See Fig. 47).

The requirement that v_j should vanish at the origin gives one complex boundary equation with K complex unknowns a_m, or two real boundary equations with 2K real unknowns. In particular, the contribution to v_j from the two exponential waves is $2\ \phi_o\ (-k - jb)$, and from the Fourier wave is $\sum_{m=1}^{K} a_m$, which can be divided into real and imaginary parts, $\sum_{m=1}^{K} (a_r + j\ a_i)_m$. Equating the real and imaginary parts gives

$$\sum_{m=1}^{K} (a_r)_m = 2\ \phi_o\ k \tag{20}$$

$$\sum_{m=1}^{K} (a_i)_m = 2\ \phi_o\ b \tag{21}$$

Another complex equation with the same unknowns is gotten by substituting the sum of the three component flows into the coupled boundary equation at a specific location on the x-axis. In particular, substituting and grouping all the known terms onto the left we obtain

$$(e^{bx-jkx} + e^{-bx+jkx})\ (2\ \phi_o - 2\ \phi_o\ (k-jb)\ \frac{w_o}{}$$

$$+\ 2\ \phi_o\ (-k-jb)\ (b-jk)^2\ \frac{V_o^2}{\omega^2}$$

$$+\ j\ \phi_o 2\frac{V_o}{\omega}\ (b-jk)\ (-k-jb)\ (e^{bx-jkx} - e^{-bx+jkx})$$

=

$$\sum_{m=1}^{K} \frac{2}{V_o} \frac{a_m}{k_o m} \cos k_o mx + \sum_{m=1}^{K} a \cos k_o mx$$

$$-j \frac{2V_o}{\omega} \sum_{m=1}^{K} -a_m k_o m \sin k_o mx - \frac{V_o^2}{\omega^2} \sum_{m=1}^{K} -a_m k_o^2 m^2 \cos k_o mx \qquad (22)$$

In this equation the terms of the right travelling wave have been cancelled; the right wave by itself satisfies the equation. One such equation can be written for each specific location x, and thus a system of equations with the same unknowns can be written. K -1 coupled boundary equations plus the equation for v_j at the origin would uniquely specify the K unknowns. If these K locations are situated closely enough within the distance x_m, and the desired decay with increasing x is manifest, we infer that the solution is reasonably accurate.

These equations involve complex quantities and so when converted to real numbers result in twice the number of equations and unknowns. These equations are arranged in a matrix form:

$$\begin{bmatrix} RHS_{11} & RHS_{12} & \cdots & RHS_{1,2K} \\ RHS_{21} & RHS_{22} & & \\ \vdots & & & \\ \vdots & & & \\ \vdots & & & \\ RHS_{2L,1} & & & RHS_{2L,2K} \\ 1 & 1 & \cdots 0 & 0 \cdots \\ 0 & 0 & \cdots 1 & 1 \cdots \end{bmatrix} \cdot \begin{bmatrix} a_{r1} \\ \vdots \\ a_{rK} \\ a_{i1} \\ \vdots \\ a_{iK} \end{bmatrix} = \begin{bmatrix} LHS_1 \\ LHS_2 \\ \vdots \\ LHS_{2L,1} \\ 2\emptyset_o k \\ 2\emptyset_o b \end{bmatrix} \tag{23}$$

Each row is an equation written for a particular location x, $0<x\leq x_m$. The last two equations specify the zero velocity condition at the origin (Eqns 20 and 21). The solution of these $(2L + 2)$ equations was done on the C.D.C. 6400 computer using the FLUXPK Matrix Package (3).

In practice solutions of these $(2L + 2)$ equations and $(2L + 2)$ unknowns gave rise to a high frequency oscillation in the values of v_j of the Fourier wave along x. The frequency corresponded with the frequency of the last component of the Fourier series. As a consequence, the desired decay with increasing x did not occur. A mathematical

ill-conditioning was suspected since the spacing of the locations was precisely the half wavelength of the highest Fourier component. It was decided to make the number of unknowns in the given set of equations two less than the number of equations, causing a redundancy in the system of equations. Since no exact solution is possible a minimization process sugrested by Dr. Brown was used. The details follow.

The syster of equations

$$\begin{bmatrix} R_{11} & R_{12} \cdots & R_{1K} \\ R_{21} & R_{22} \cdots & R_{2K} \\ R_{31} & \cdots & \cdot \\ \cdot & & \\ \cdot & & \\ \cdot & & \\ \cdot & & \\ R_{L1} & \cdots & R_{LK} \end{bmatrix} \begin{bmatrix} a_1 \\ a_2 \\ \cdot \\ \cdot \\ a_K \end{bmatrix} = \begin{bmatrix} c_1 \\ c_2 \\ \cdot \\ \cdot \\ \\ \\ \\ \\ c_L \end{bmatrix} \qquad (24)$$

where K<L has more equations than unknowns. This is rearranged as shown on the following page.

$$\begin{bmatrix} R_{11} & R_{12} \cdots & R_{1K} \\ R_{21} & R_{22} \cdots & R_{2K} \\ R_{31} & \cdots & \cdot \\ \cdot & & \\ \cdot & & \\ \cdot & & \\ \cdot & & \\ R_{L1} & \cdots & R_{LK} \end{bmatrix} \begin{bmatrix} a_1 \\ a_2 \\ \cdot \\ \cdot \\ \cdot \\ a_K \end{bmatrix} - \begin{bmatrix} c_1 \\ c_2 \\ \cdot \\ \cdot \\ \cdot \\ \cdot \\ \cdot \\ c_L \end{bmatrix} = \begin{bmatrix} E_1 \\ E_2 \\ \cdot \\ \cdot \\ \cdot \\ \cdot \\ \cdot \\ E_L \end{bmatrix} \tag{25}$$

where E is the deviation from zero caused in every equation by the final solution a_K. This present method requires that the sum of the error squared $\sum_{n=1}^{L} E_n^2$ be minimized.

Thus,

$$\left(\sum_{n=1}^{K} R_{1n}a_n - c_1 \right)^2 + \left(\sum_{n=1}^{K} R_{2n}a_n - c_2 \right)^2 + \cdots$$

$$\cdots + \left(\sum_{n=1}^{K} R_{Ln}a_n - c_L \right)^2 = \text{Minimum} \tag{26}$$

Differentiating the left hand side of this equation with respect to $a_1, a_2 \cdots a_K$ and setting equal to zero we obtain K equations with K unknowns.

$$\frac{\delta E}{\delta a_n} = \sum_{i=1}^{L} \left(\sum_{j=1}^{K} R_{ij}a_j - c_i \right) R_{in} = 0 \tag{27}$$

$$\begin{bmatrix} \sum_{j=1}^{L} R_{j1}R_{j1} & \sum_{j=1}^{L} R_{j1}R_{j2} & \cdots \\ \sum_{j=1}^{L} R_{j2}R_{j1} & \sum_{j=1}^{L} R_{j2}R_{j2} & \cdots \\ \vdots & & \\ \sum_{j=1}^{L} R_{jK}R_{j1} & \sum_{j=1}^{L} R_{jK}R_{j2} & \cdots \end{bmatrix} \begin{bmatrix} \\ \\ \\ \\ \\ a_K \end{bmatrix} = \begin{bmatrix} \sum_{j=1}^{L} R_{j1}C_j \\ \sum_{j=1}^{L} R_{j2}C_j \\ \vdots \\ \sum_{j=1}^{L} R_{jK}C_j \end{bmatrix} \tag{23}$$

The solution of such a system of equations with K unknowns and K equations yielded good results, so long as the component errors were weighted reasonably.

Since the process involves a redundancy of equations and the final solution is just a best fit for the given equations, a freedom of choice exists in the emphasis of any particular equation which will tell in the result. The weighting of a particular equation is enhanced by multiplying the equation throughout by a big weighting factor. In the present work initial answers did not yield correct results near the origin. By weighting the origin equations to a magnitude comparable with the other equations a reasonable solution was obtained.

The final result, the sum of the exponential and Fourier waves, satisfies all boundary conditions. This was obtained in the form of transverse velocity of the wave at every discrete point. The phase velocity of this wave, which is of particular interest, can be obtained by a simple derivation.

The transverse velocities are of the form

$$v_j(x) = \left(f(x) + j\,g(x)\right) e^{j\omega t}$$
$$= \left(f(x)\cos\omega t - g(x)\sin\omega t\right)$$
$$+ j\left(g(x)\cos\omega t + f(x)\sin\omega t\right)$$

where f and g are the real and imaginary parts which were listed out seperately by the computer.

The vanishing of the real component of v_j, $\left(f(x)\cos\omega t - g(x)\sin\omega t\right)$, defines the crossover points of the transverse velocity wave.

Thus, for the crossover points,

$$\frac{f(x)}{g(x)} = \tan\omega t$$

Differentiating with respect to x,

$$\left[\frac{f'(x)\,g(x) - g'(x)\,f(x)}{g(x)^2}\right]\frac{dx}{dt} = \omega\sec^2\omega t$$

The desired phase velocity of the crossovers is $\frac{dx}{dt}$, or

$$v_{pc} = \omega \cdot \frac{(g^2+f^2)}{(f'g-g'f)} \qquad (29)$$

The amplitude of the wave envelope at every point x is $\sqrt{g^2 + f^2}$.

The phase velocity of the crests or troughs of the wave, v_{pp}, was similarly arrived at by defining the location of the crests and troughs (or peaks) where $\frac{dv_i}{dx} = 0$.

The relation is

$$v_{pp} = \omega \cdot \frac{g'^2 + f'^2}{f''g' - f'g''} \tag{30}$$

At the origin the phase velocities of the crossovers and those of the peaks must be, and indeed were, different by a factor of 2.

At the origin

$$v_{pc} = \text{Lim}_{x \to 0} \left[\frac{g^2 + f^2}{f'g - g'f} \right]$$

Using L'Hospital's rule,

$$v_{pc} = 2 \cdot \left[\frac{g'^2 + f'^2}{g'f'' - g''f'} \right] = 2 \cdot v_{pp} \tag{31}$$

The theoretical phase velocity curves are shown in Fig. 55. Experimental data were taken seperately for the two phase velocities shown in Figs. 14 to 25.

A typical computer solution of the inviscid wave theory is presented in detail in what follows.

Figures 47 to 51 show the results of the inviscid theory for a representative Strouhal number of 0.0689. For the rightward wave,

$$b = 1.45 \quad \text{in}^{-1}$$

$$k = 1.23 \quad \text{in}^{-1} \qquad \text{(See Fig. 40)}$$

ϕ was rather arbitrarily taken to be 0.1.

Sixty discrete locations were evenly distributed over a six inch length; the number of Fourier components was two less at 5%. The Strouhal number is referred to a nozzle width of 1/8 inches, giving a wavelength of 5·12 inches.

The results of the transverse velocities are seperated into their real and imaginary parts. If the real part is taken to be the velocity at instant zero, the negative of the imaginary part is the velocity at a quarter of a time period later. The velocity for the second half of the cycle is the negative of that for the first half, by recalling that

$$v_j = (v_{rl} + j\, v_{im})$$

$$v_j\, e^{j\omega t} = (v_{rl} \cos \omega t - v_{im} \sin \omega t)$$

$$+ j(v_{im} \cos \omega t + v_{rl} \sin \omega t)$$

The real part of the second expression is the actual velocity, giving

$$v_j = + v_{rl} \quad \text{at} \quad \text{time} = 0$$

$$= - v_{im} \quad \text{at} \quad \text{time} = 1/4 \text{ time period}$$

$$= - v_{rl} \quad \text{at} \quad \text{time} = 1/2 \text{ time period}$$

$$= + v_{im} \quad \text{at} \quad \text{time} = 3/4 \text{ time period}$$

$$= + v_{rl} \quad \text{at} \quad \text{time} = 1 \text{ time period}$$

The important decisions in these computations were the spacing between every discrete location at which the boundary conditions are satisfied and the total number of

[illegible] limit on the number of locations that can be included (this is 50 with the present program) for a computer memory of 1300($_{oct.}$ words).

Figure 47 shows the transverse velocities at the initial time. The component solutions are shown separately. As can be seen, the left and right wave have both a negative magnitude of 0·12 at the origin. In Fig. 48 the Fourier wave together with the left wave is shown to exactly cancel the right wave magnitude at the origin. Note that the Fourier wave shows good convergence for large x. Figs. 49 and 50 show these same effects at a quarter time period. Figure 51 shows the total wave which is the solution of the inviscid theory for a Strouhal number of 0·0639. The condition at the origin is seen to be satisfied. Figures 52, 53 and 54 show the total wave for three other Strouhal numbers. Note the distance (marked on the plot) where the Fourier wave decays to less than 2 percent of its original value at the origin. Beyond this point the right wave is virtually the only contributing component of the solution which thus can be extended by the reader.

Figure 55 shows the phase velocities of the crossovers and peaks seperately for the four Strouhal numbers. For distances where the effect of the compensating Fourier plus

[illegible] the [illegible] [illegible], the [illegible] with [illegible] to the value [illegible] [illegible] [illegible] theory ([illegible] 1.) [illegible] [illegible] [illegible] numerical [illegible] [illegible] [illegible]. The theoretical limit for [illegible] = 0 (Eqn. 31) can be reached if the curves are judiciously extrapolated to the left. The kink in the phase velocity plots near the origin is an error from numerical differentiation. The slope of the transverse velocity curve at the origin was computed as a first order approximation while for the other points a second order approximation of the Taylor series was used. Phase velocity computations involve slopes and curvatures of the transverse velocity curve and hence the first two points on the plot are unreliable.

3.3. The Exponential-viscous Rivoting Jet

The next step is to introduce jet decay and spreading while retaining the inviscid field, as described earlier in section 3.1. Thus, the viscous terms in the coupled boundary equation are retained. The simplest solution which can be found is for an exponentially decaying velocity and exponentially increasing width, for constant jet momentum. Measurements of the decay of the centerline velocity of the non-oscillating jet show the centerline velocity is somewhat different, and the wall shear reduces the jet momentum, but the assumption nevertheless gives a fair model. Figures 33

$$\frac{2}{w_o}\, e^{-x/x_p}\,(y_{i+1}-y_i) = \left[\left(1 - j\,\frac{2\gamma_c}{\omega}\, e^{-x/x_p} - \frac{\gamma_c^2}{\omega^2}\, e^{-x/x_p}\right)\frac{y_{i+1}+y_i}{2}\right.$$

$$\left. + \left(-j\,\frac{2\gamma_c}{\omega}\, e^{-x/x_p} - \frac{\gamma_c^2}{\omega^2}\, e^{-x/x_p}\right)\frac{y_{i+1}+y_i}{2}\right.$$

$$\left. -\left(\frac{\gamma_c^2}{\omega^2}\, e^{-x/x_p}\right)\frac{y_{i+1}^2+y_i^2}{2}\right] \qquad (32)$$

Solutions satisfying this boundary equation were actually found by R.L. Brown for two specific frequencies, describing waves with one or two exponentially growing components that continuously shrink in wavelength and phase velocity toward the right. Unfortunately the desired boundary conditions (Eqns. 9 and 10) at x = 0 were not satisfied (as before) and because of the limited nature of the solutions their complete solutions were not pursued. This leaves us with only the simple exponentially growing wave to use as the effective right-hand boundary condition, since the Fourier and left-travelling waves should not penetrate to the right side of the computational field if left travelling energy is to be precluded. The right travelling wave satisfies a coupled

[illegible] (Eqn. 4), however, corresponds to the left of an interconnect position x_i ($0 < x < x_i$) the exponential-jet character (Eqn. 32) were used, and to the right ($x_i < x < x_f$) uniform-jet characteristics (Eqn. 5) were assumed, as suggested in Fig. 36. If x_m is sufficiently larger than x_i the Fourier solution should have an adequate opportunity to die out before x_m since it is not needed in the interval $x_i < x < x_m$ to compensate for other waves (the leftward travelling wave is very small in this region).

The method of solution follows exactly the same pattern as in the case of the inviscid jet (Eqns. 23 through 30). The compensating Fourier wave is assumed to be of the cosine Fourier series form (Eqn. 18) with the fundamental component having a wavelength equal to twice x_m (Eqn. 19). The parameters for the right wave were again taken from the table in Fig. 40. The point of note is that the Strouhal number changes with distance in the viscous region. At x_i from which distance we assume the jet to be inviscid we can write,

$$w = w_o e^{-\alpha x_i}$$

$$V = V_o e^{-\alpha x_i}$$

$$St = \frac{\omega w_o}{V_o} \cdot e^{2\alpha x_i}$$

This Strouhal number which is greater than the Strouhal number at the origin by a factor of $e^{2\alpha x_i}$ is the Strouhal

[illegible] the [illegible] boundary condition [illegible] the only wave existing beyond [illegible] must be specified by the Kutta condition. The boundary condition at the origin (Eqn. 10) gives one complex equation.

$$\sum_{n=1}^{I} (a_r)_n = 2\,\phi_{0r} \tag{20}$$

$$\sum_{n=1}^{I} (a_i)_n = 2\,\phi_{0i} \tag{21}$$

for discrete values of $x=x_i$ the coupled boundary equation with viscous terms is written out to form a system of equations. As before the Fourier wave terms in this equation are grouped together to form a rectangular matrix multiplied by a column matrix of the unknown Fourier coefficients. On the other side of the equation the left and right wave terms which involve known quantities are grouped together. This equation is written out in terms of the non-dimensional quantities;

$$K_o = k_o w_o$$

$$b_n = b \cdot w_o$$

$$k_n = k \cdot w_o$$

$$X = x/w_o$$

$$\zeta to\,. = \frac{\omega w_o}{V_o}$$

$$\phi_n = \phi_o/w_o$$

$$A = \alpha \cdot w_o \quad , \quad \alpha = 1/\mu_r$$

$$2\,\beta_{1}\,e^{(b_n - j\,k_n)x}\,e^{-\lambda x}$$

$$-\,\beta_{1}\,e^{(b_n - j\,k_n)x}\,(-k_n - j\,b_n)\left[\,2 - j\,\frac{\lambda}{\beta_{to}}\,e^{-\lambda x} - \right.$$

$$\left. j\,2\,\frac{e^{-\lambda x}}{\beta_{to}}\,(b_n - j\,k_n) - \left\{\frac{e^{-\lambda x}}{\beta_{to}}\,(b_n - j\,k_n)\right\}^{2}\right]$$

Right wave terms

$$+\,2\,\phi_{n}\,e^{(b_n + j\,k_n)x}\,e^{-\lambda x}$$

$$-\,\phi_{n}\,e^{(-b_n + j\,k_n)x}\,(-k_n - j\,b_n)\left[\,1 - j\,\frac{e^{-\lambda x}}{\beta_{to}}\,\lambda\right.$$

$$\left. -\,j\,2\,\frac{e^{-\lambda x}}{\beta_{to}}\,(-b_n + j\,k_n) - \left\{\frac{e^{-\lambda x}}{\beta_{to}}\,(-b_n + j\,k_n)\right\}^{2}\right]$$

Left wave terms

$$=$$

$$2\,e^{-\lambda x}\left(\sum_{n=1}^{K}\frac{a_n}{K_o n}\,\cos K_o n x\right)$$

$$+\left[\left(1 - j\,\frac{\lambda\,e^{-\lambda x}}{\beta_{to}}\right).\sum_{n=1}^{K} a_n \cos K_o n x\right.$$

$$+\left(j\,\frac{2}{\beta_{to}}\,e^{-\lambda x}\right).\sum_{n=1}^{K} a_n\,b_o n \sin K_o n x$$

$$\left.+\left(\frac{e^{-\lambda x}}{\beta_{to}}\right)^{2}.\sum_{n=1}^{K} a_n K_o^{2}\,n^{2}\cos K_o n x\right]$$

Fourier terms

[illegible] for the [illegible] equation for the inviscid case (Eq. 7) is written out to complete this system of equations. This system of equations is solved by the minimization procedure described in section 3.2 (Eqs. 8 through 9).

The complete solution found this way is of course accurate only for values of x considerably smaller than x_1. The N_p question is how many points are needed to achieve accurate results over a useful distance. As noted in section 3.2 the inviscid equations written for $x>x_1$ had to be spaced such that there were at least 10 locations per wave length of the right wave. This criterion was used in this theory also. Since the total number of locations had an upper limit, the total distance x_m was thus fixed.

Evaluation of the results of this theory are presented in the Appendix of this thesis.

3.4. The Viscous Drag on a Jet between two Plates.

The previous discussion on the pivoting jet with viscous drag assumed an exponential decay of the jet velocity. A more accurate representation is desired. Results of an analysis done by F.T. Brown are compared with the experiment in Figs. 33 to 38. Fairly good agreement is seen to exist.

[illegible] the jet [illegible] the two-dimensional wall jet
[illegible] to [illegible] parabolic shape in terms of the two
[illegible] (i.e.). [illegible] observed in the experiment.
The profile of the jet in the plane of the field as it
emerges out of the nozzle is assumed to be the Gaussian's
similarity profile (4) for the two dimensional flow of a
straight jet. Experimentally observed profiles had a nearly
parabolic shape inside the core of the jet but the entrained-
flow portion of the jet did not show up well (Fig. 7).

Using the momentum integral equation as a starting point the rate of change of momentum at any distance x of the jet is equated to the viscous drag acting at the location. This gives a differential equation relating velocity, width and the location of the jet.

Next, the energy integral equation is used to equate the dissipation of energy from the viscous drag of the plates and from the viscosity existing in the entraining of fluid, to the rate of decrease of energy of the jet. This gives another differential equation relating the velocity and width of the jet at any particular location x.

Solving these two equations gave the required results.

This problem was solved numerically using the LEANS package in the Lehigh University computer center (5). The Runge-Kutta Merson method of solving differential equations was used.

The differential equations governing the flow are given

$$\frac{\quad}{\quad} \cdot \left(\frac{\quad}{\quad} - \frac{\quad}{\quad}\right) \tag{34}$$

$$\frac{\quad}{\quad} = -\left(\frac{\quad}{\quad} - \frac{\quad}{\quad}\right) \tag{35}$$

where

$$\quad = \frac{\quad}{\quad} \cdot \frac{a}{\nu} u_{c.l.}$$

$$\quad = \frac{x}{a}$$

$$W = \frac{w}{a}$$

$u_{c.l.}$ = Center line velocity of the jet

a = Width of the nozzle = 1/4 ins.

ν = Kinematic viscosity of the fluid

x = Actual distance in inches along the direction of propogation

w = A representative measure of the actual width of the jet.

The initial conditions for this set of equations is known from the Reynolds number of the flow.

$$Re = \frac{Q}{2a\nu} \tag{35}$$

where Q is the flow rate in the nozzle.

Then

$$U_o = Re/W_o \tag{36}$$

$$W_o = 25/36 \tag{37}$$

This value of W_o, the dimensionless width of the jet just as

[illegible] velocity profile for a plane jet in the region, [illegible] definition of flow rate and momentum,

$$\text{flow rate, } Q = 2 \int_0^a w \, dr \tag{37}$$

$$\text{momentum, } K = 2 \int_0^a w^2 \, dr \tag{38}$$

With respect to w we can deduce that,

$$w = \frac{K}{2aQ}$$

$$\text{Thus, } \quad w_c = \frac{Q}{K_c} \cdot \frac{1}{2a^3} \tag{40}$$

The particular values for the flow rate Q_o at the origin and momentum K_o at the origin are wholly dependent on what velocity profile exists just inside the nozzle. Assumption of a double parabolic profile (shown in Fig. 57) yields a value of W_c given above. In fact the velocity profile itself is Reynolds number sensitive and the assumed value would apply only at very low Reynolds numbers. The similarity assumption itself breaks down near the nozzle and the solution should not be expected to agree with experiment near the nozzle. The best value of W_o for the region far from the nozzle is also expected to be different from that near the nozzle. In fact the experimental values did not correspond to the theoretical computations for the given value. Results for $W_o = 0{\cdot}8$ and $0{\cdot}9$ are seen from Fig. 37 to give better matching. Note that assumption of a single

[illegible] the [illegible] value [illegible] the problem; unstable [illegible] [illegible] of ν_c of .3, the [illegible] of a cable with [illegible] (ν_c .5) [illegible] ν_c of 1.

It was then decided to use that value of ν_c for each hypothetical number which gave the closest fit to the experimental data.

This study was directed to obtain the physics of the operation of a circumferentially oscillating ribbon jet. The theory recorded assumes a completely inviscid jet with a surrounding inviscid field of fluid. Results are useful only in a qualitative way, since real jets decay rapidly with increasing distance from the nozzle. A more complete theory involving viscous drag was developed and initial results computed, which look encouraging, but some further minor changes are necessary.

The experimental data covers a range of flow patterns classified according to Reynolds numbers and dimensionless Strouhal frequencies computed from the flow rate at the nozzle exit. Figures 60 and 61 show typical flow patterns as taken with a 16mm movie camera. Lowering the Strouhal frequency clearly increases the wave length as seen in Fig. 61. Lowering the Reynolds number shortens the range of the linear behaviour. A low Reynolds number is shown in Fig. 60 where one of the wave patterns has a very high Strouhal number. The amplitude of the wave actually decays instead of growing, possibly because of the effect of non-linearities (also see Fig. 26). A quantitative correlation between the flow pattern and the two dimensionless parameters has not yet been established from the experimental data, but should be attempted when the results of the more

[illegible] theory or experiment.

Quantitatively, lower critical numbers for pipe, boundary layer flow and plane wake, as expected from the inviscid theory. A reversible undulation was observed in the plane velocity plots, however. This undulation may be explained as follows. The part of the jet inside the oscillating nozzle does not oscillate in unison, as if rigidly fixed, with the nozzle. At either extreme angle position the transverse momentum of the jet inside the nozzle forces the bulk of the flow toward the wall of the nozzle. Flow seperation might occur from the opposite wall, but this is not known. The gross features of the flow can be clearly seen by observing the dye trace inside the nozzle. This effect spoils the pure sinusoidal pivoting motion of the jet at the nozzle exit, which eventually shows up in the phase velocity. Presumably this is an amplitude sensitive (i.e. nonlinear) effect, but this question was not investigated. Aside from the undulations, phase velocities for a given flow pattern under similar conditions of Reynolds and Strouhal numbers but different amplitudes of oscillation of the jet were identical in the linear region of the flow.

Growth of amplitude of the wave patterns abstracted from the movie projection are shown in Figs. 26 to 32. The growth in the region closer to the nozzle is not substantially greater than the linear growth shown by a straight line.

[illegible] the jet [illegible] the [illegible] with [illegible] theoretical. [illegible] theoretical [illegible], [illegible] [illegible] [illegible] (Fig. 12 to 1). [illegible] [illegible] [illegible] with the more complete wind-jet theory, namely in the [illegible], namely [illegible] the velocity [illegible] and the [illegible] of the jet surrounding the [illegible] of [illegible]. This supposition may be great enough to explain the contraction observed in Fig. 21 and 20.

Results of the center line velocity of the undisturbed jet showed good agreement with the theory. The theory assumes a similarity profile, which is not accurate near the nozzle exit producing a local deviation from the experiment. The mean velocity profile of the jet inside the nozzle was not observed. Different profiles influence the theory only so far as one parameter, U_o, is concerned. This could be taken account of empirically for any flow situation by using that value of U_o which yields the best fit to the experimental data. The more complete theory for the propagation of waves should ultimately incorporate the decay of the jet velocity as deduced by the center line velocity theory.

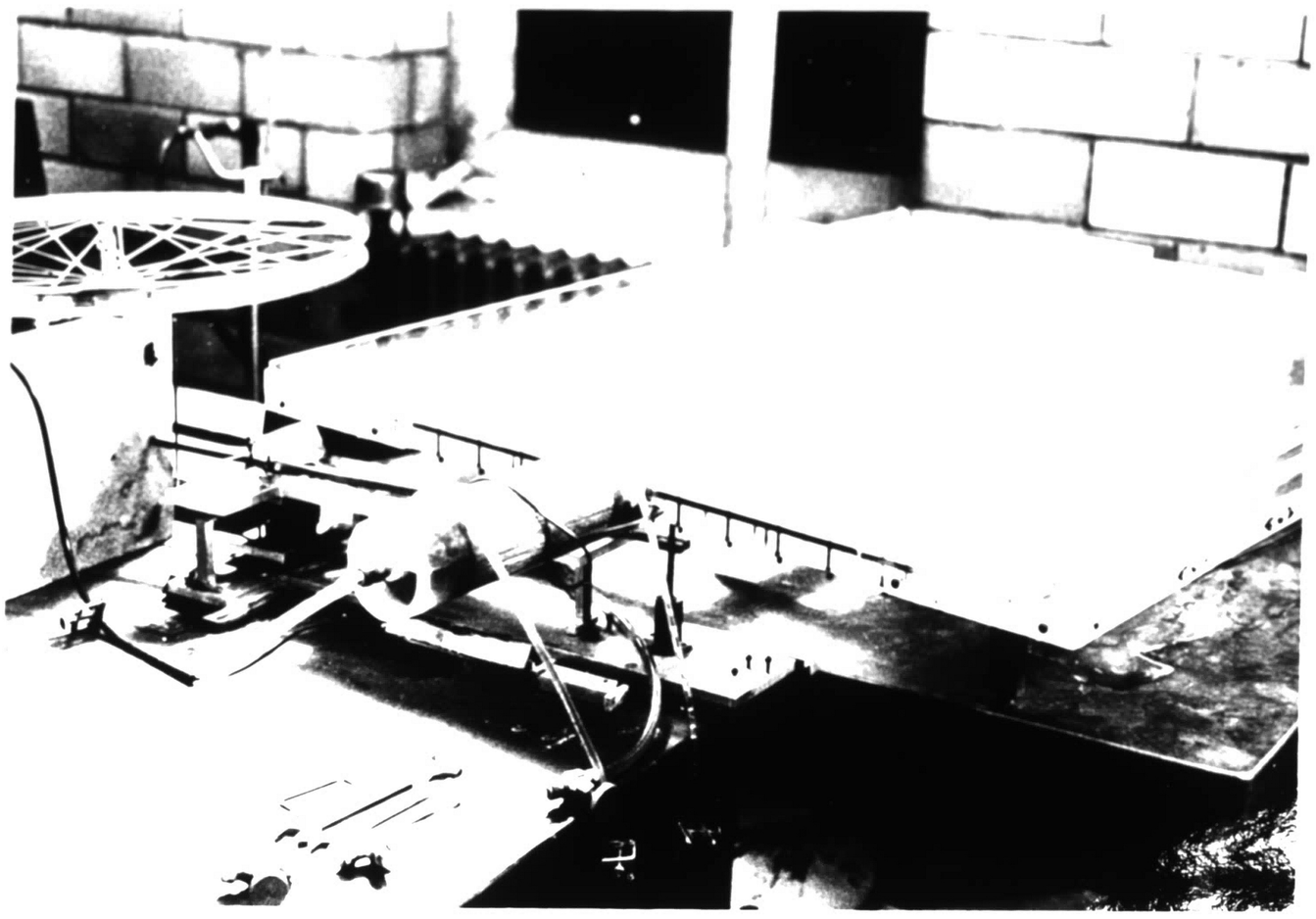

FIG. 1. THE EXPERIMENTAL APPARATUS

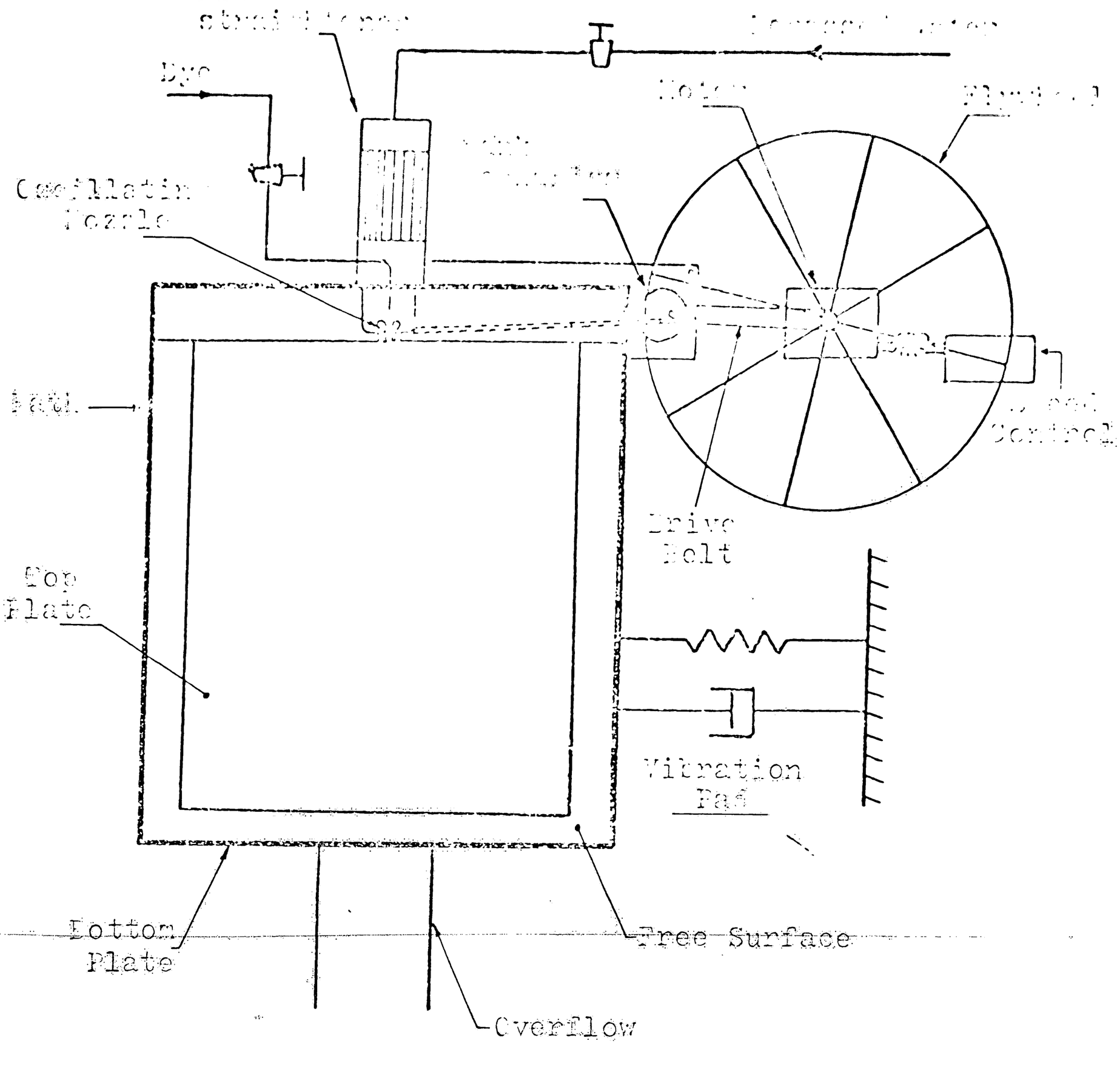

FIG. 2. T-P MAIN APPARATUS

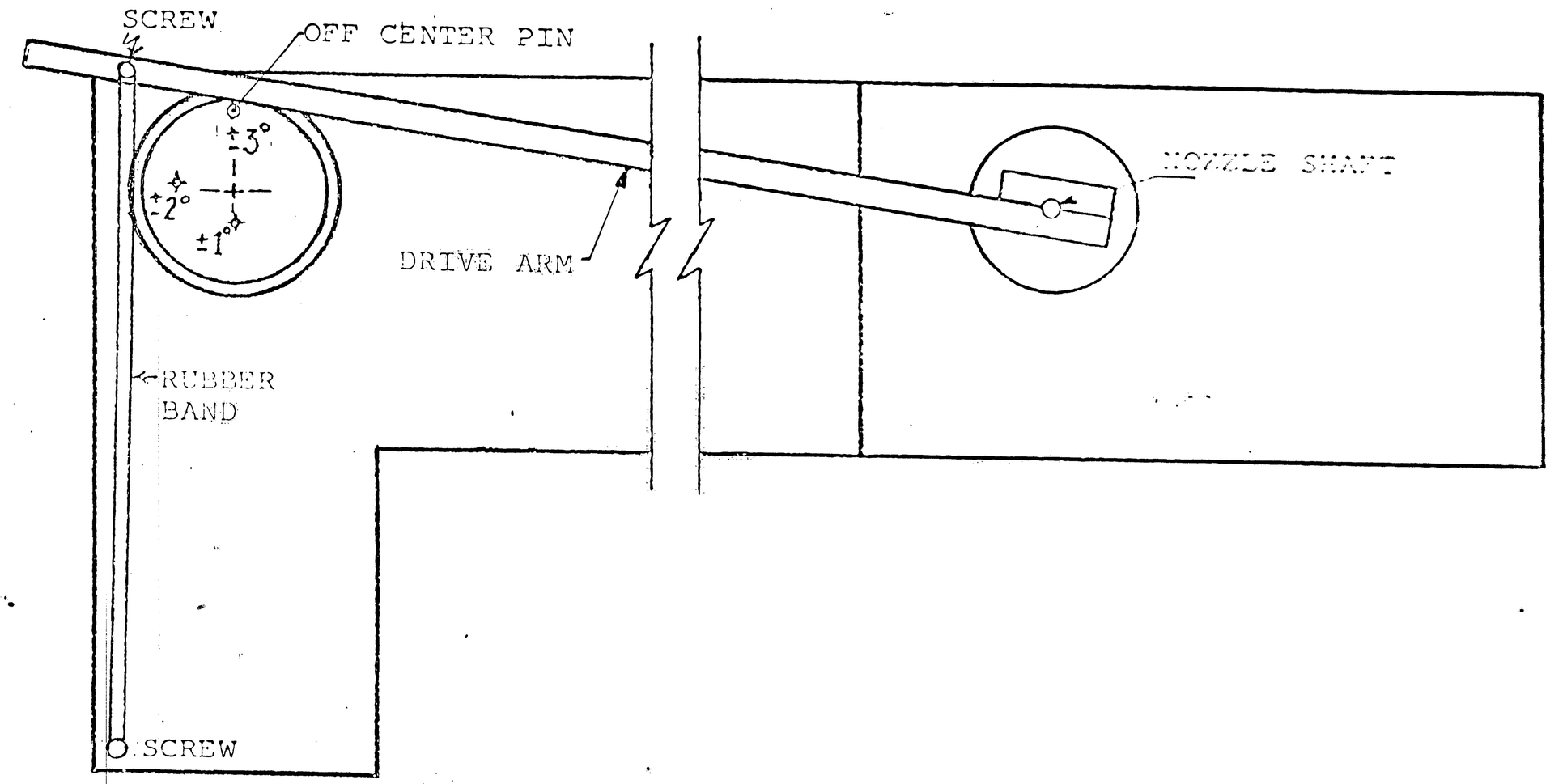

FIG. 3. TRIVEC ISOMATIC

±1°, ±2°, ±3° Drive Mechanism

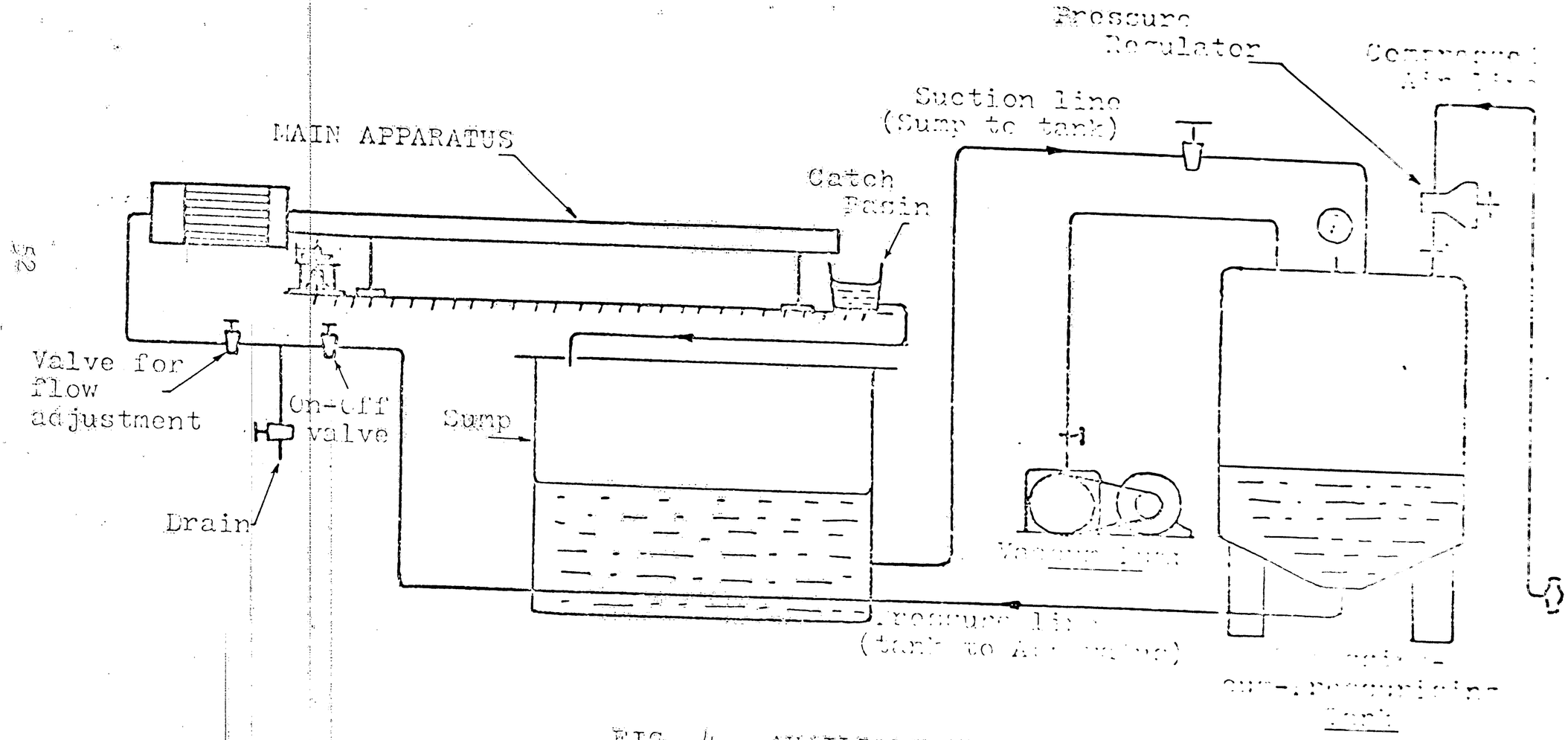

FIG. 4 AUXILIARY APPARATUS

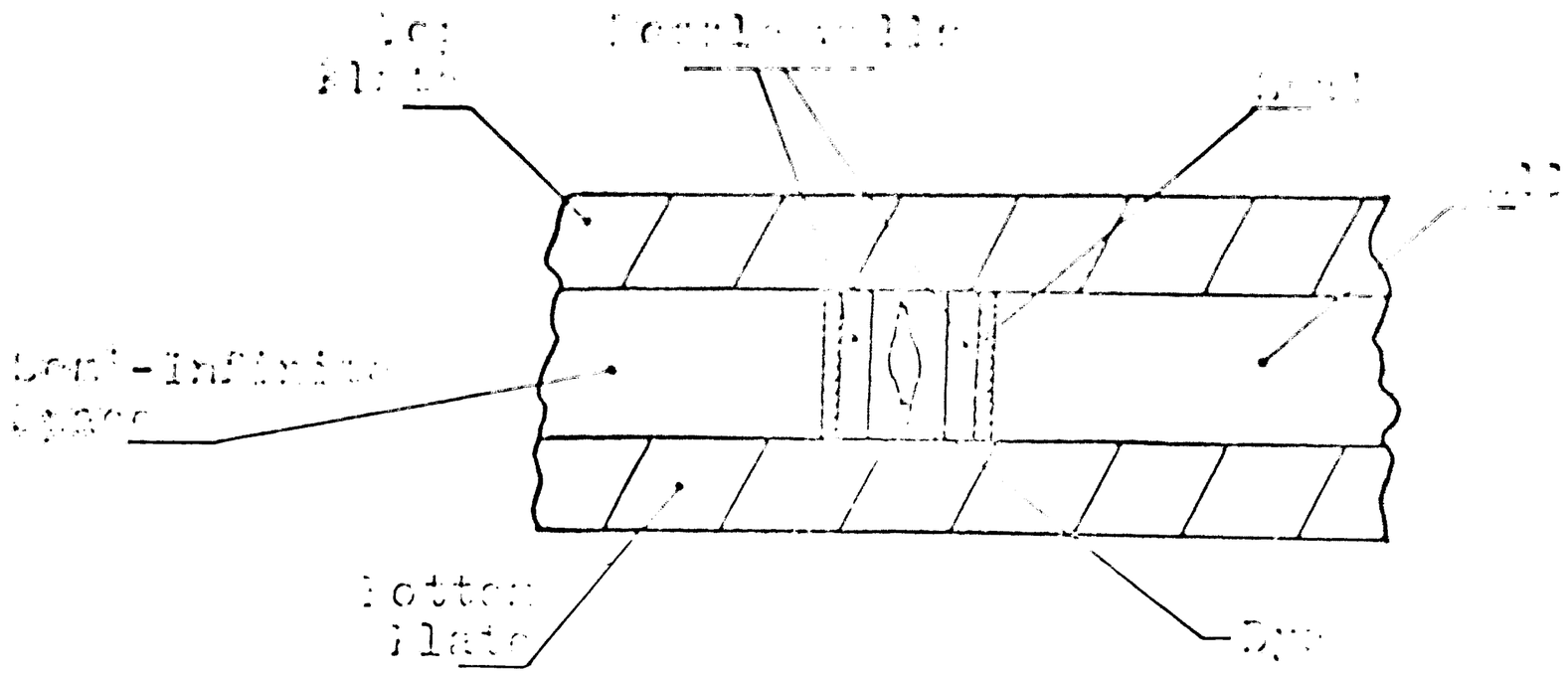

FIG. 5 SIDE VIEW OF NOZZLE

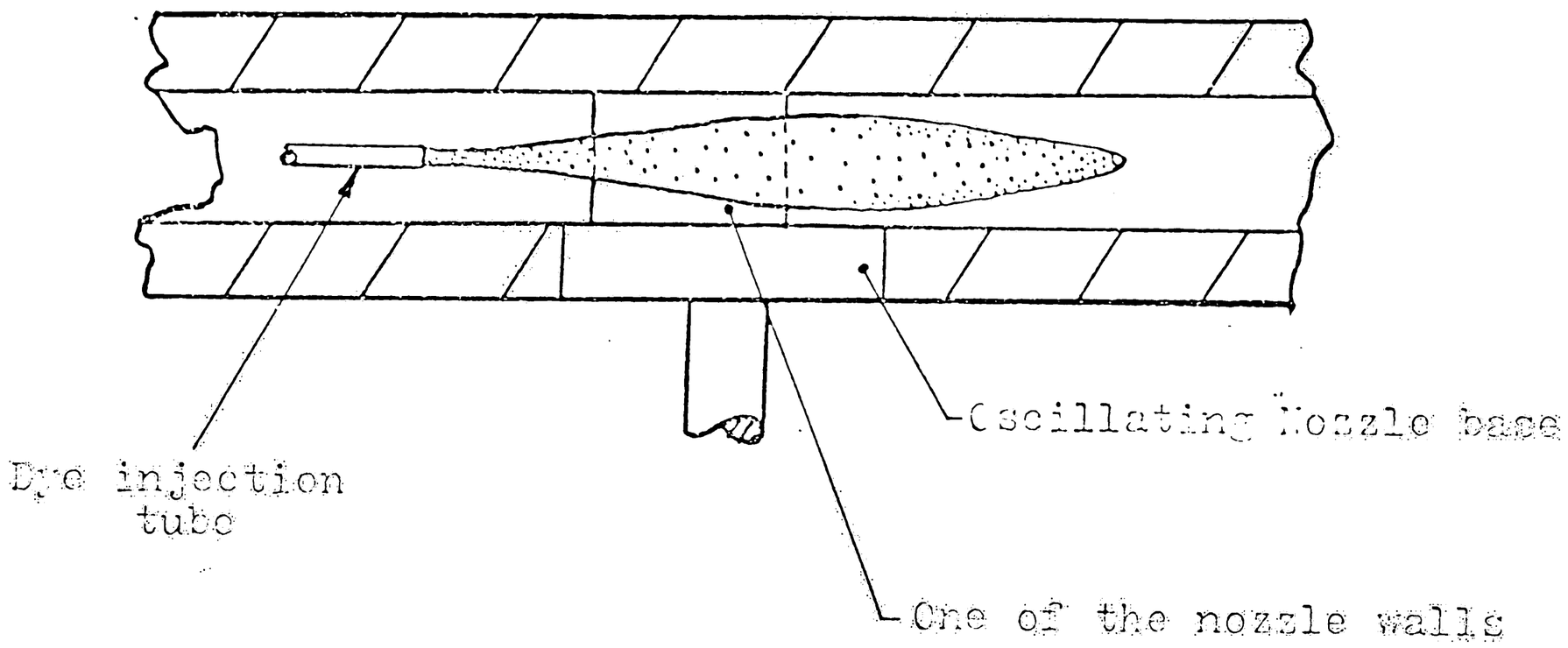

FIG. 6 SIDE VIEW OF NOZZLE

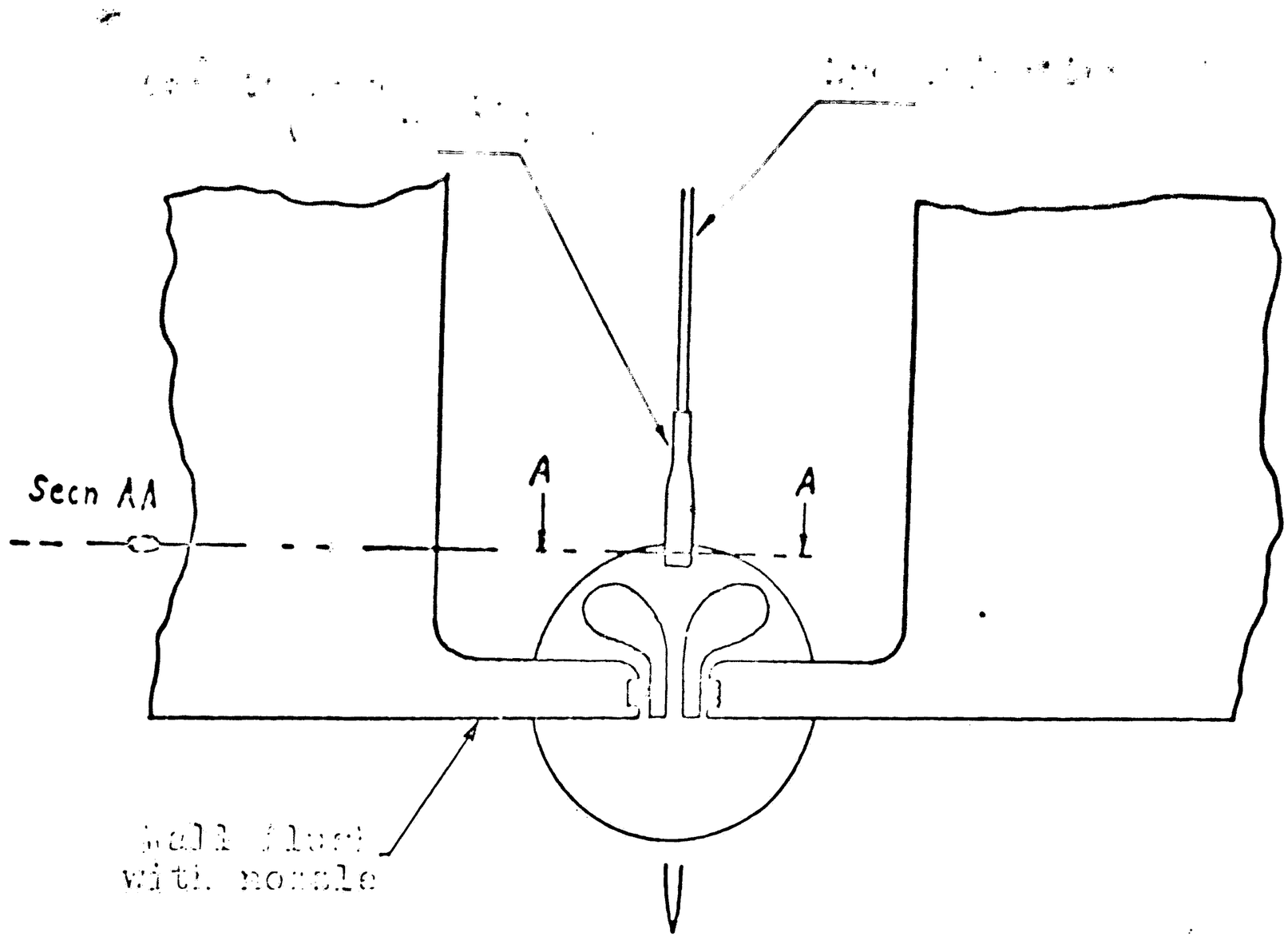

Velocity profiles in the plane of the semi-infinite field.

FIG. 7 THE SEMI-INFINITE FIELD

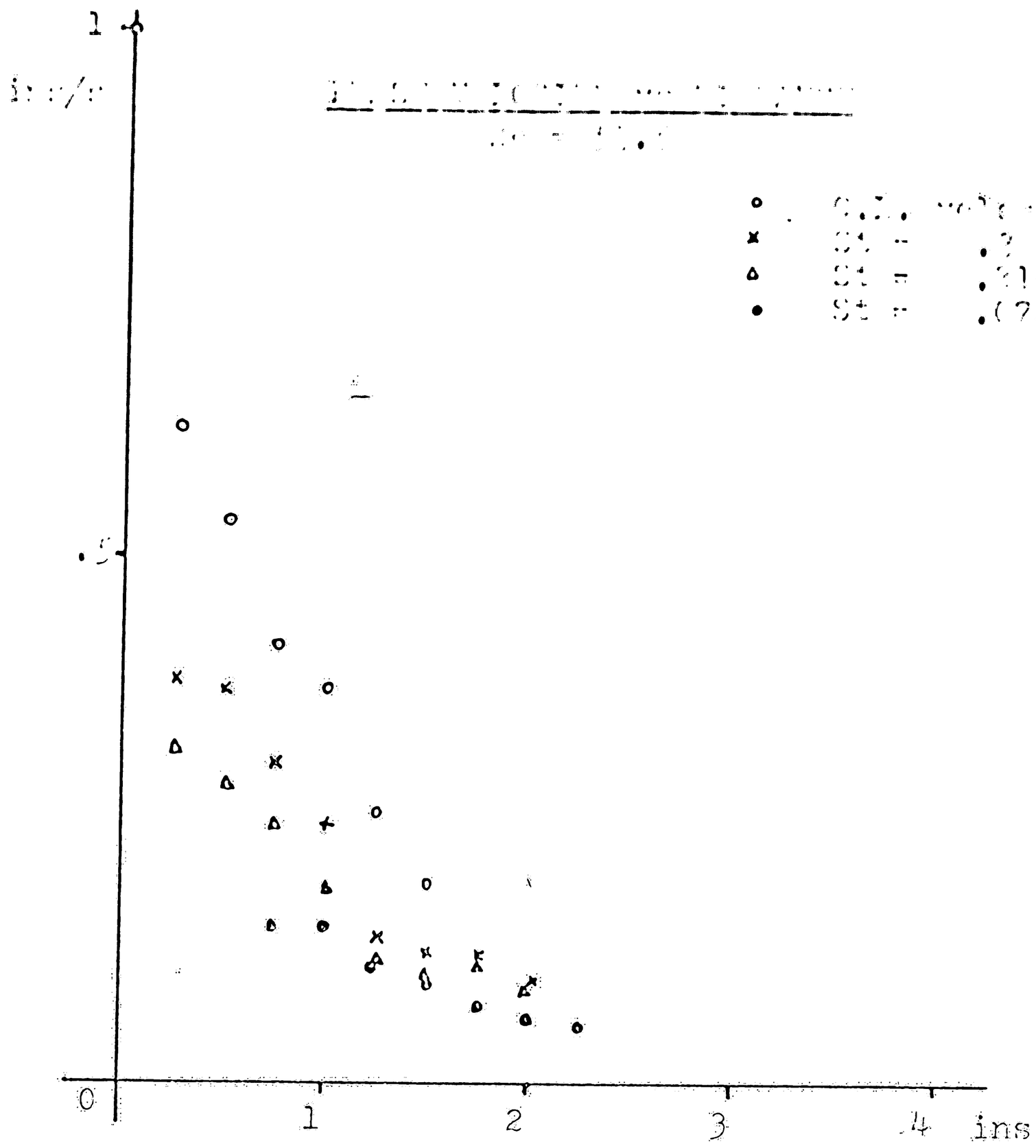

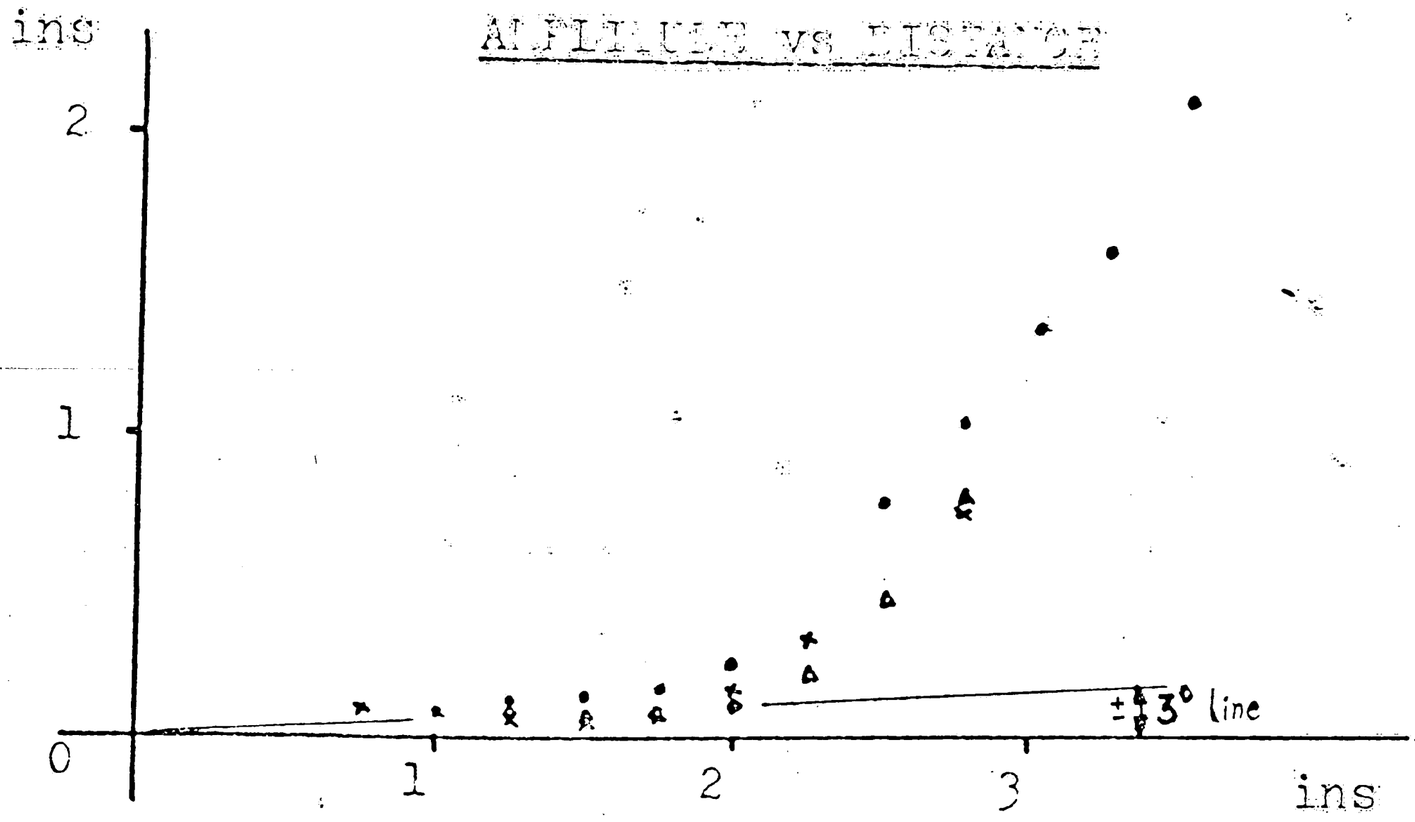

AMPLITUDE vs DISTANCE

Fig. 8

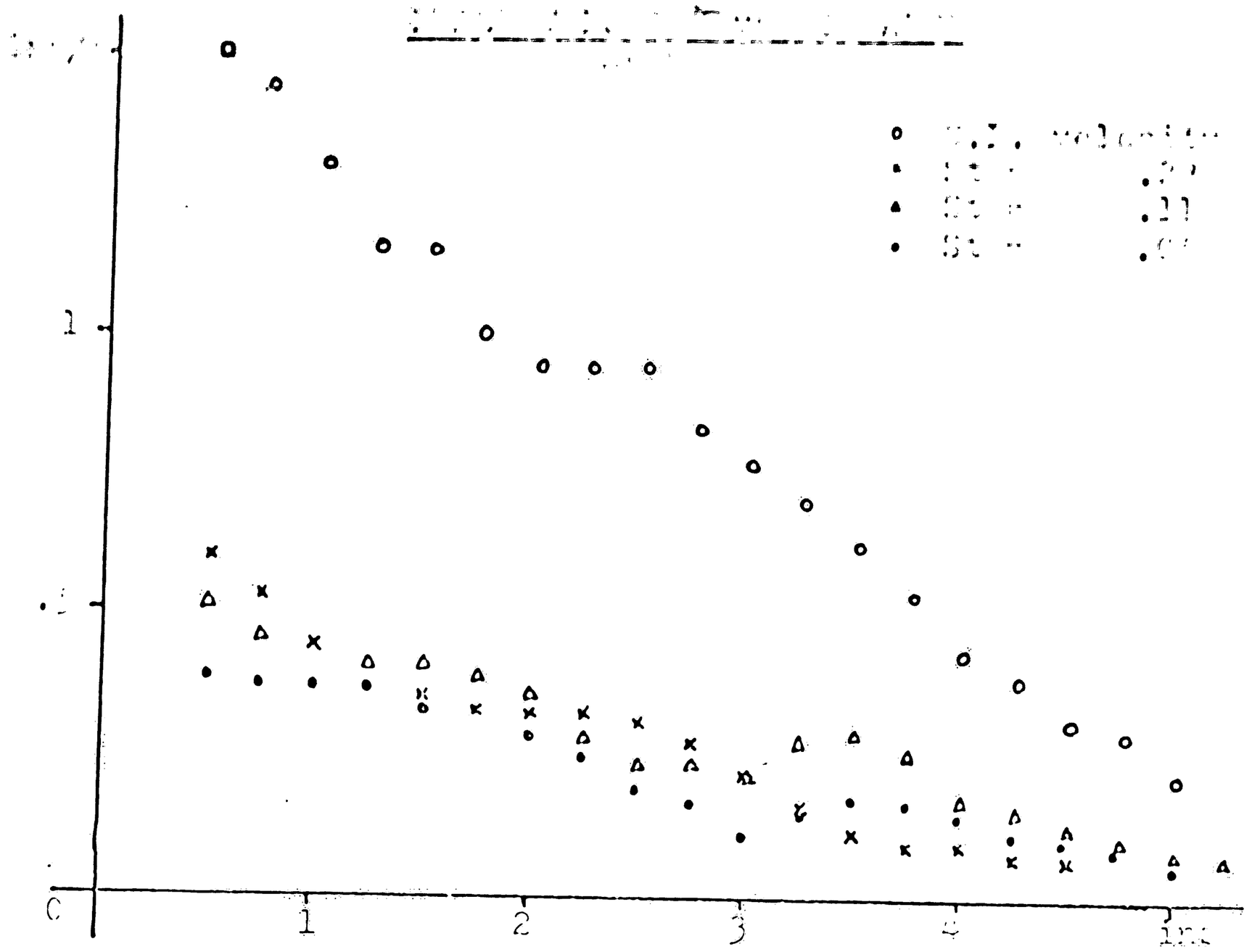

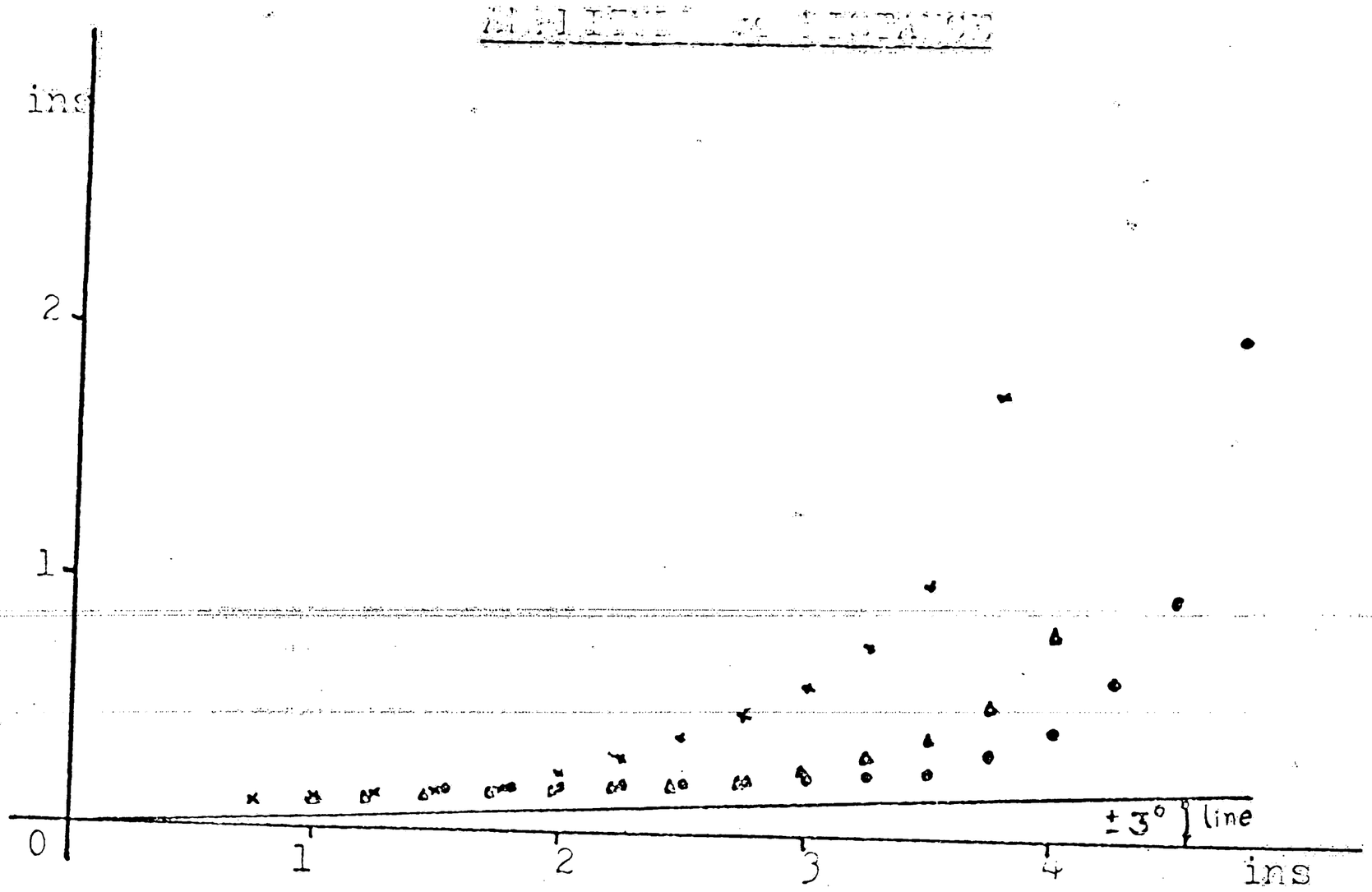

Fig. 9

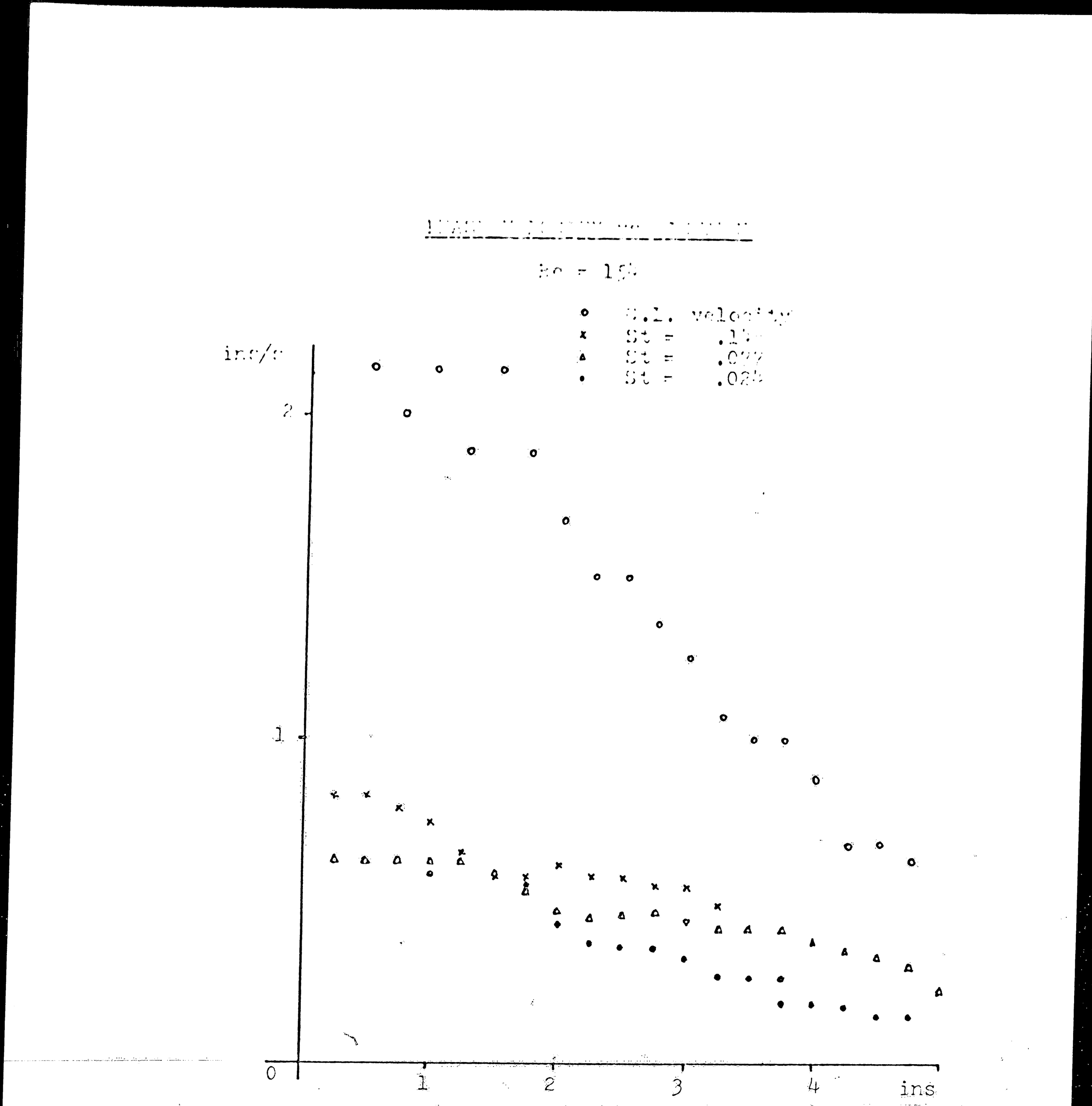

Fig. 10

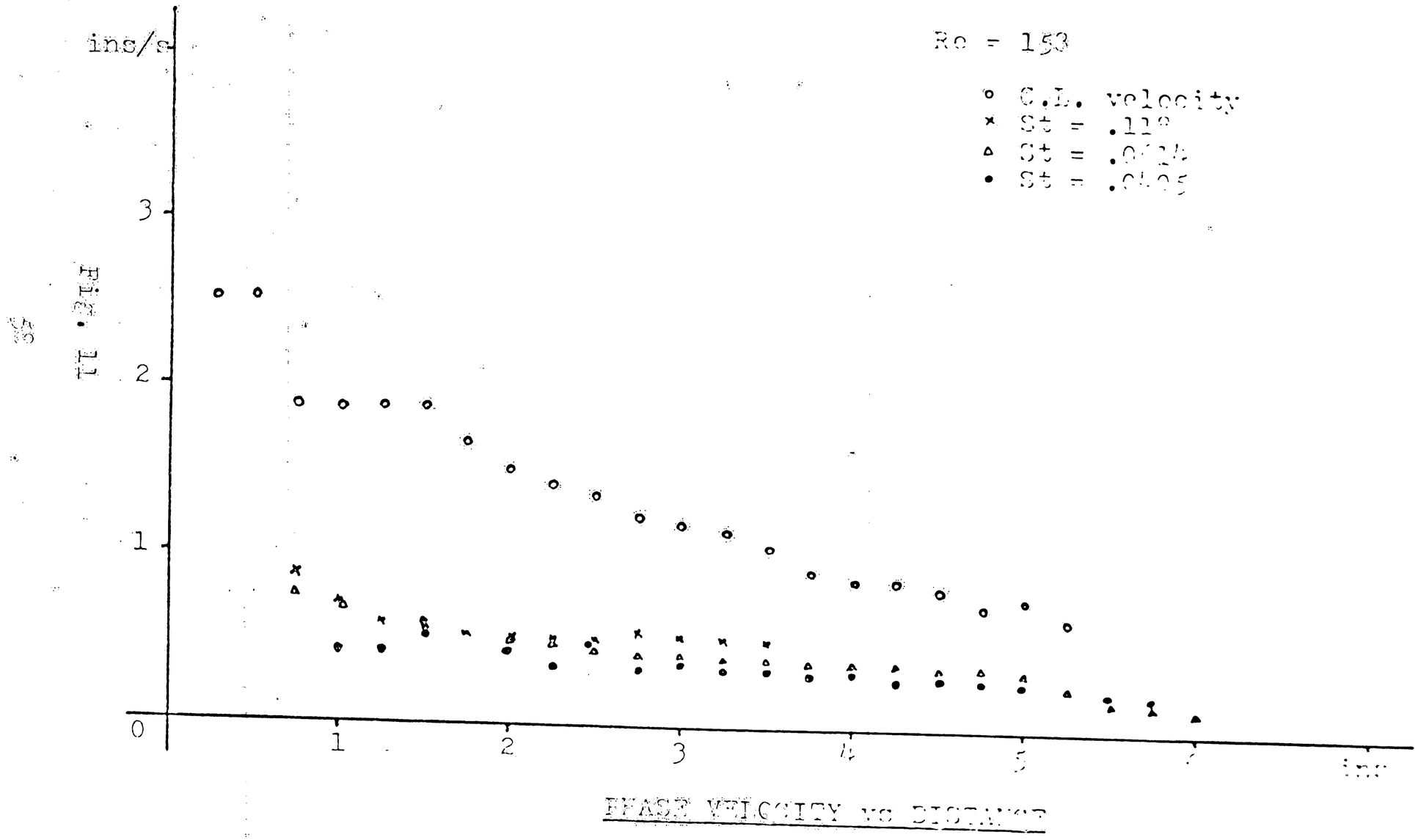

PHASE VELOCITY VS DISTANCE

PHASE VELOCITY vs DISTANCE

Re = 193

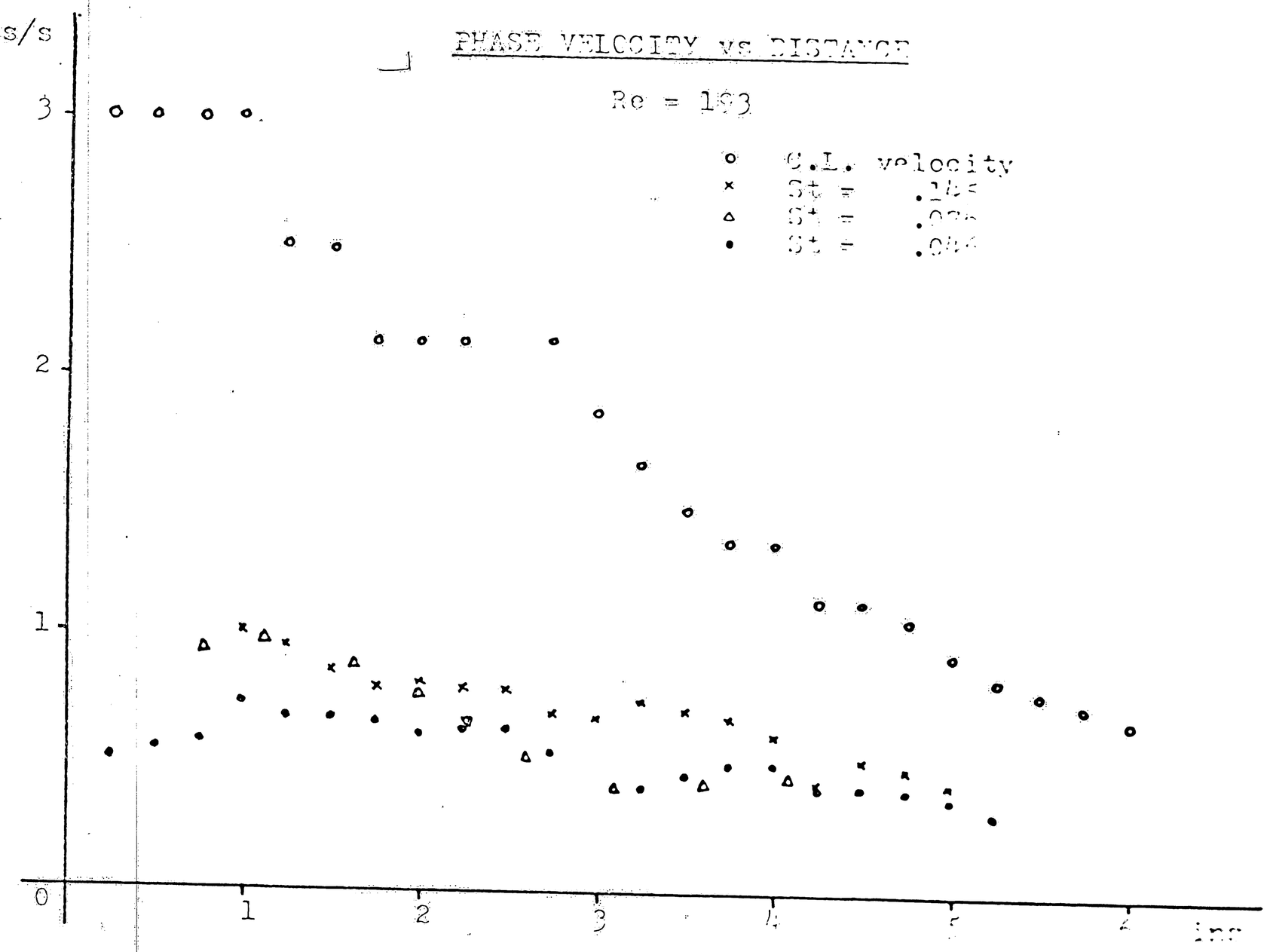

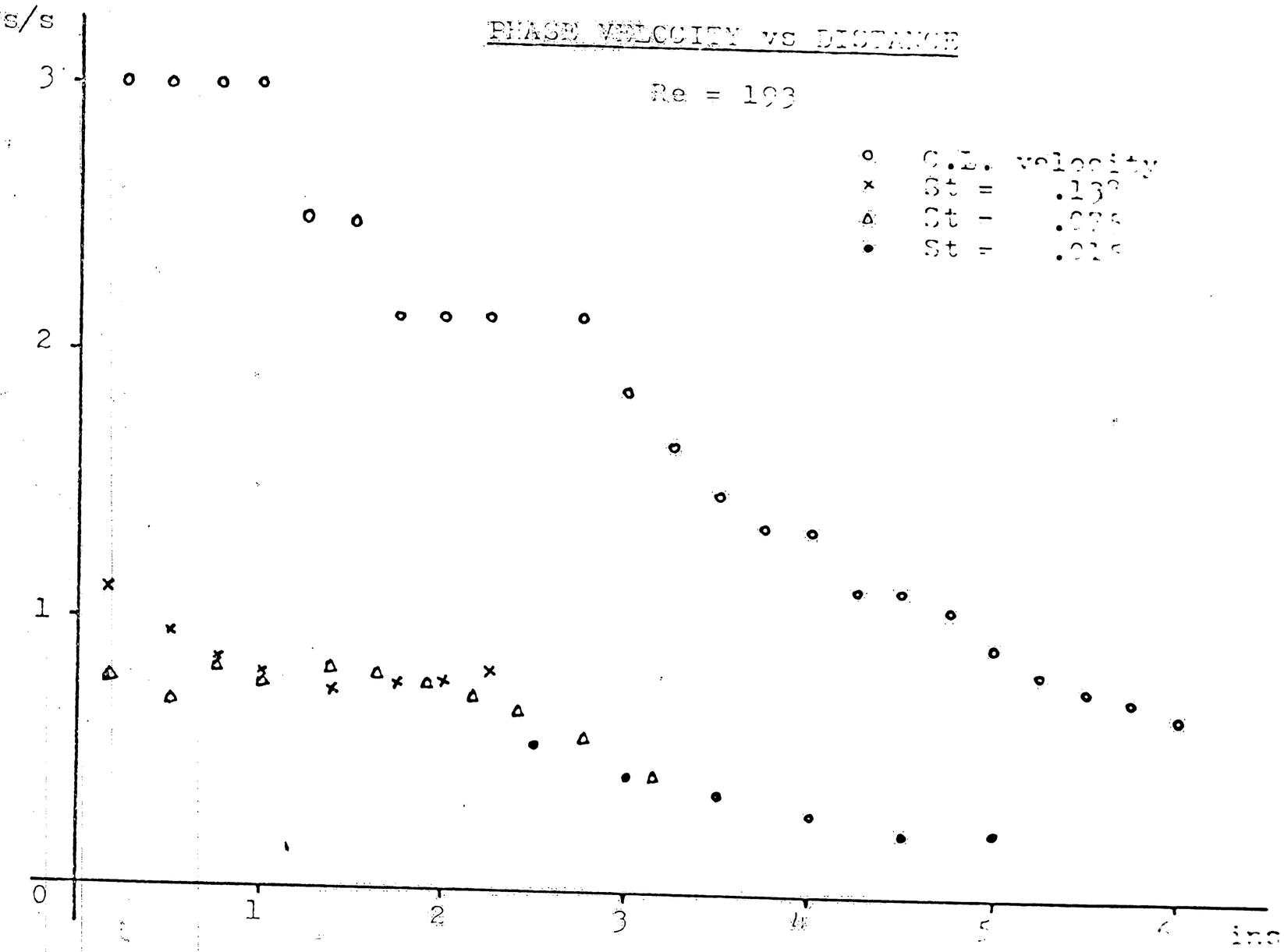
PHASE VELOCITY vs DISTANCE
Re = 193
o C.L. velocity
× St = .13
Δ St = .
• St = .
ins/s
3
2
1
0
1
2
3
4
5
ins

Fig. 13

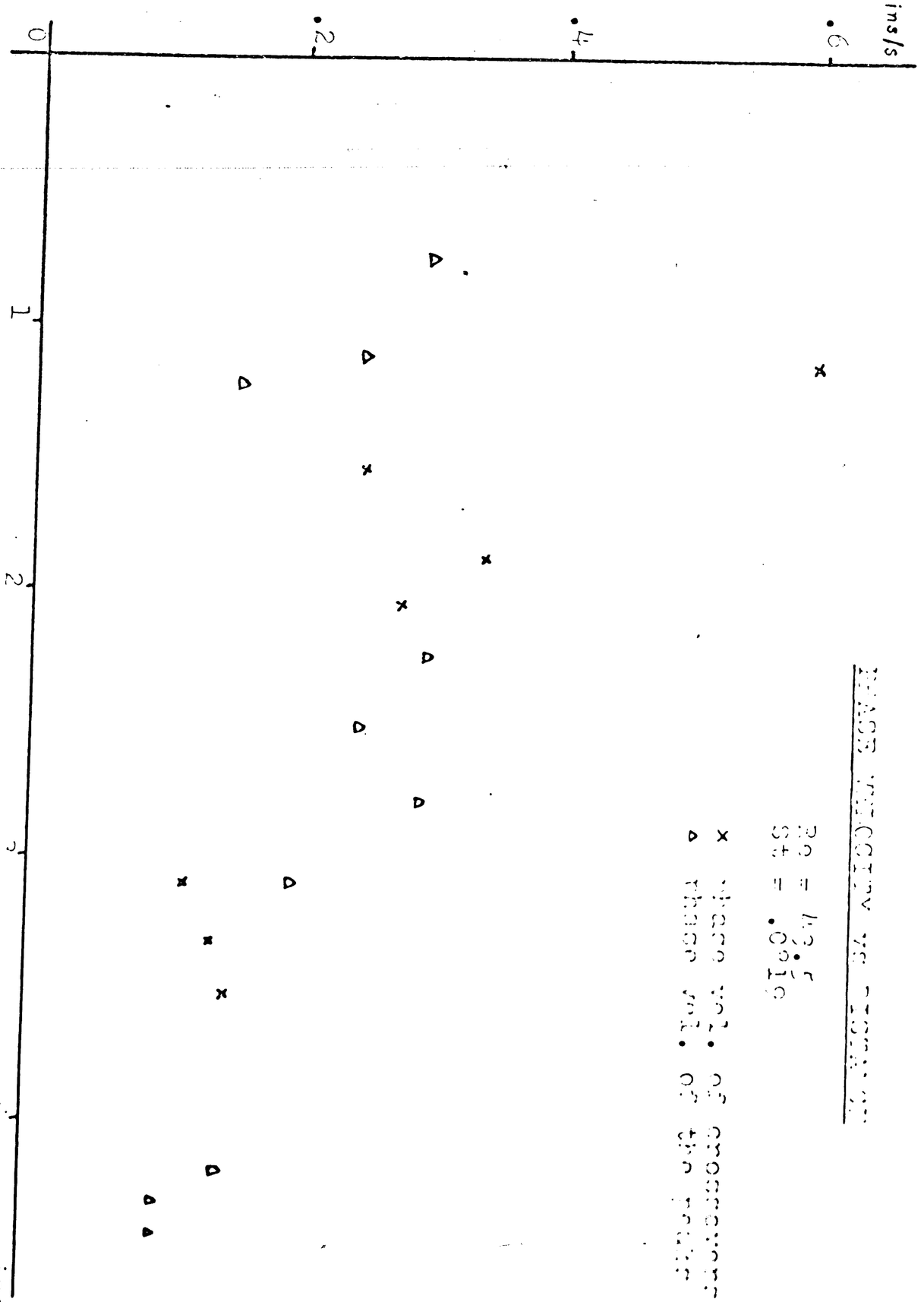

Fig. 14

PHASE VELOCITY VS DISTANCE

Δσ = 42.9
Δt = .121

× phase vel. of crossovers
Δ phase vel. of the peaks

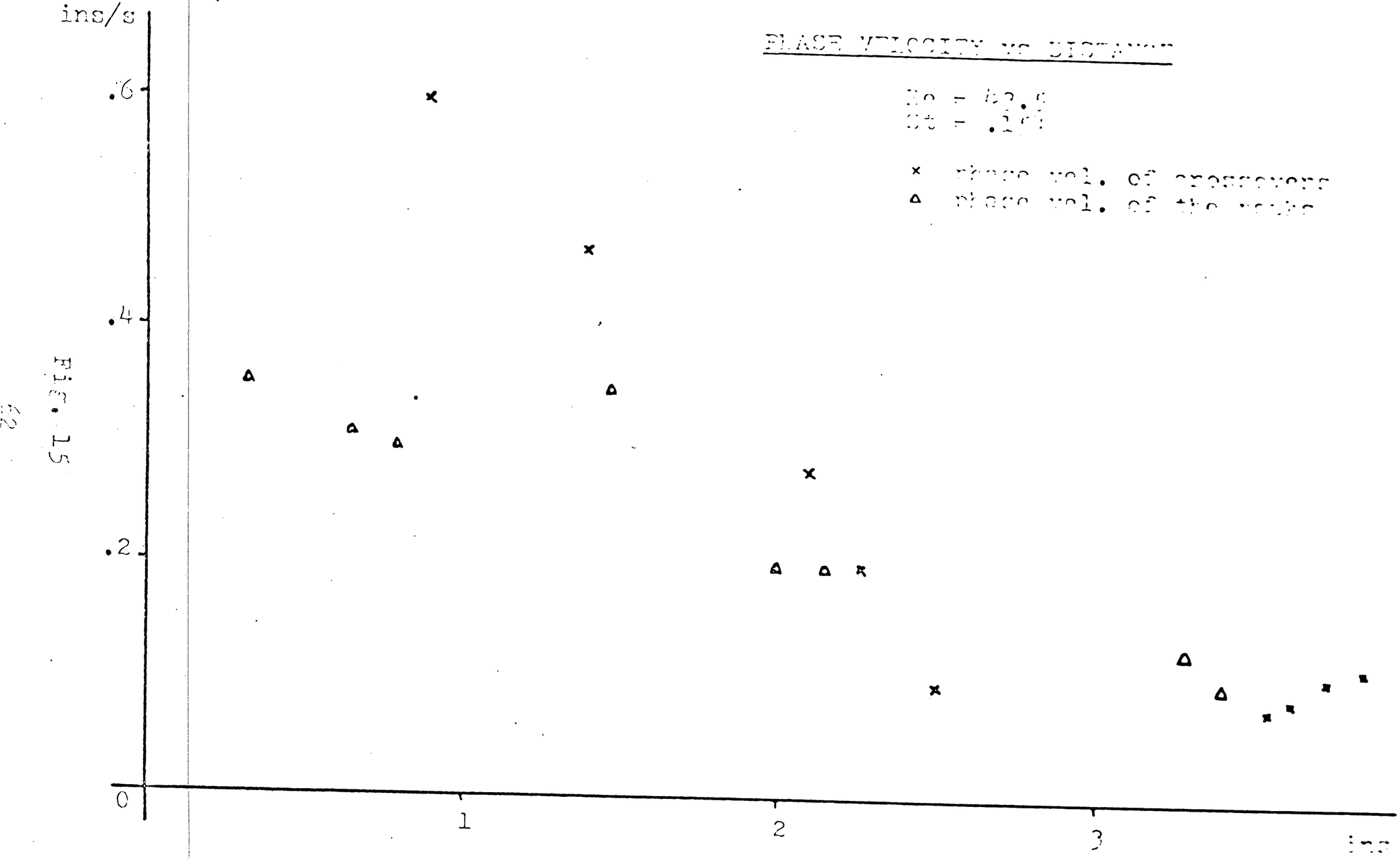

Fig. 15
52

PHASE VELOCITY vs FREQUENCY

Ko 43.5
σt .475

× phase vel. of crossovers
△ phase vel. of peaks

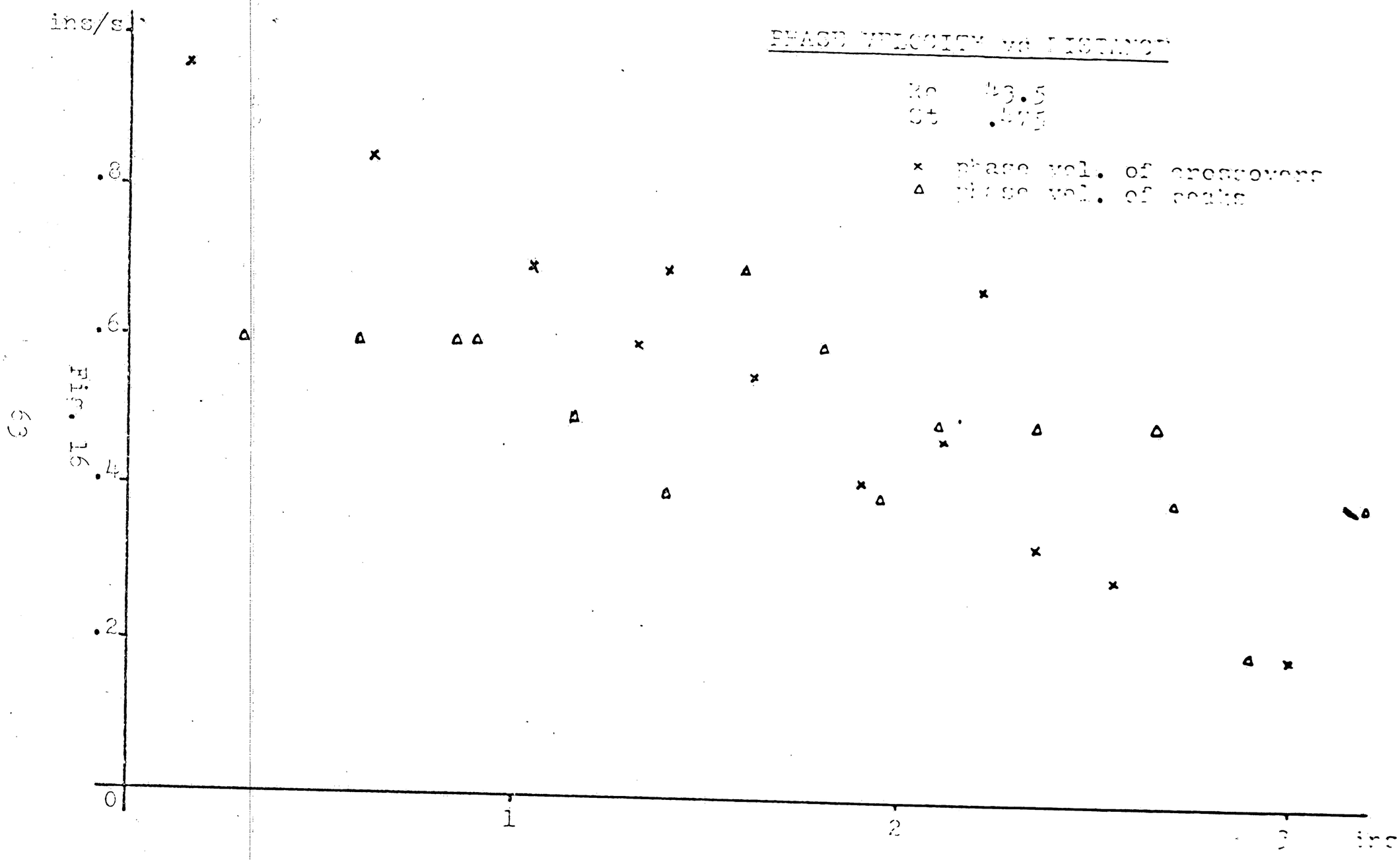

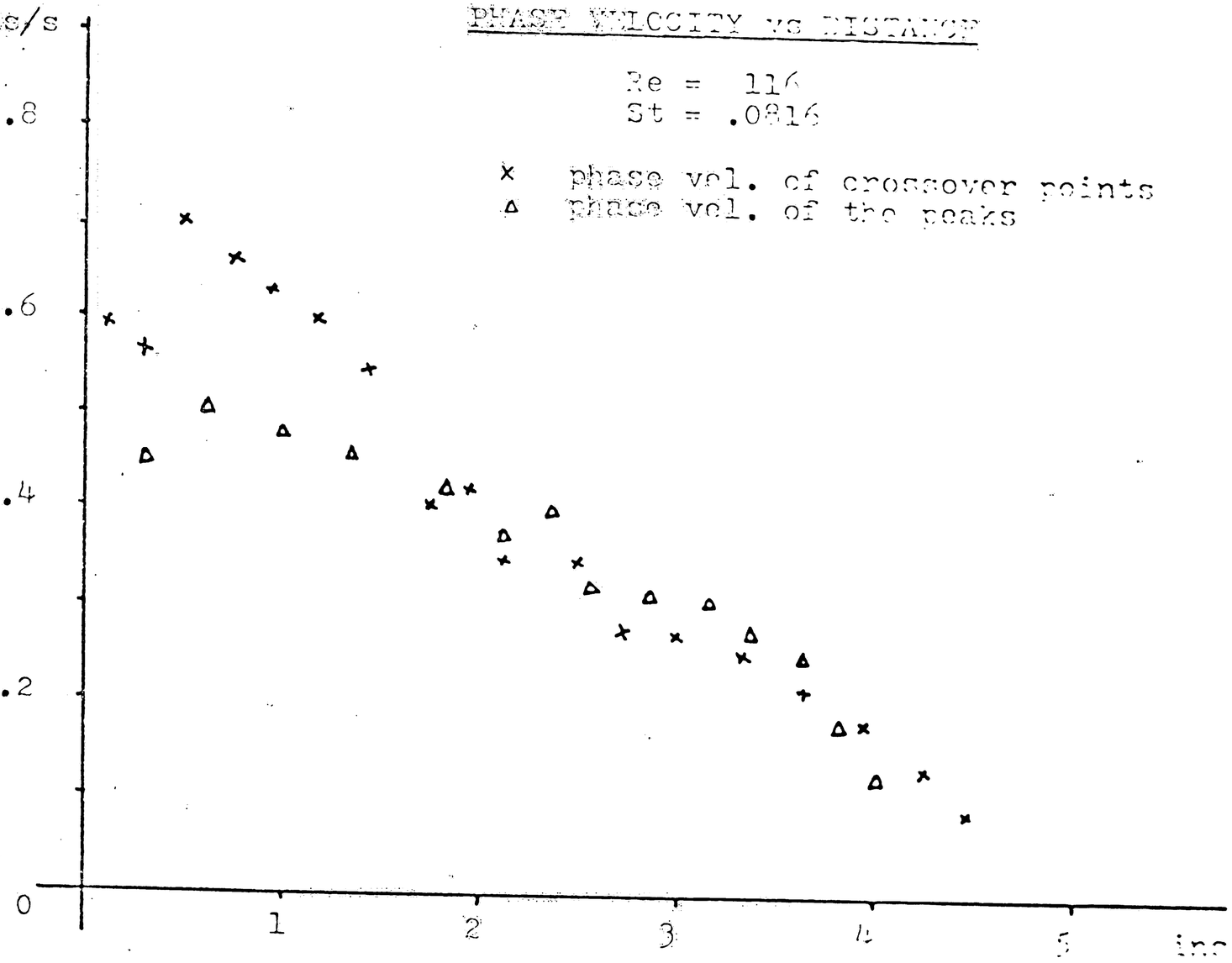
PHASE VELOCITY vs DISTANCE
Re = 116
St = .0816
x phase vel. of crossover points
Δ phase vel. of the peaks
ins/s
.8
.6
.4
.2
0
1
2
3
4
5
ins

Fig. 17

Fig. 18

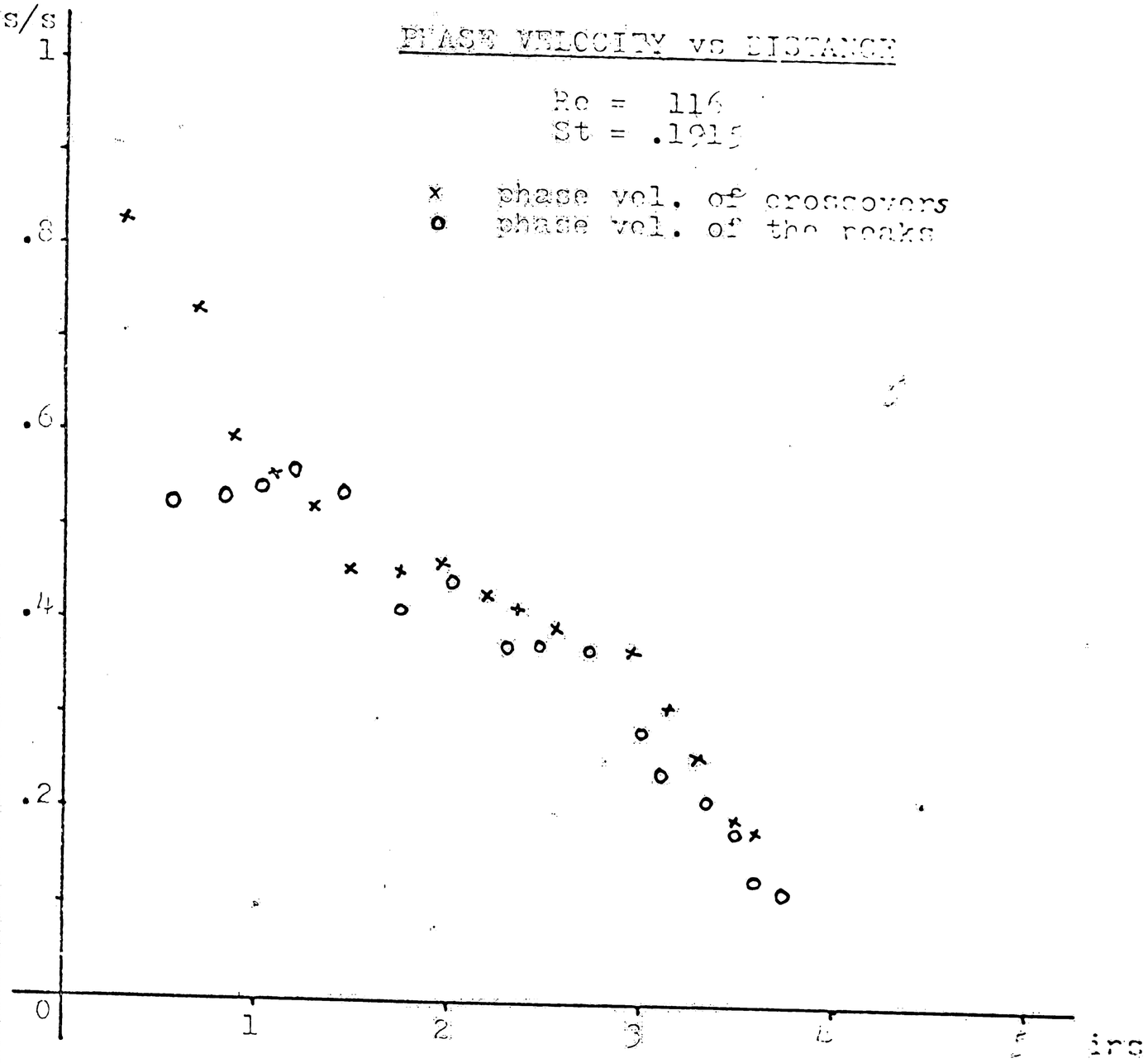

PHASE VELOCITY vs DISTANCE

Re = 116
St = .1915

x phase vel. of crossovers
o phase vel. of the peaks

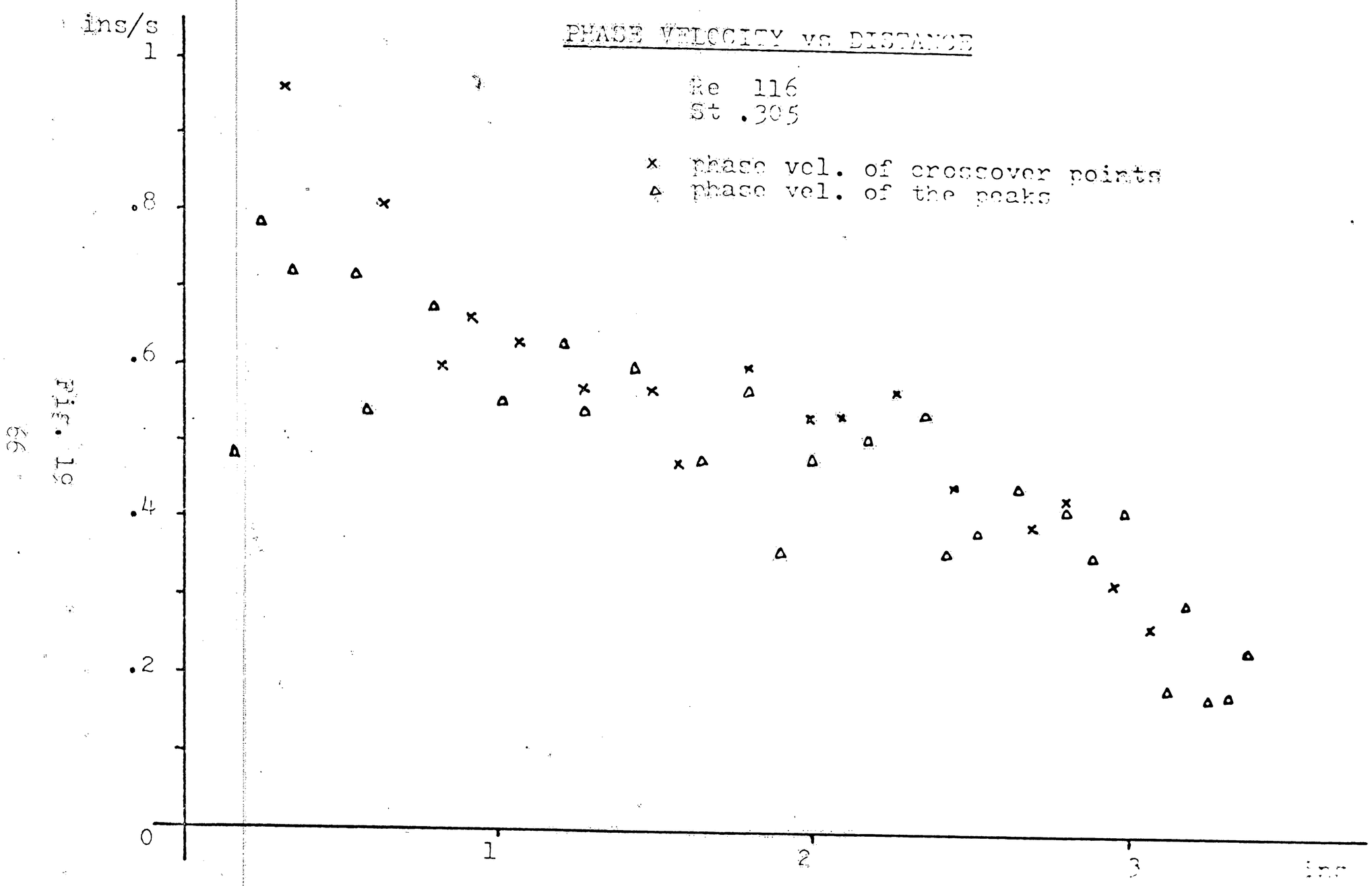
PHASE VELOCITY vs DISTANCE
Re 116
St .305
× phase vel. of crossover points
△ phase vel. of the peaks
ins/s
1
.8
.6
.4
.2
0
1
2
3
in.

PHASE VELOCITY vs WAVELENGTH

Ro = 177
St = .032

× phase vel. of experiment
△ phase vel. of theory

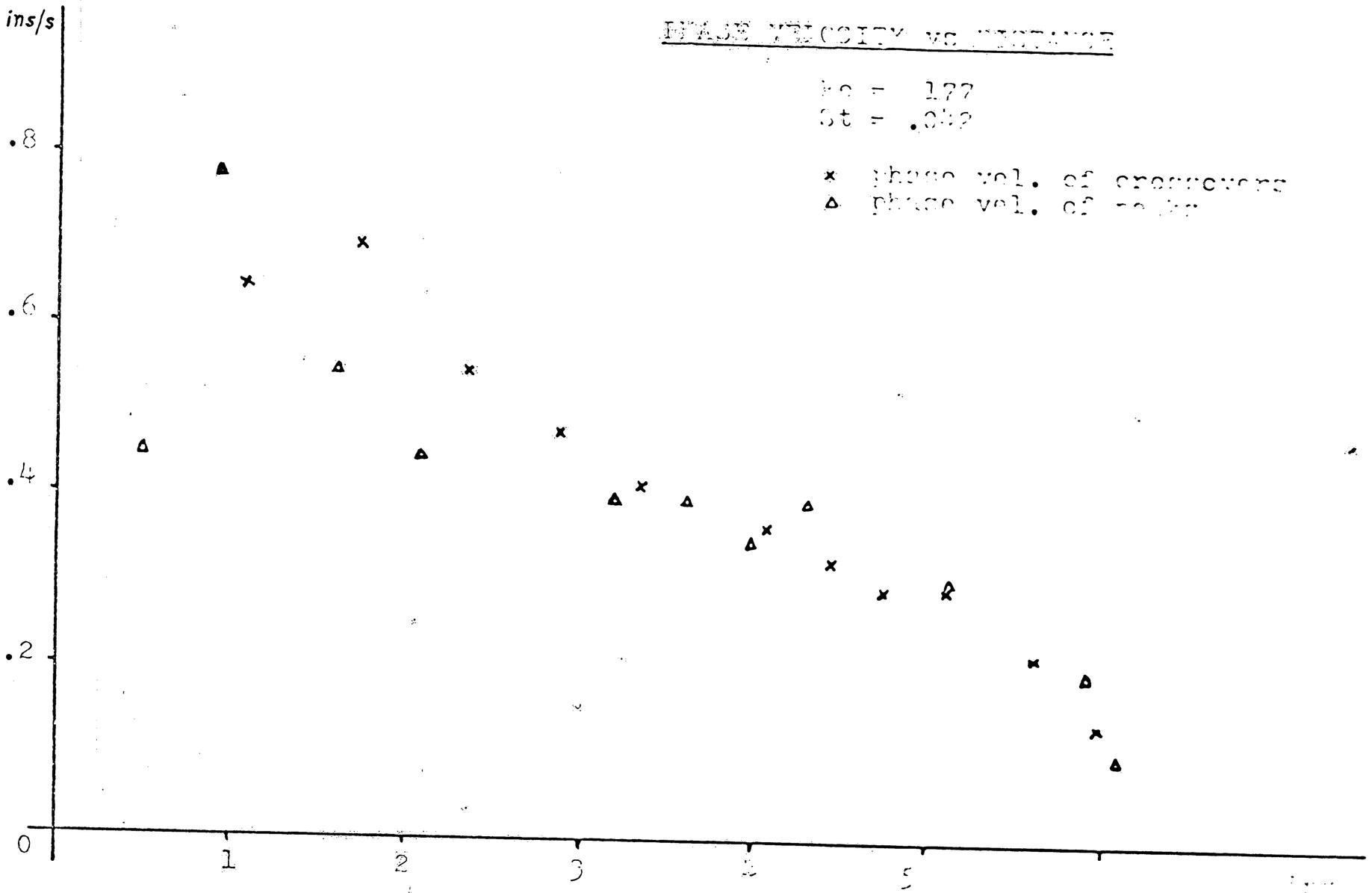

Fig. 20

PHASE VELOCITY vs FREQUENCY

Re = 1[illegible]
St = .0[illegible]

x phase vel. of crossover
Δ phase vel. of the peaks

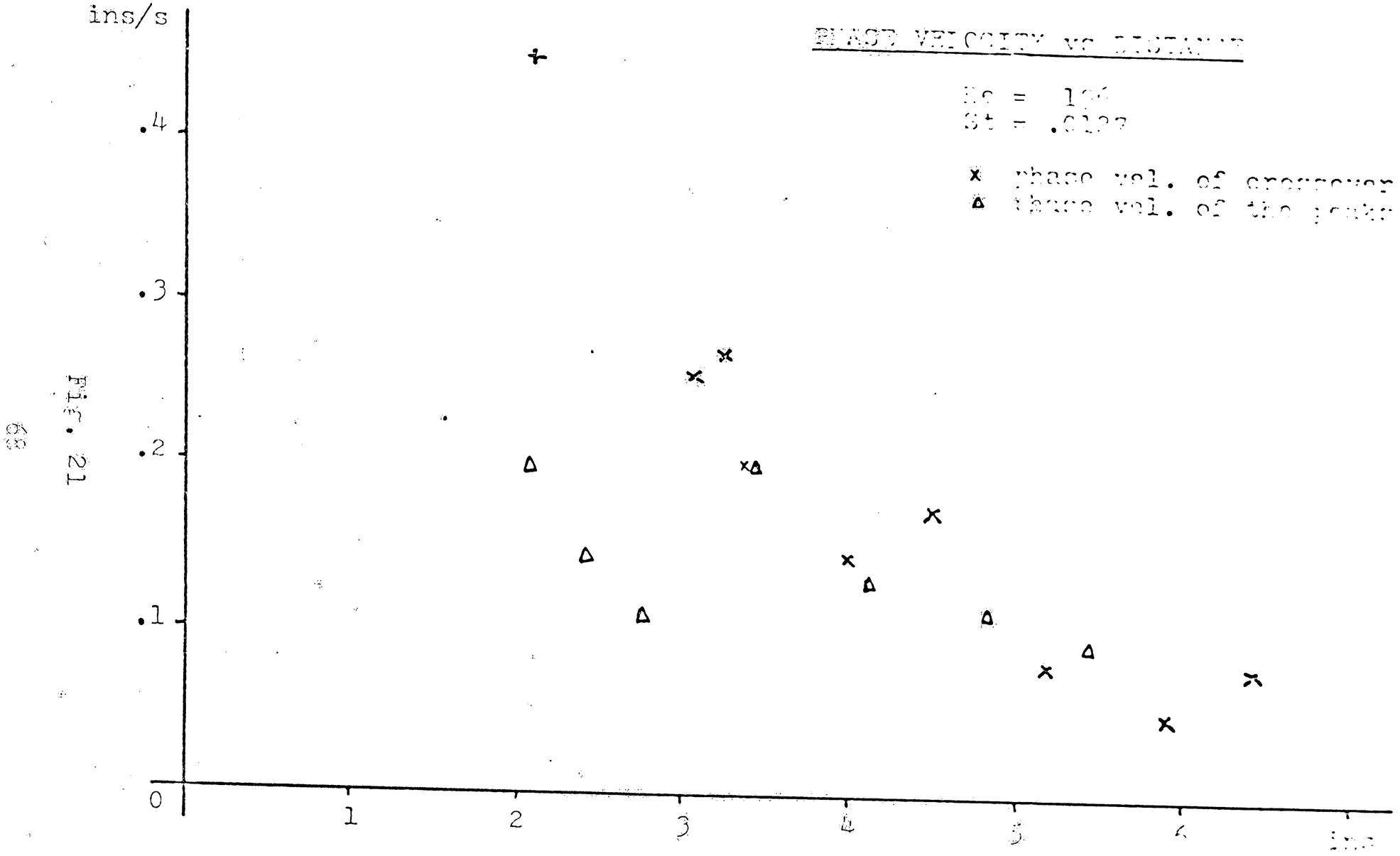

PHASE VELOCITY vs DISTANCE

Re = 196
St = .0323

x phase vel. of crossover points
Δ phase vel. of the peaks

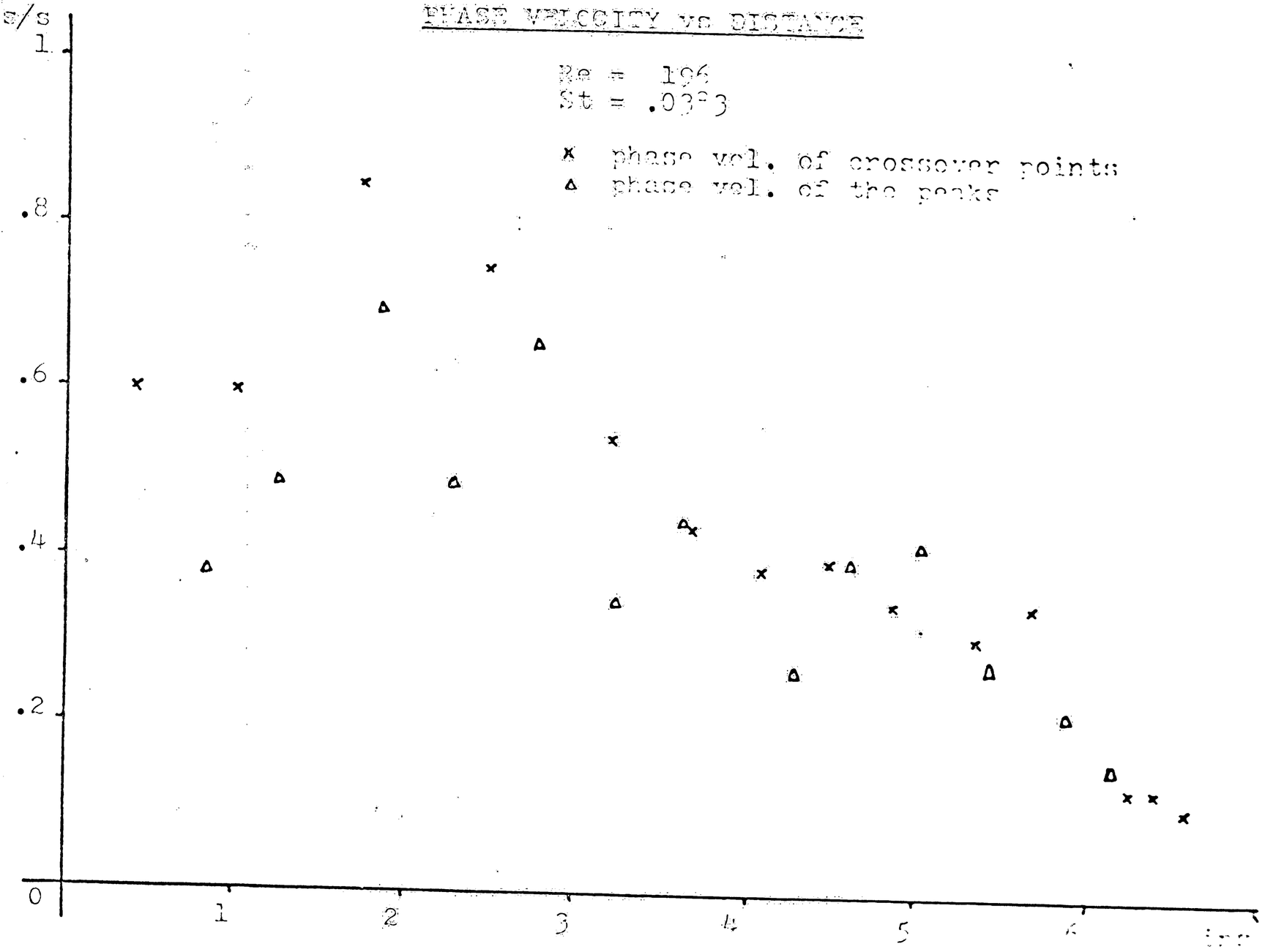

FIG. 23

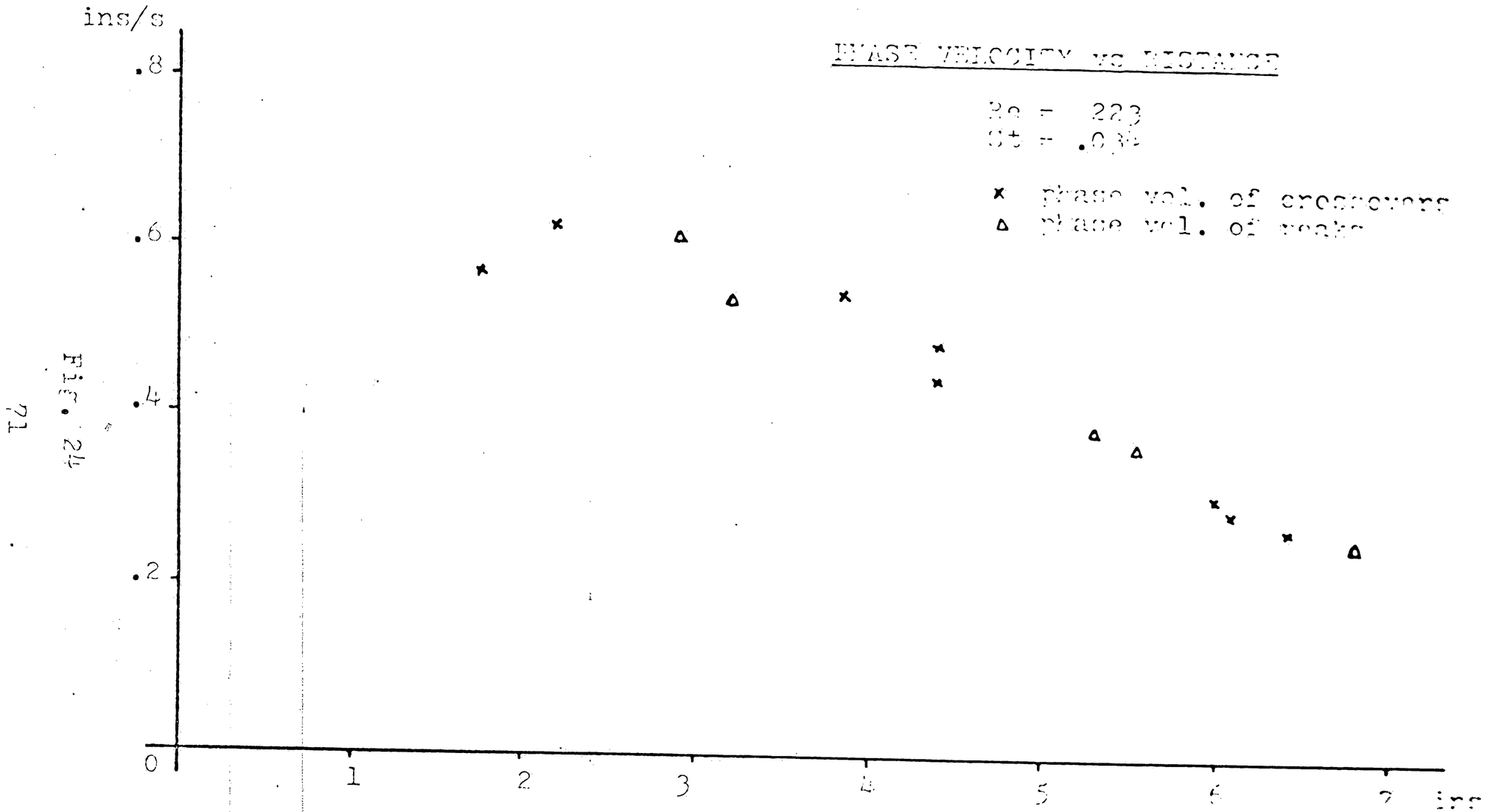
PHASE VELOCITY VS DISTANCE
Re = 223
St = .03
x phase vel. of crossovers
Δ phase vel. of peaks
ins/s
.8
.6
.4
.2
0
1
2
3
4
5
ins

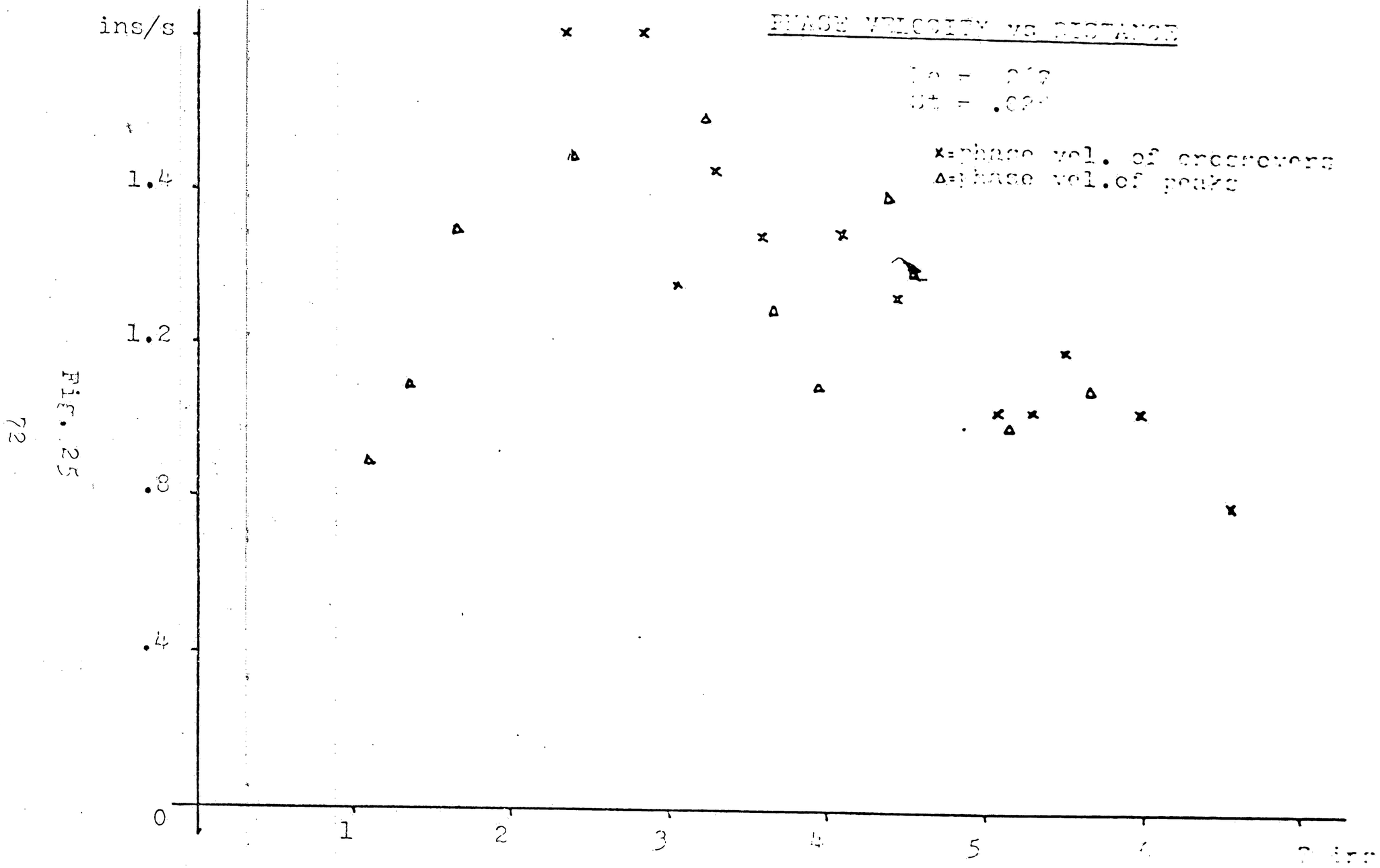
PHASE VELOCITY VS DISTANCE
x=phase vel. of crossovers
Δ=phase vel.of peaks
ins/s
1.4
1.2
.8
.4
0
1
2
3
4
5

Fig. 23

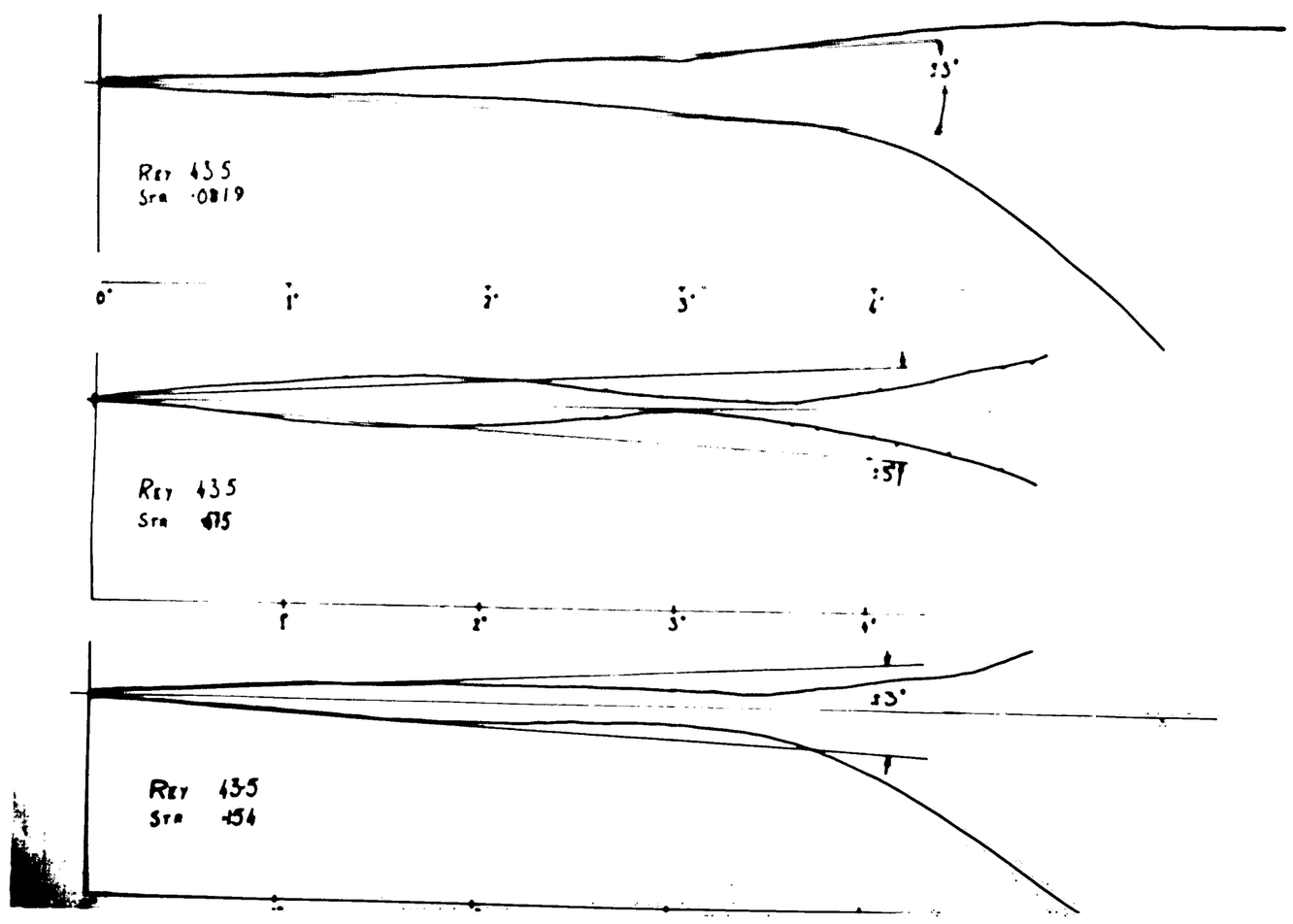

FIG. 26. AMPLITUDE GROWTH

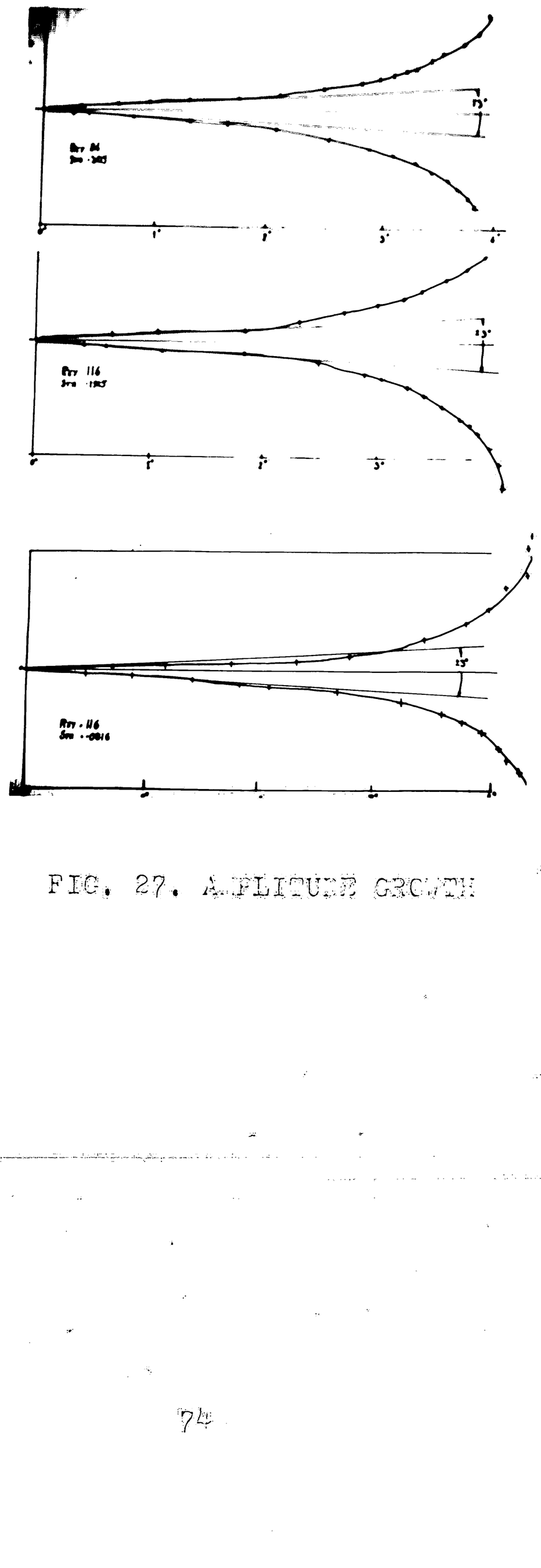

FIG. 27. AMPLITUDE GROWTH

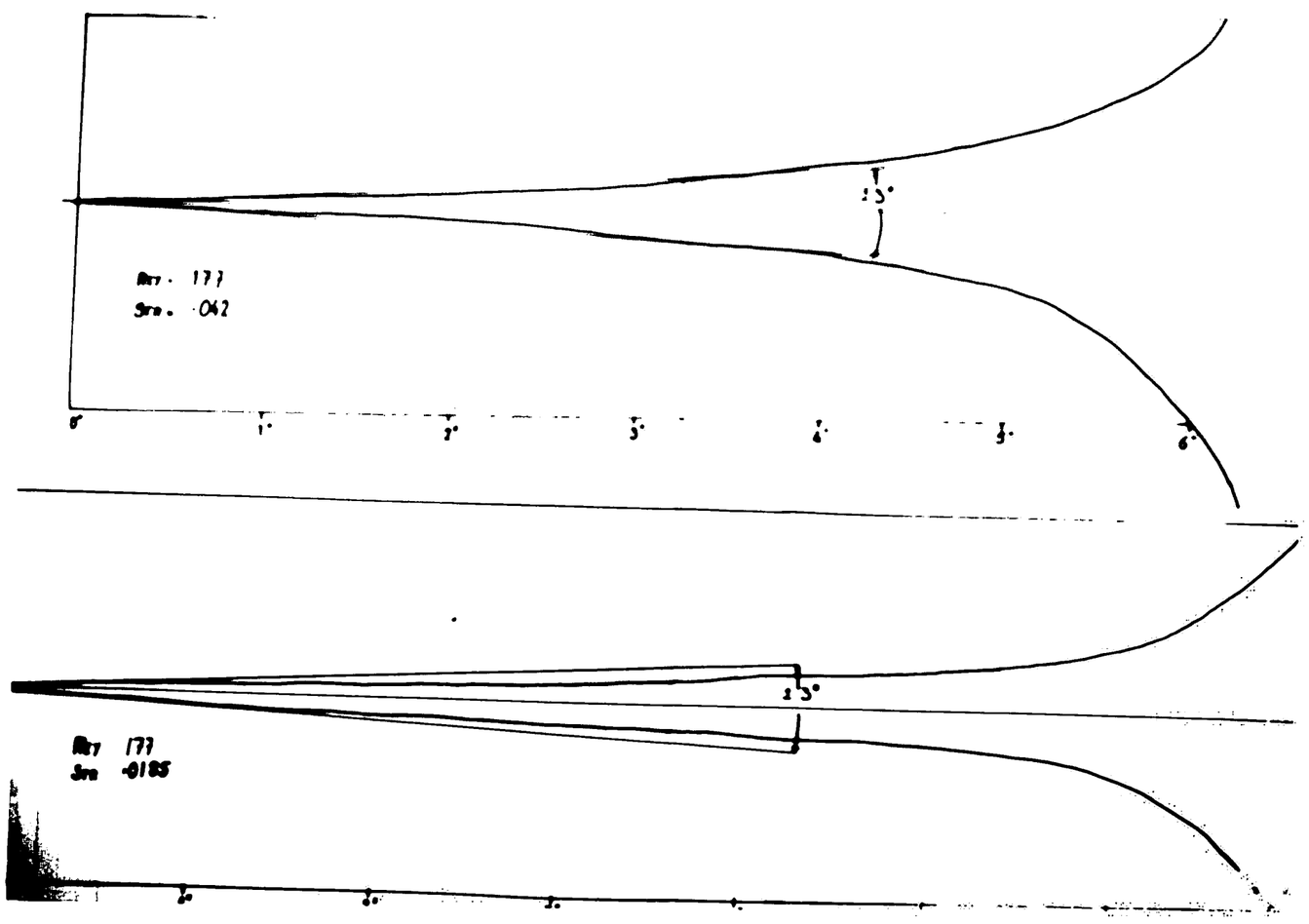

FIG. 23. AMPLITUDE GROWTH

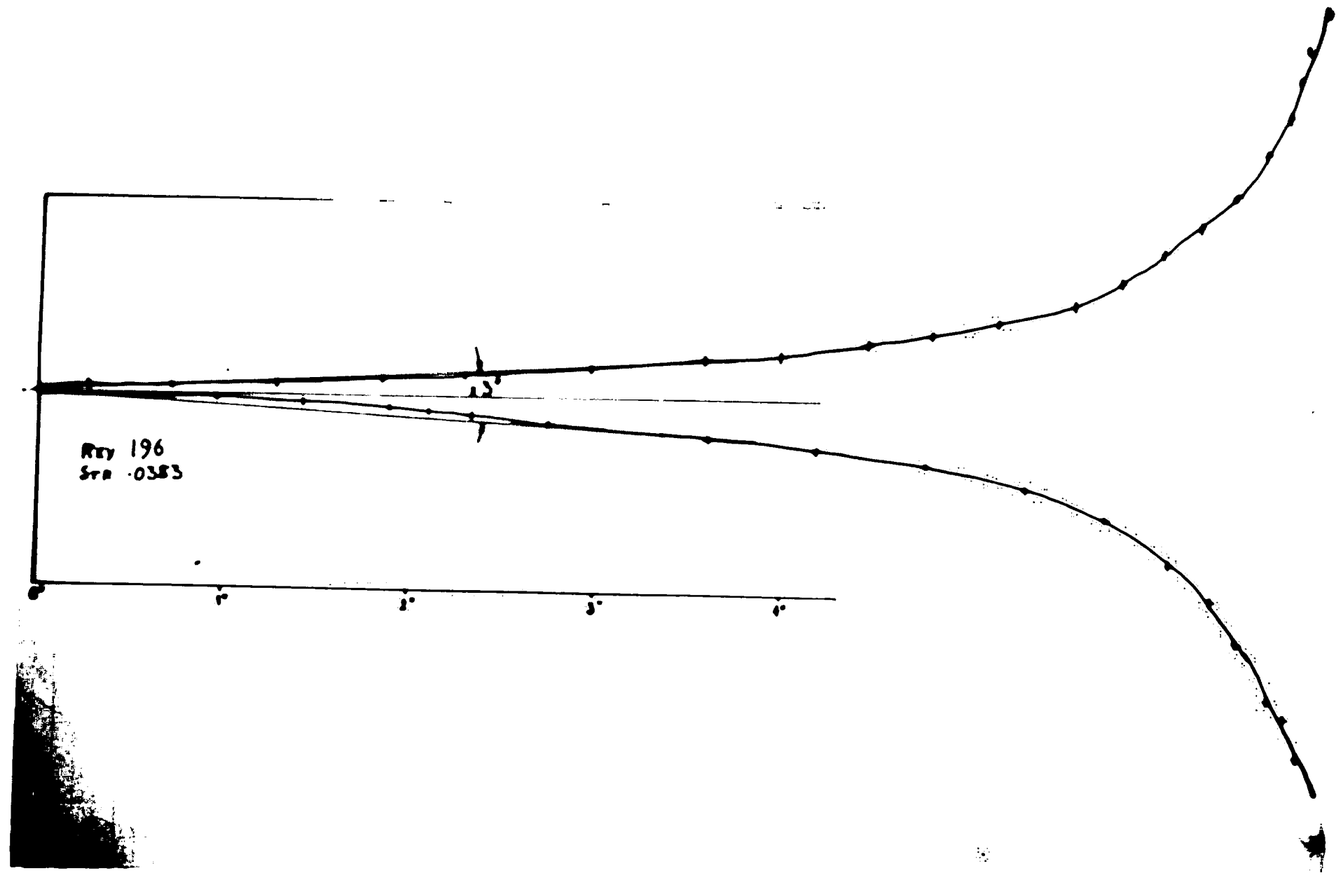

FIG. 29. AMPLITUDE GROWTH

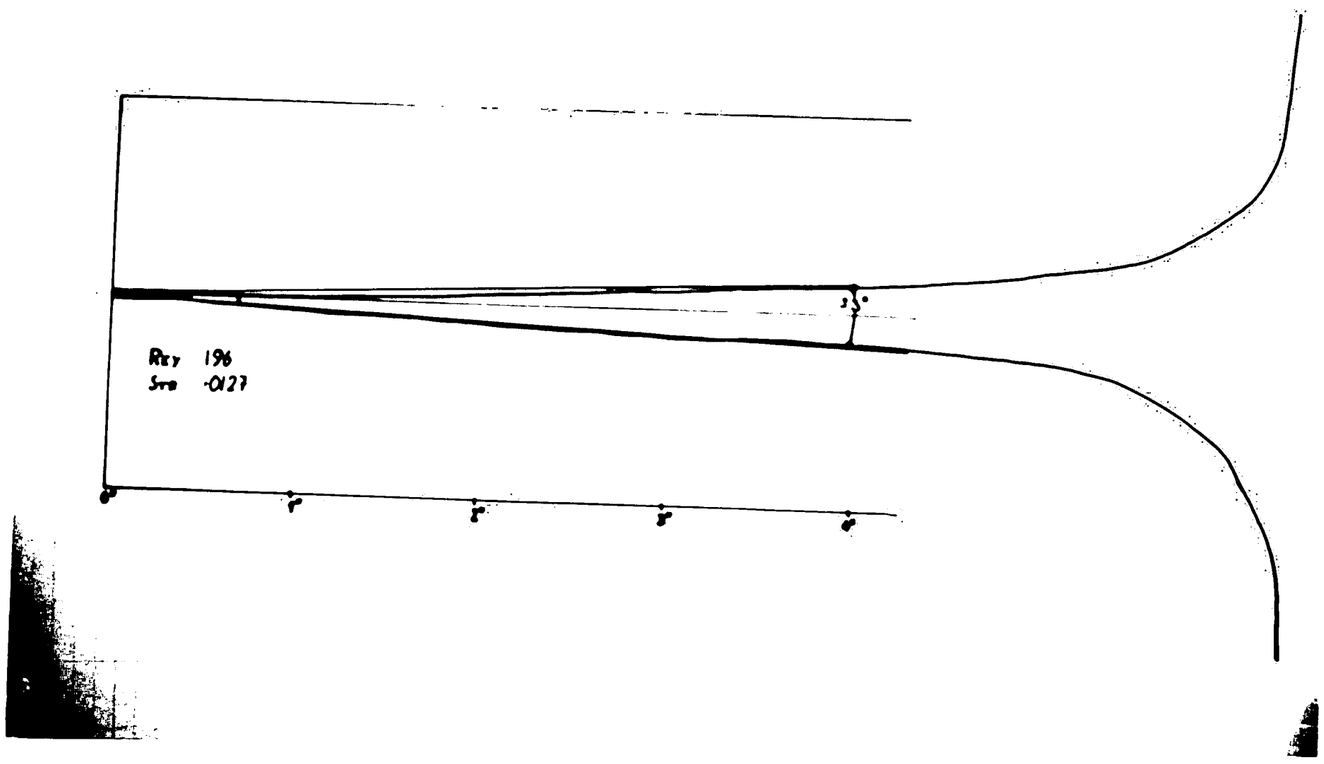

FIG. 30. AMPLITUDE GROWTH

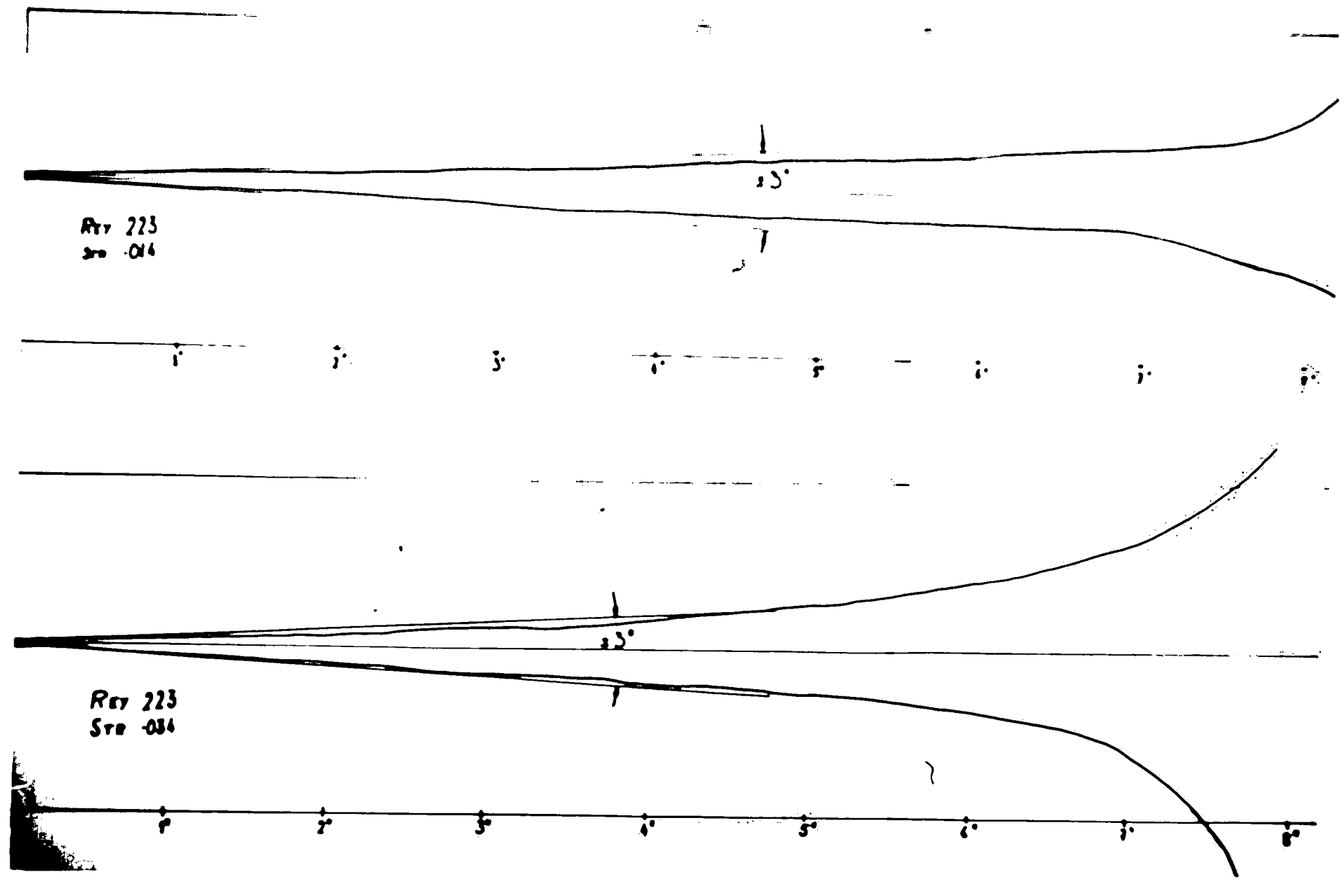

FIG. 31. AMPLITUDE GROWTH

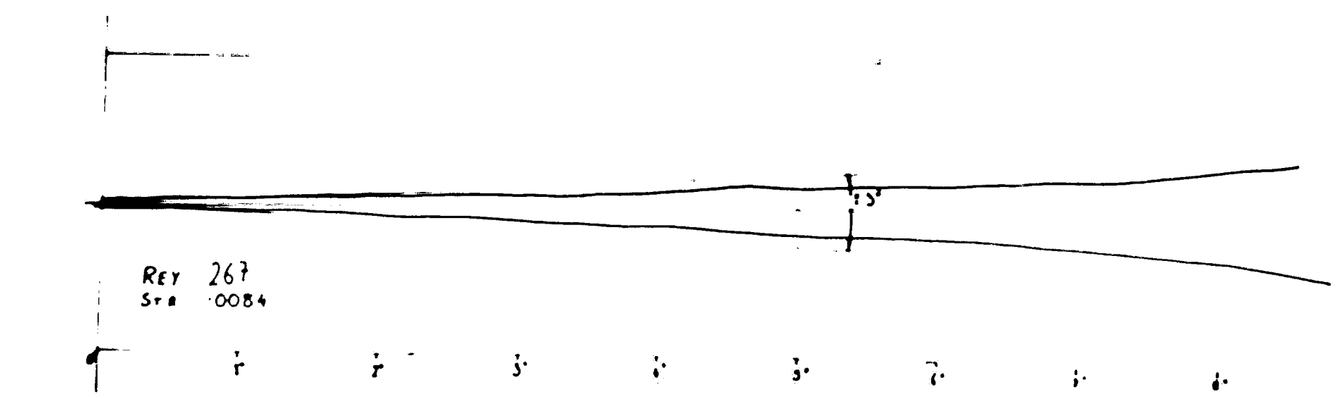

FIG. 32. AMPLITUDE GROWTH

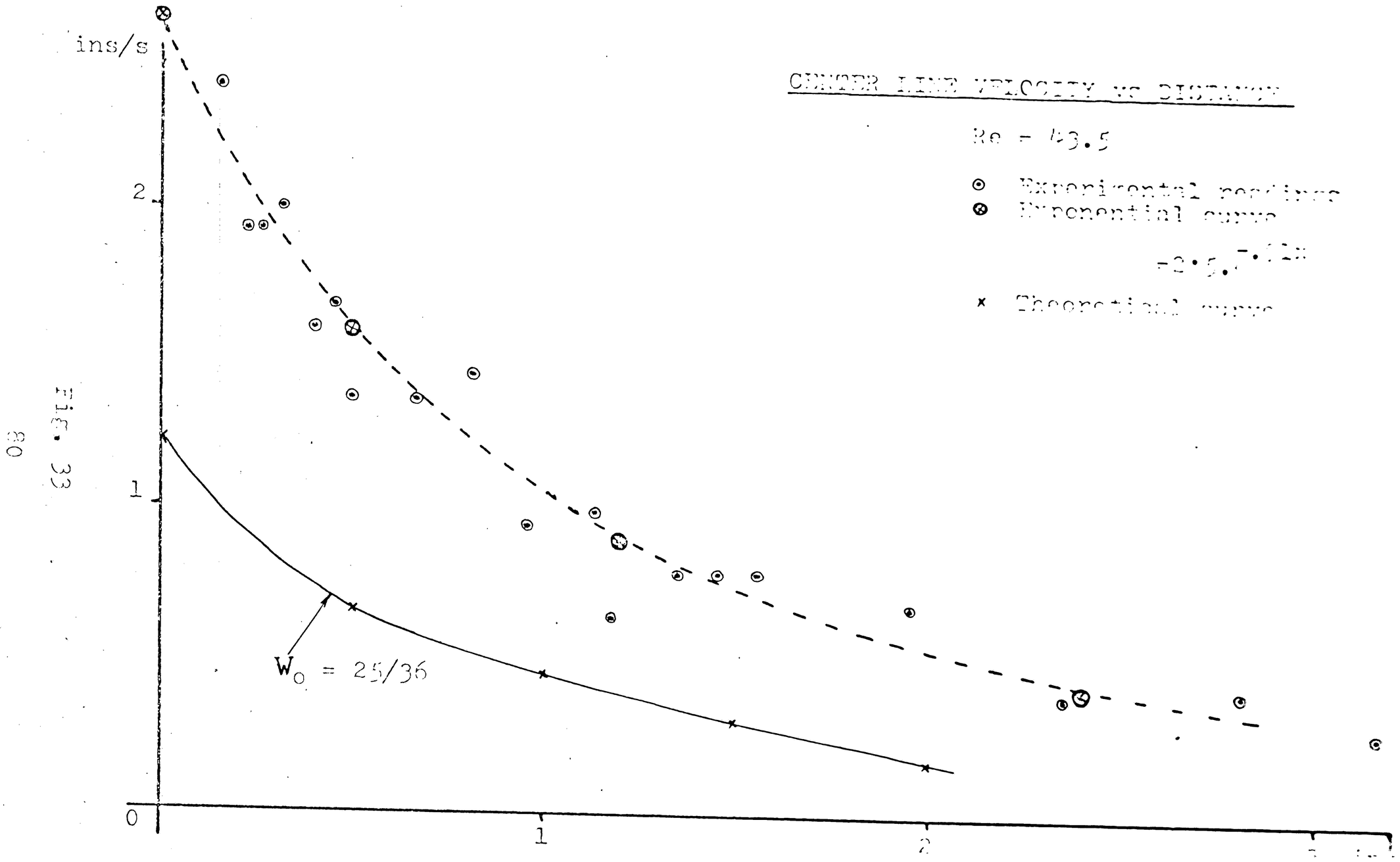

Fig. 33

CENTER LINE VELOCITY VS DISTANCE

Re = 43.5

⊙ Experimental readings
⊗ Exponential curve

$= 2 \cdot 5 \cdot e^{-.12x}$

× Theoretical curve

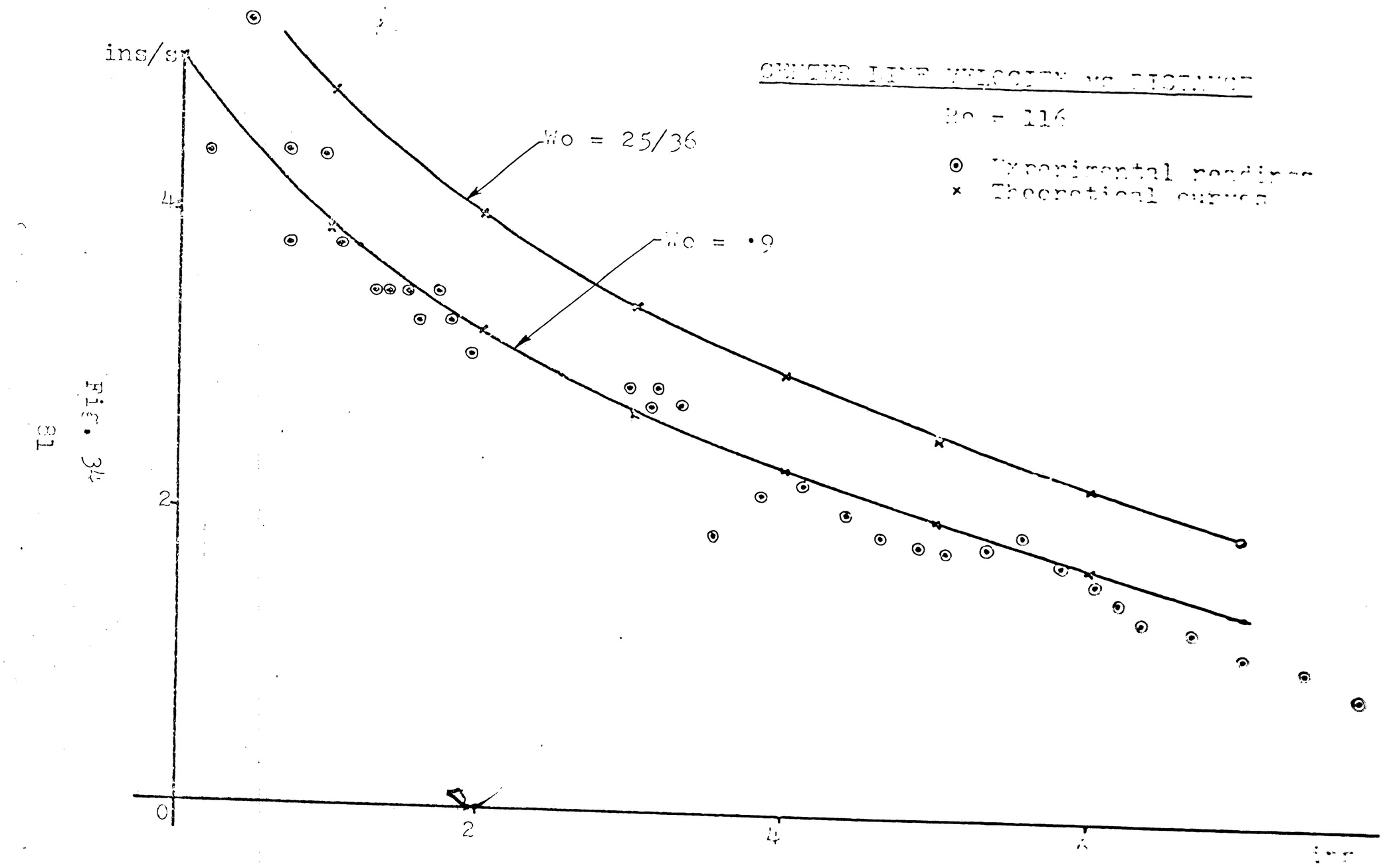

CENTRE LINE VELOCITY vs DISTANCE

Re = 116

⊙ Experimental readings
× Theoretical curves

.31
.81

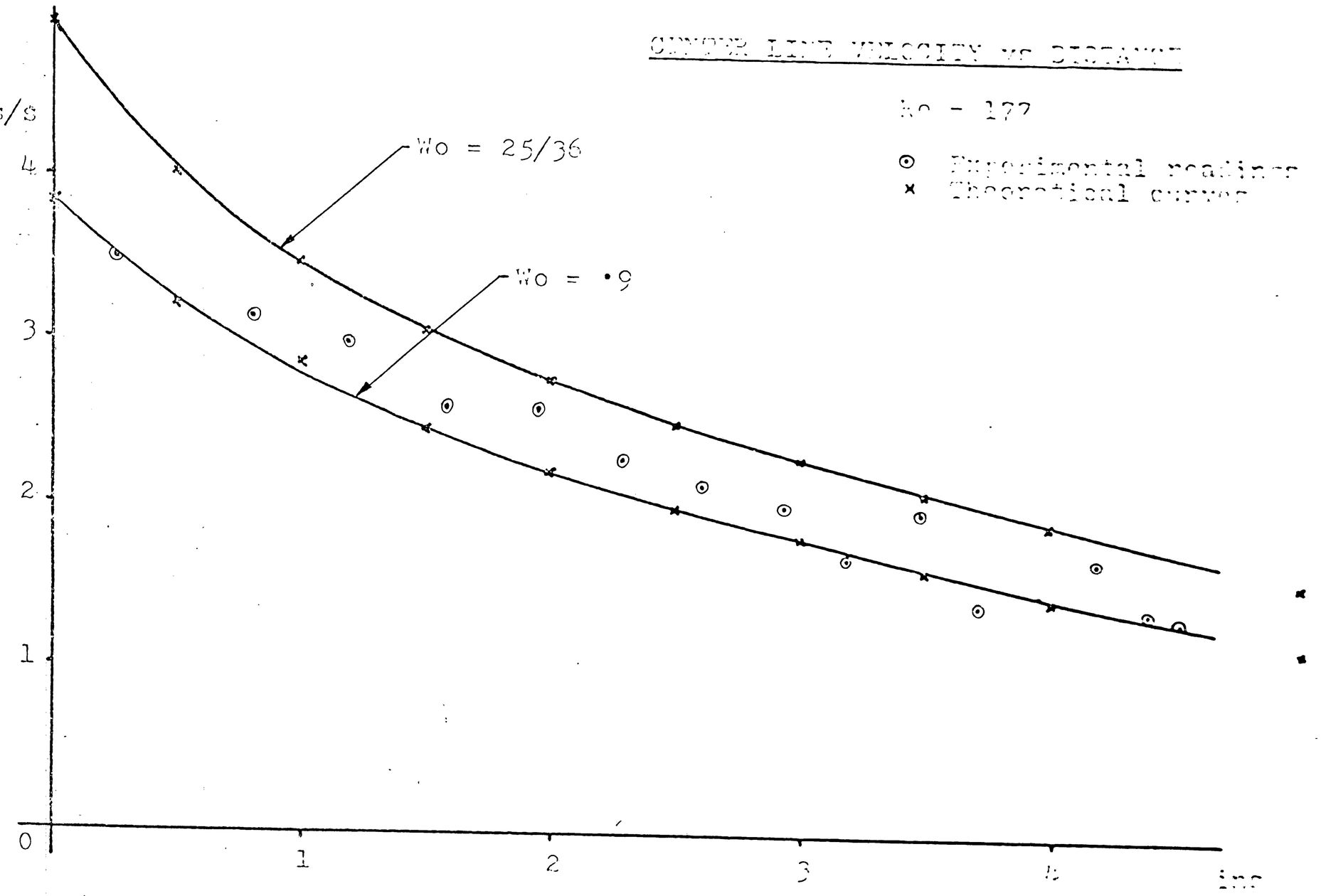
CENTER LINE VELOCITY vs DISTANCE
ho - 177
⊙ Experimental readings
× Theoretical curves
ins/s
4
3
2
1
0
Wo = 25/36
Wo = •9
1
2
3
4
ins

Fig. 35

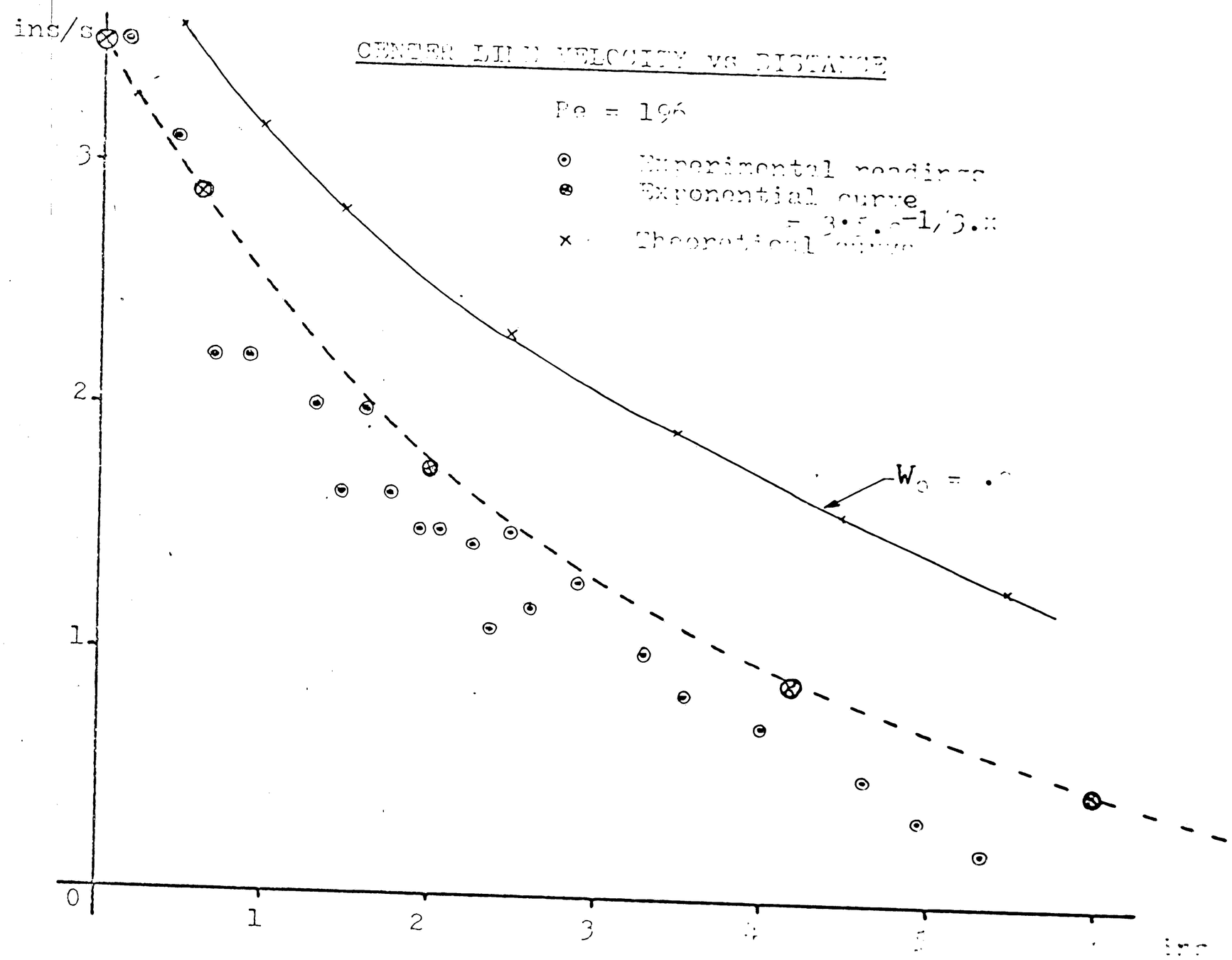
CENTER LINE VELOCITY vs DISTANCE
Re = 196
Experimental readings
Exponential curve
Theoretical values
ins/s
3
2
1
0
1
2
3
W_o = .

Fig. 36

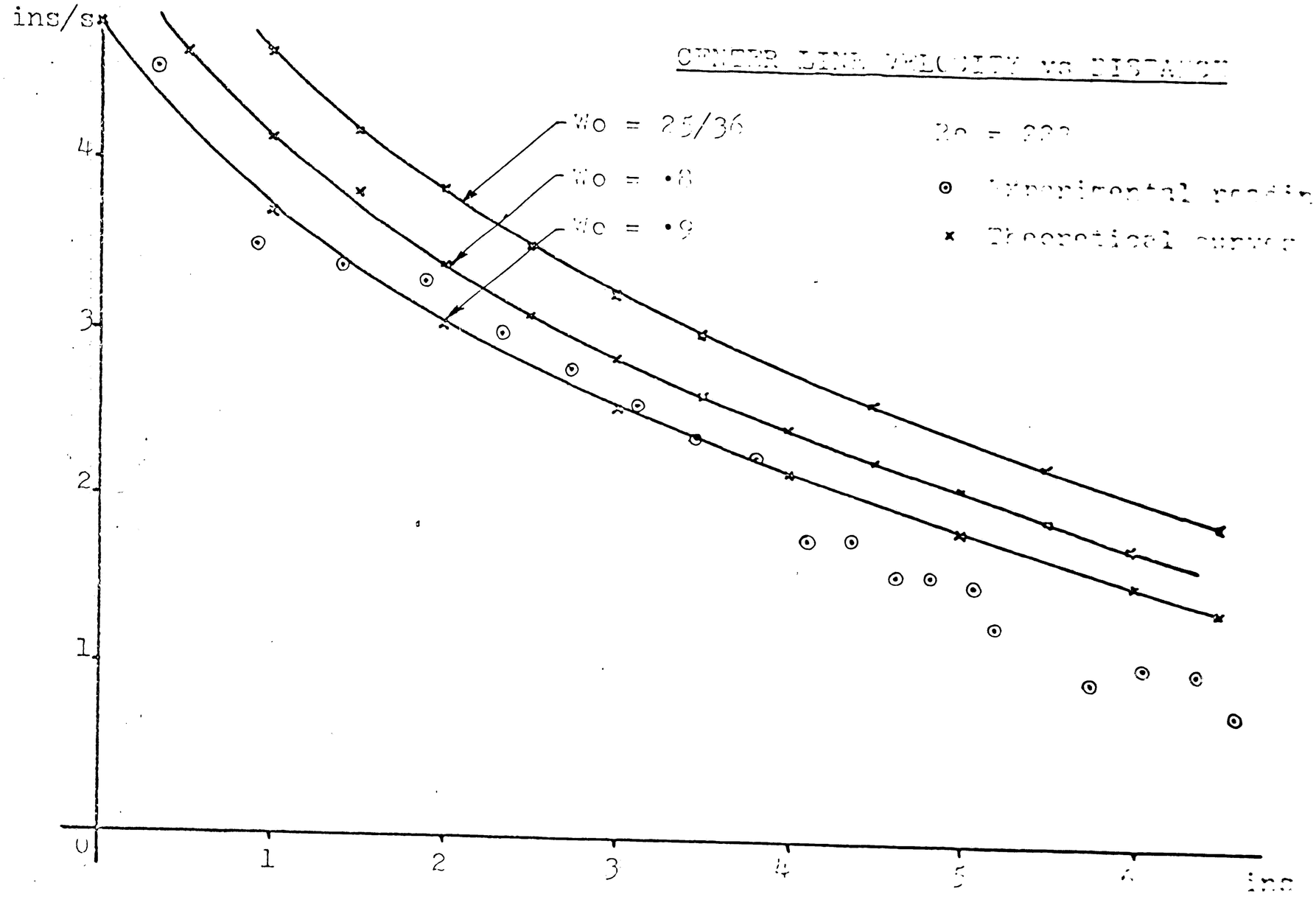
CENTER LINE VELOCITY vs DISTANCE
Wo = 25/36
Wo = •8
Wo = •9
Re = 222
⊙ Experimental readings
× Theoretical curves
ins/s
4
3
2
1
0
1
2
3
4
5
ins

Fig. 37

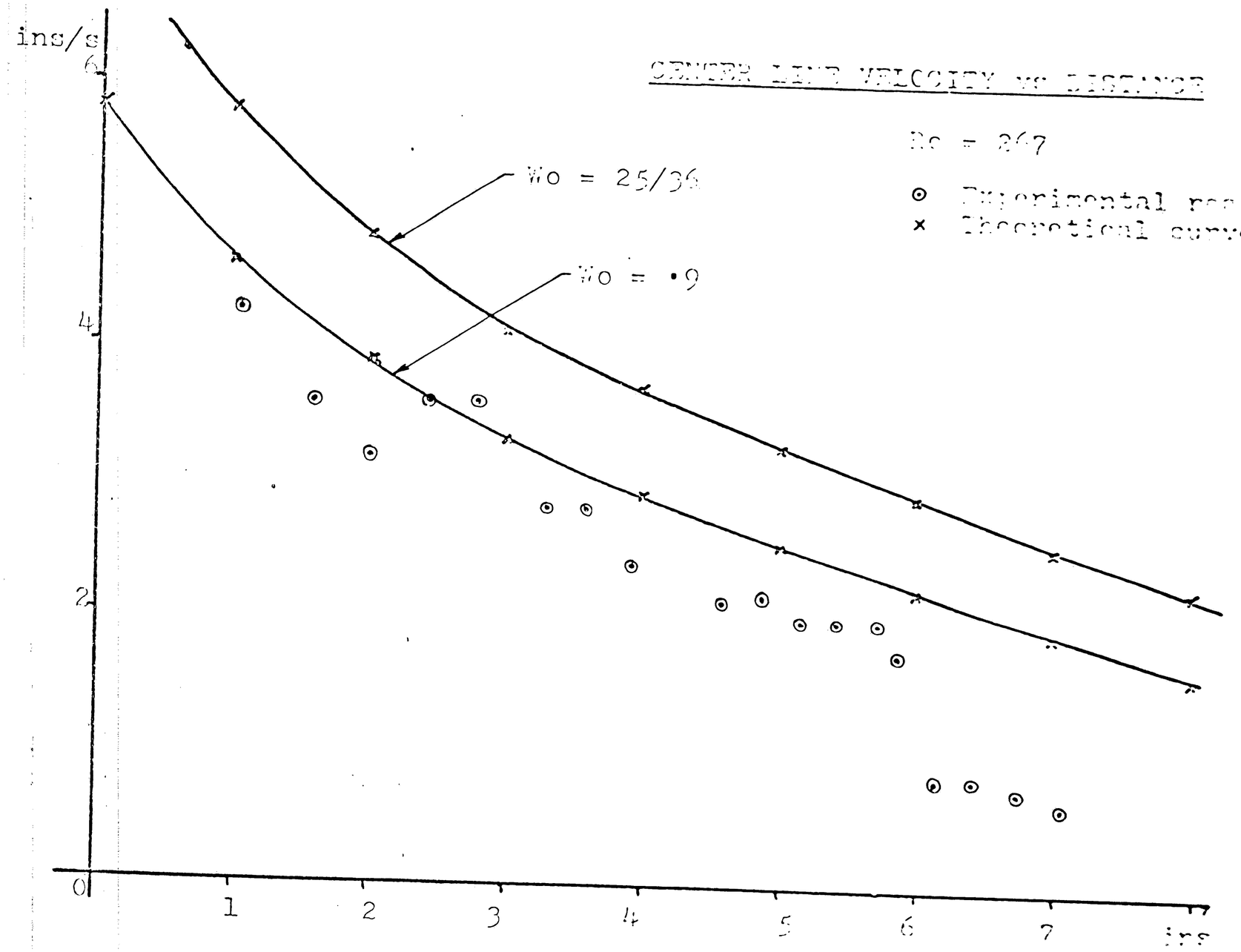
CENTER LINE VELOCITY VS DISTANCE
Re = 267
⊙ Experimental readings
× Theoretical curves
Wo = 25/36
Wo = .9
ins/s
6
4
2
0
1
2
3
4
5
6
7
ins

53

Fig. 3.3.3

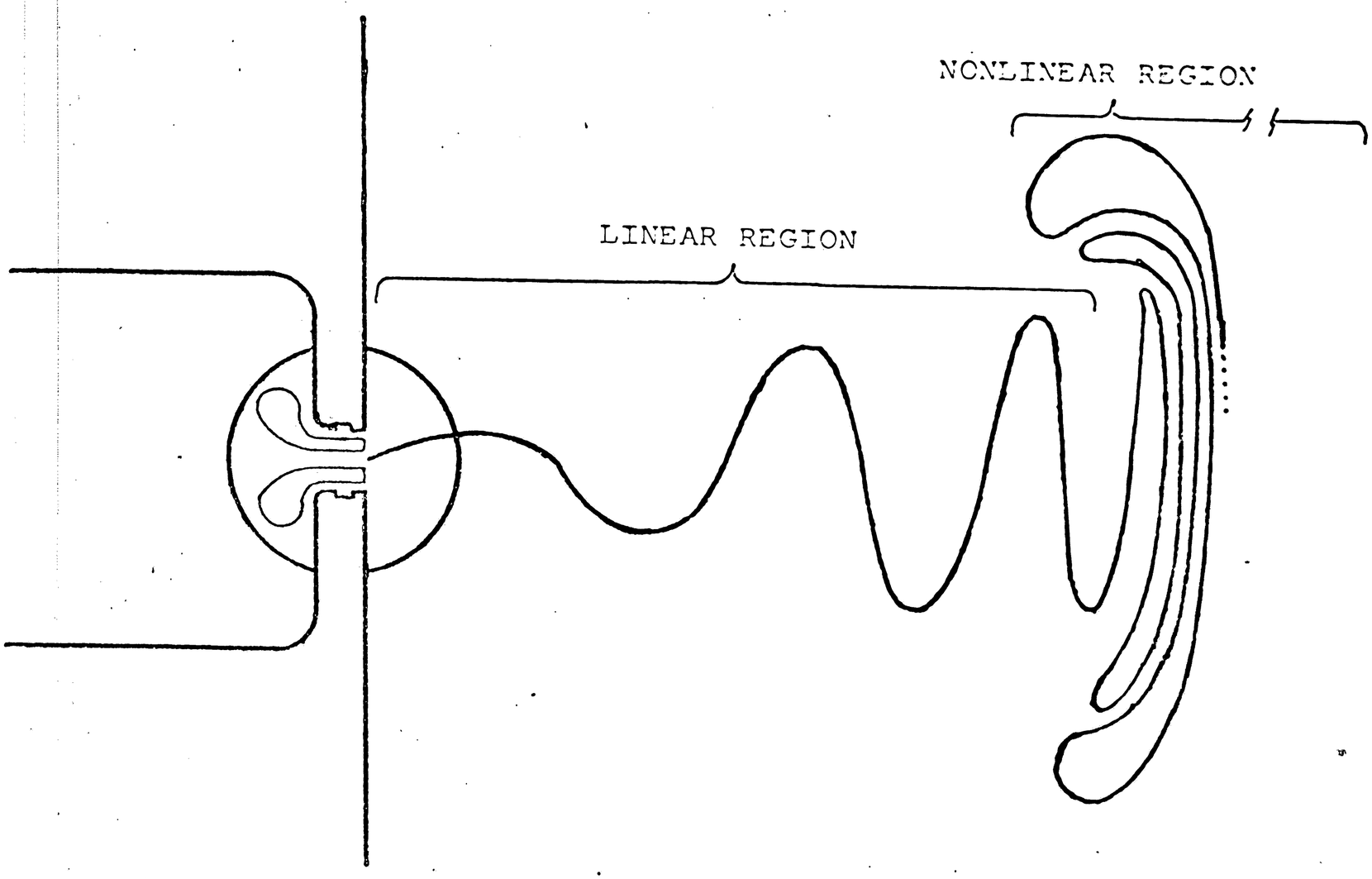

Appearance of Jet

Fig. 39

W = 1/8 ins.

ST	VP/V0	W*B	W*K
1.189559	.7600	9.181047	12.521679
1.133277	.7550	8.905746	12.008233
1.080000	.7500	8.640000	11.520000
1.029535	.7450	8.383363	11.055411
.981704	.7400	8.135418	10.613020
.936343	.7350	7.895775	10.191491
.893300	.7300	7.664067	9.789590
.852434	.7250	7.439949	9.406172
.813616	.7200	7.223097	9.040179
.776725	.7150	7.013204	8.690624
.741648	.7100	6.809983	8.356593
.708281	.7050	6.613160	8.037235
.676529	.7000	6.422478	7.731755
.646299	.6950	6.237695	7.439414
.617509	.6900	6.058578	7.159520
.590078	.6850	5.884910	6.891426
.563935	.6800	5.716483	6.634527
.539009	.6750	5.553101	6.388258
.515237	.6700	5.394576	6.152086
.492558	.6650	5.240730	5.925513
.470916	.6600	5.091394	5.708071
.450257	.6550	4.946408	5.499319
.430531	.6500	4.805616	5.298844
.411692	.6450	4.668873	5.106255
.393695	.6400	4.536040	4.921184
.376498	.6350	4.406982	4.743286
.360063	.6300	4.281572	4.572232
.344353	.6250	4.159688	4.407713
.329332	.6200	4.041214	4.249439
.314967	.6150	3.926038	4.097132
.301228	.6100	3.814053	3.950531
.288085	.6050	3.705156	3.809388
.275510	.6000	3.599250	3.673469
.263477	.5950	3.496240	3.542552
.251961	.5900	3.396037	3.416425
.240939	.5850	3.298552	3.294889
.230387	.5800	3.203704	3.177752
.220285	.5750	3.111411	3.064834
.210612	.5700	3.021597	2.955964
.201350	.5650	2.934188	2.850978
.192480	.5600	2.849113	2.749719
.183985	.5550	2.766303	2.652041
.175849	.5500	2.685692	2.557802
.168055	.5450	2.607216	2.466866
.160590	.5400	2.530815	2.379107
.153438	.5350	2.456429	2.294401
.146587	.5300	2.384002	2.212632
.140023	.5250	2.313478	2.133688
.133735	.5200	2.244804	2.057463
.127711	.5150	2.177930	1.983854
.121939	.5100	2.112805	1.912765
.116409	.5050	2.049383	1.844103
.111111	.5000	1.987616	1.777778
.106035	.4950	1.927461	1.713705
.101173	.4900	1.868874	1.651802
.096515	.4850	1.811814	1.591992
.092052	.4800	1.756240	1.534200
.087777	.4750	1.702114	1.478353
.083683	.4700	1.649397	1.424384
.079761	.4650	1.598053	1.372225
.076004	.4600	1.548047	1.321814
.072407	.4550	1.499345	1.273091
.068962	.4500	1.451912	1.225996
.065664	.4450	1.405718	1.180473
.062506	.4400	1.360730	1.136470
.059483	.4350	1.316920	1.093935
.056589	.4300	1.274256	1.052817
.053819	.4250	1.232711	1.013069
.051169	.4200	1.192258	.974645
.048633	.4150	1.152869	.937501
.046207	.4100	1.114519	.901595
.043886	.4050	1.077181	.866885
.041667	.4000	1.040833	.833333
.039544	.3950	1.005450	.800901
.037516	.3900	.971008	.769551
.035576	.3850	.937486	.739250
.033723	.3800	.904861	.709963
.031953	.3750	.873113	.681657
.030261	.3700	.842221	.654301
.028646	.3650	.812164	.627865
.027104	.3600	.782923	.602320
.025633	.3550	.754480	.577637
.024228	.3500	.726816	.553790
.022889	.3450	.699913	.530751
.021611	.3400	.673753	.508496
.020393	.3350	.648319	.487001
.019232	.3300	.623596	.466241
.018127	.3250	.599566	.446194
.017073	.3200	.576215	.426837
.016071	.3150	.553526	.408151
.015117	.3100	.531486	.390113
.014209	.3050	.510079	.372705
.013347	.3000	.489291	.355907
.012526	.2950	.469110	.339700
.011747	.2900	.449520	.324067
.011008	.2850	.430510	.308991
.010306	.2800	.412067	.294453
.009640	.2750	.394177	.280439
.009009	.2700	.376830	.266933
.008411	.2650	.360013	.253919
.007845	.2600	.343714	.241383
.007309	.2550	.327923	.229310
.006803	.2500	.312629	.217687
.006324	.2450	.297821	.206500
.005872	.2400	.283488	.195737
.005446	.2350	.269621	.185385
.005044	.2300	.256209	.175432
.004665	.2250	.243242	.165866
.004309	.2200	.230712	.156675
.003973	.2150	.218609	.147850
.003659	.2100	.206924	.139378
.003363	.2050	.195648	.131251
.003086	.2000	.184773	.123457
.002827	.1950	.174290	.115987
.002585	.1900	.164192	.108832
.002358	.1850	.154469	.101982
.002147	.1800	.145114	.095429
.001950	.1750	.136120	.089163
.001768	.1700	.127479	.083178
.001598	.1650	.119184	.077464
.001440	.1600	.111228	.072014
.001295	.1550	.103603	.066820
.001160	.1500	.096303	.061874
.001036	.1450	.089322	.057171
.000922	.1400	.082652	.052701
.000818	.1350	.076288	.048460

FIG. 40. EXPONENTIAL THEORY PHASE VELOCITIES

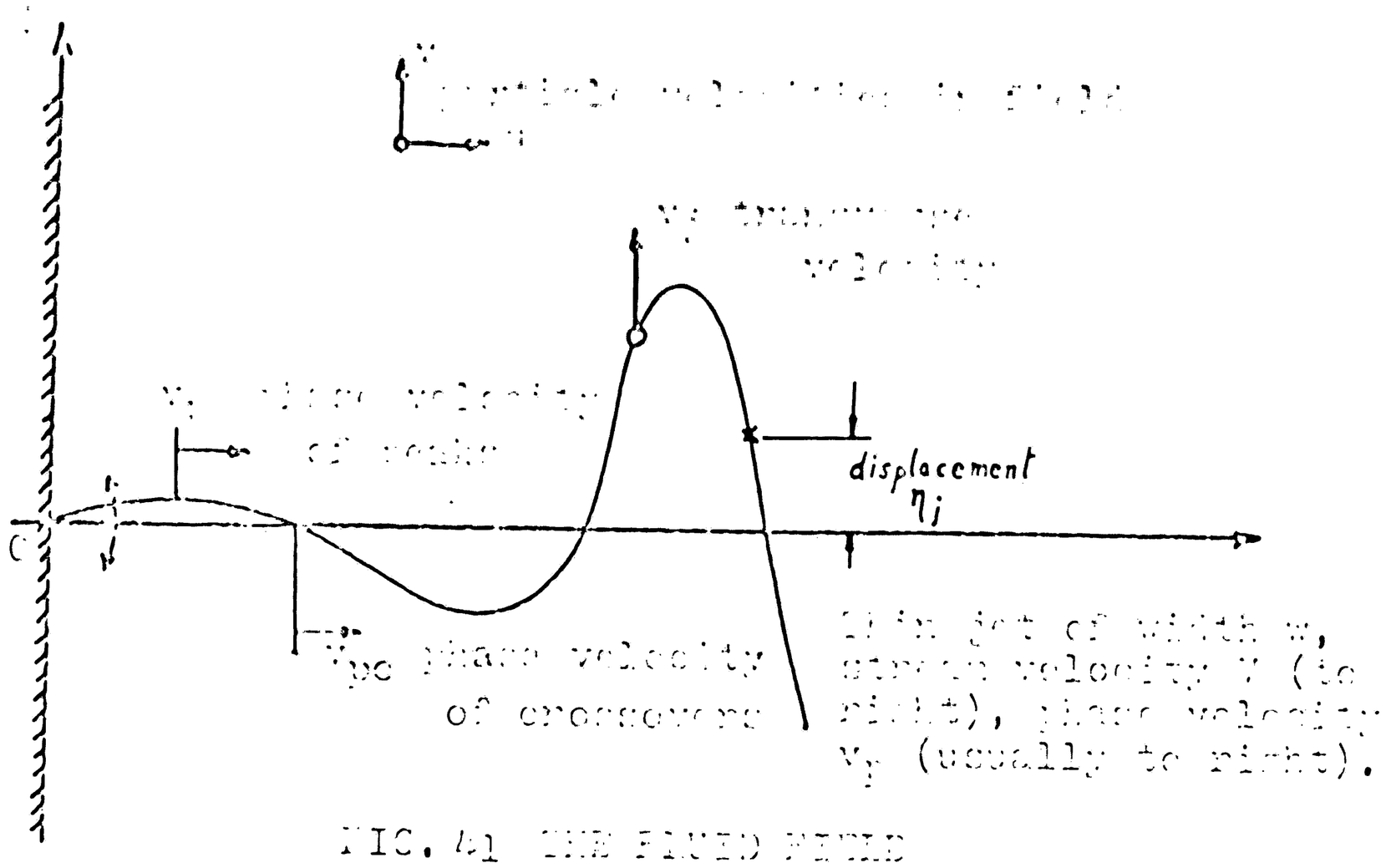

FIG. 41 THE FLUID FIELD

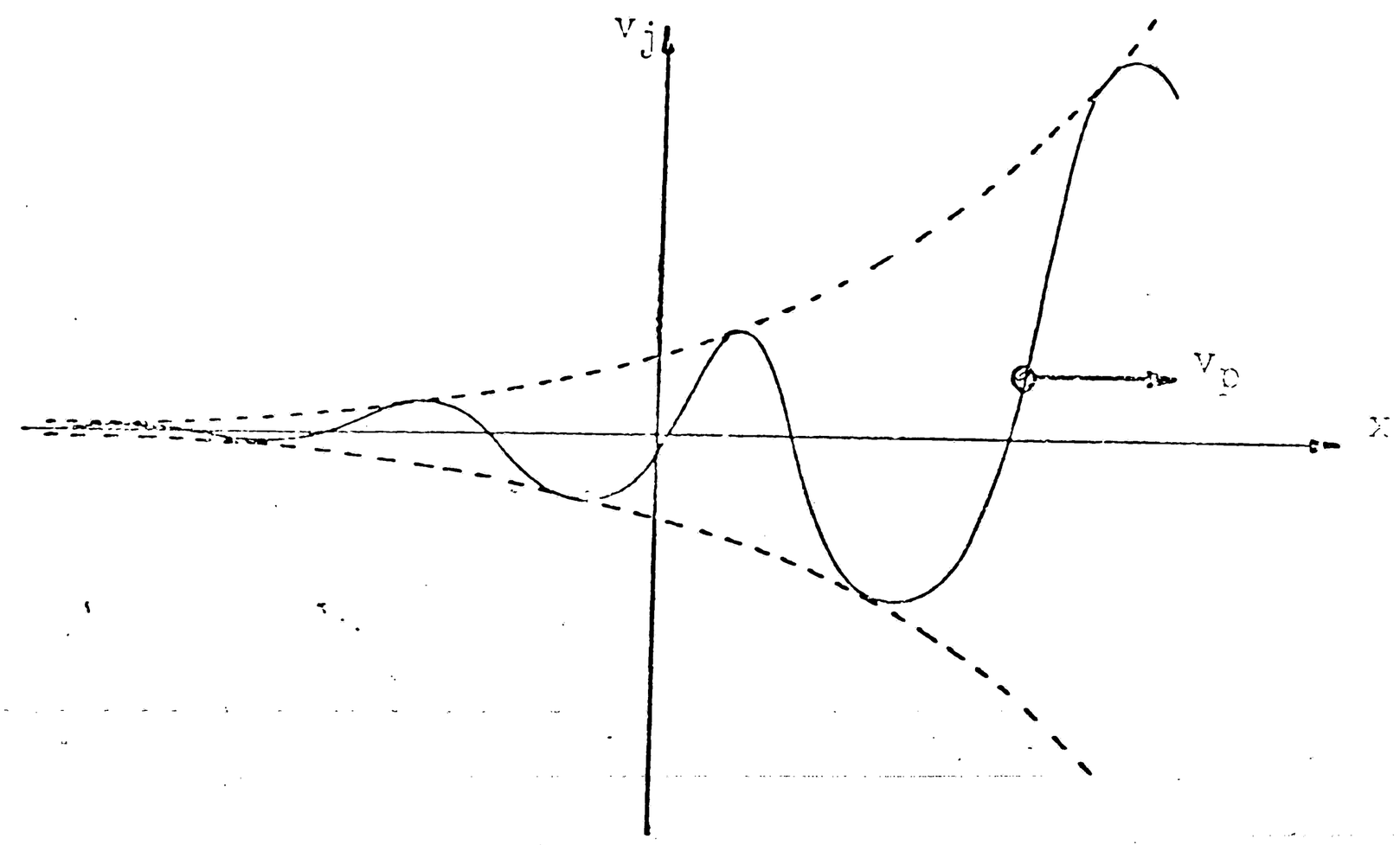

$$\phi = \phi_o \cdot e^{(bx-ky)} \; e^{j(wt-kx-by)}$$

FIG. 42 RIGHT WAVE

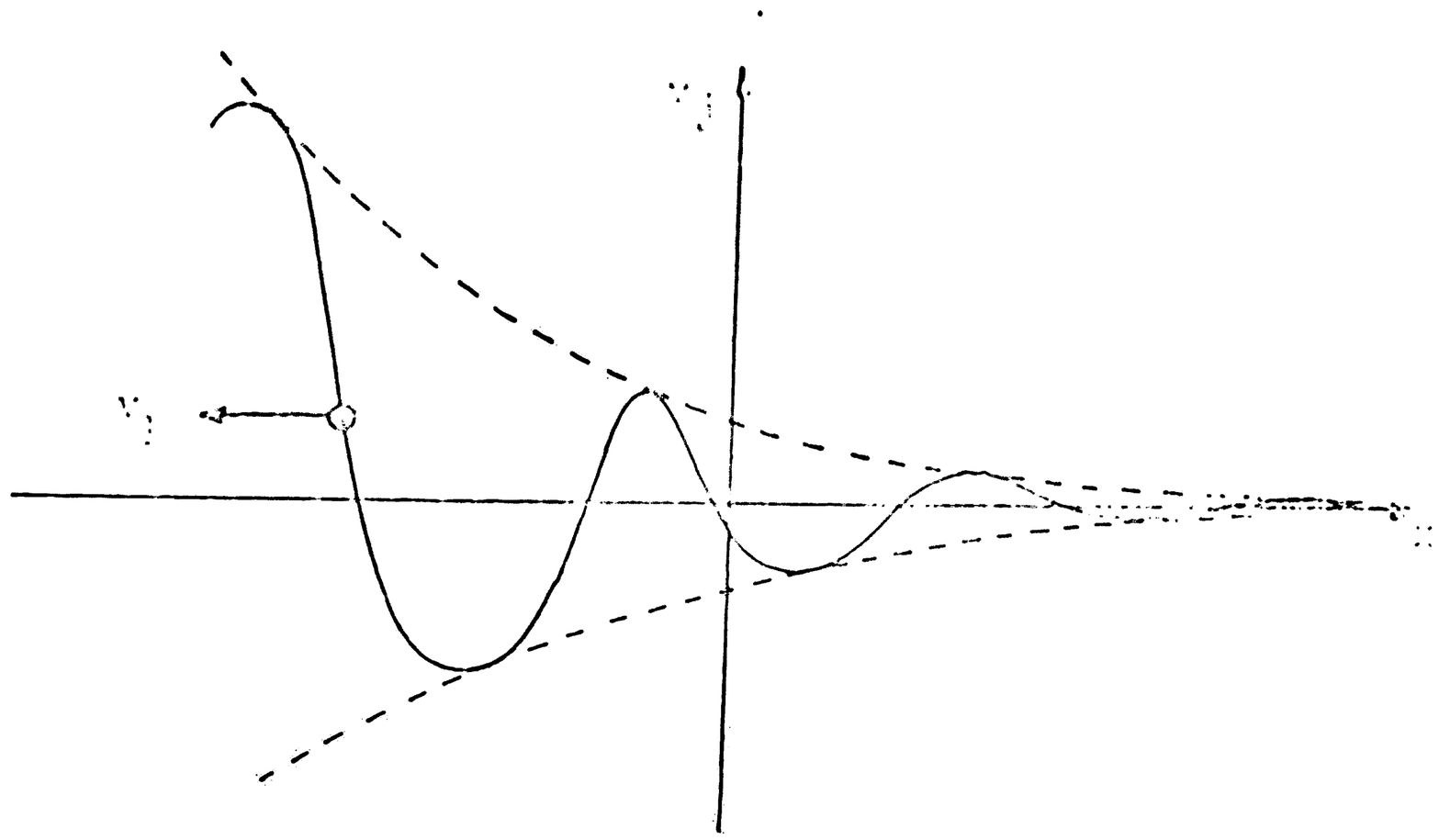

$$\phi = \phi_{0} e^{(-kx-ky)} \cdot j(\omega t+kx-ky)$$

FIG. 43 LEFT WAVE

$$U_{right\ wave} = U_{left\ wave}$$

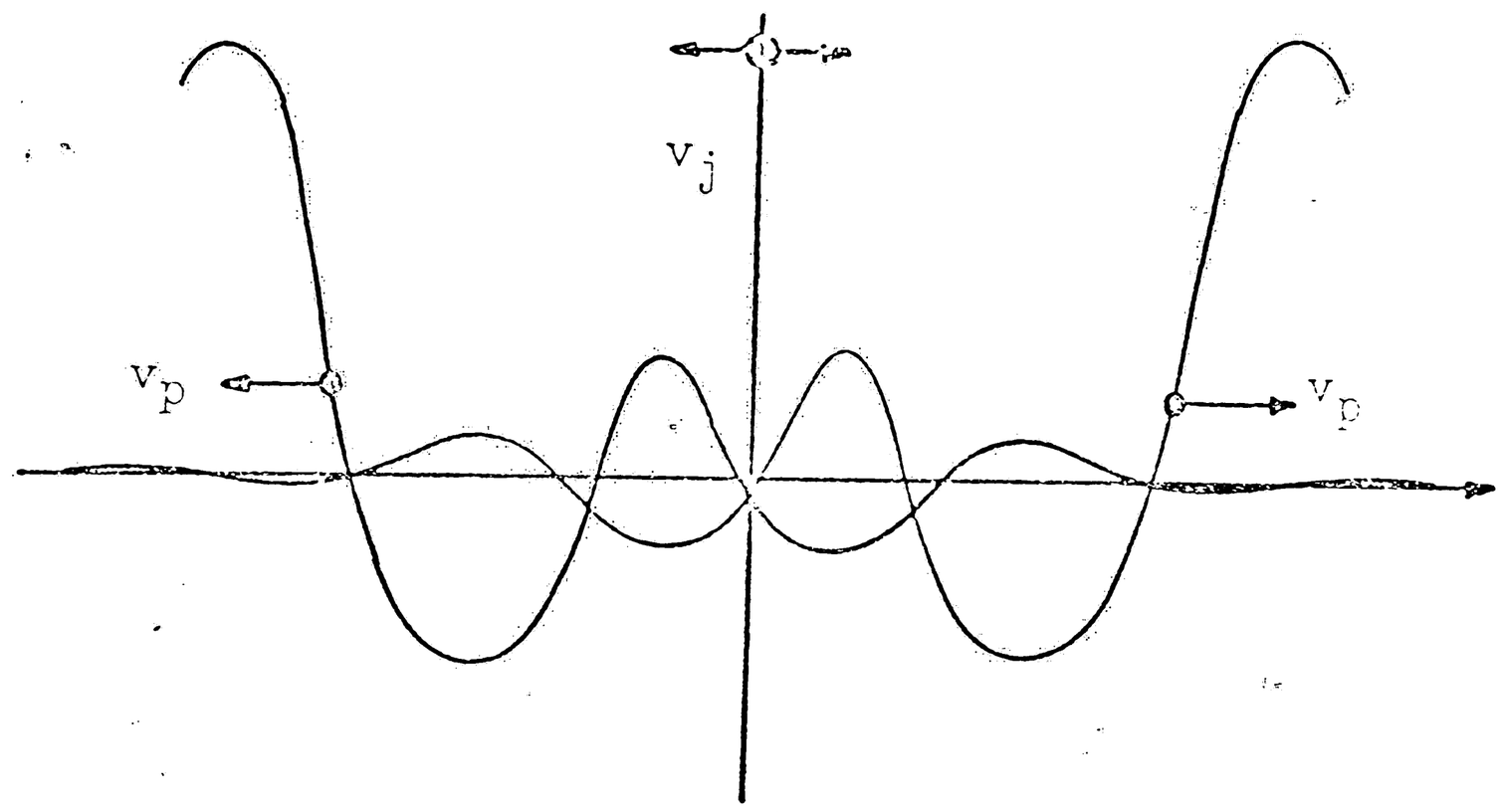

FIG. 44 SUPERIMPOSED
LEFT AND RIGHT WAVE

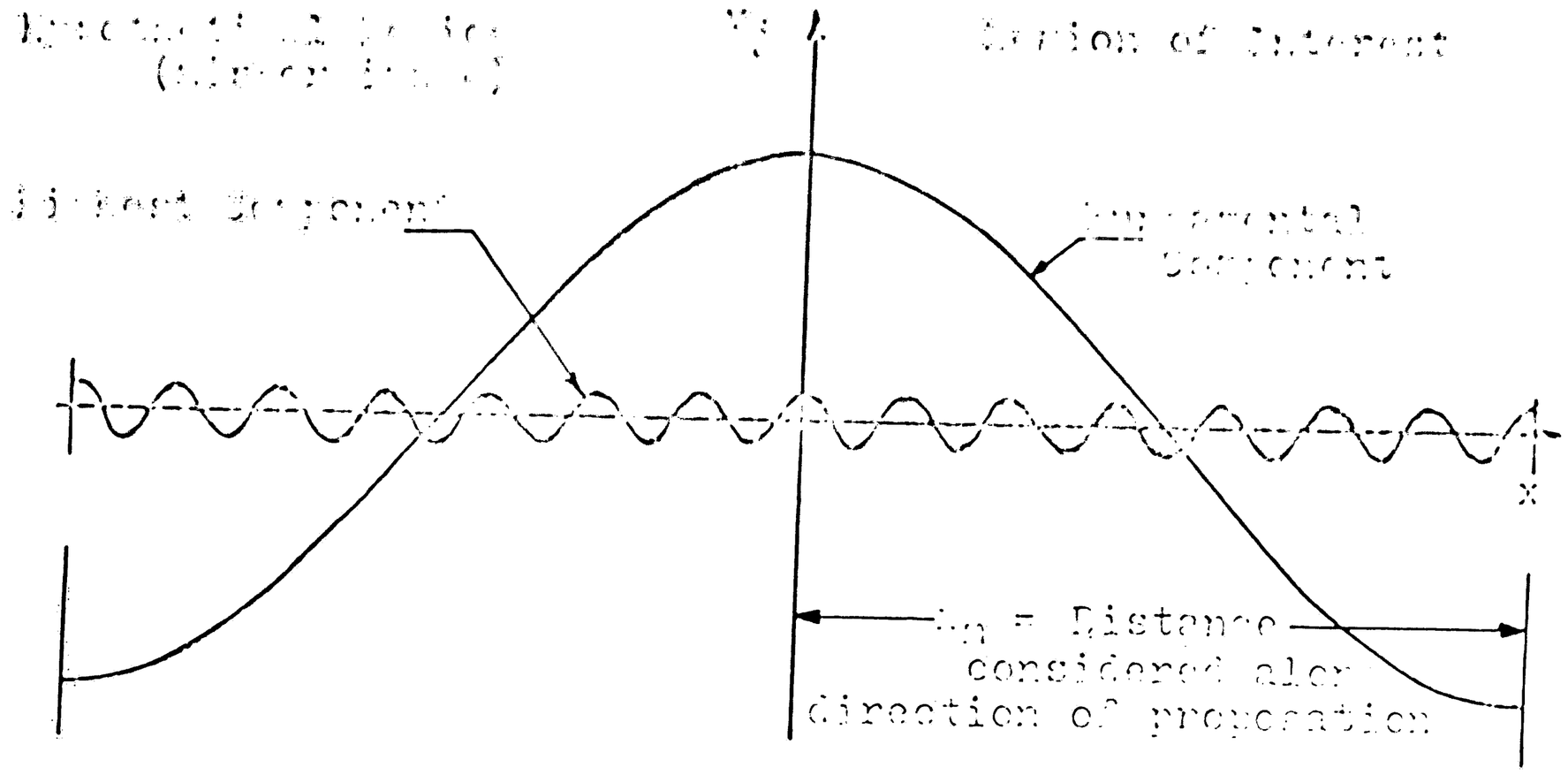

FIG. 45 FOURIER COMPONENTS

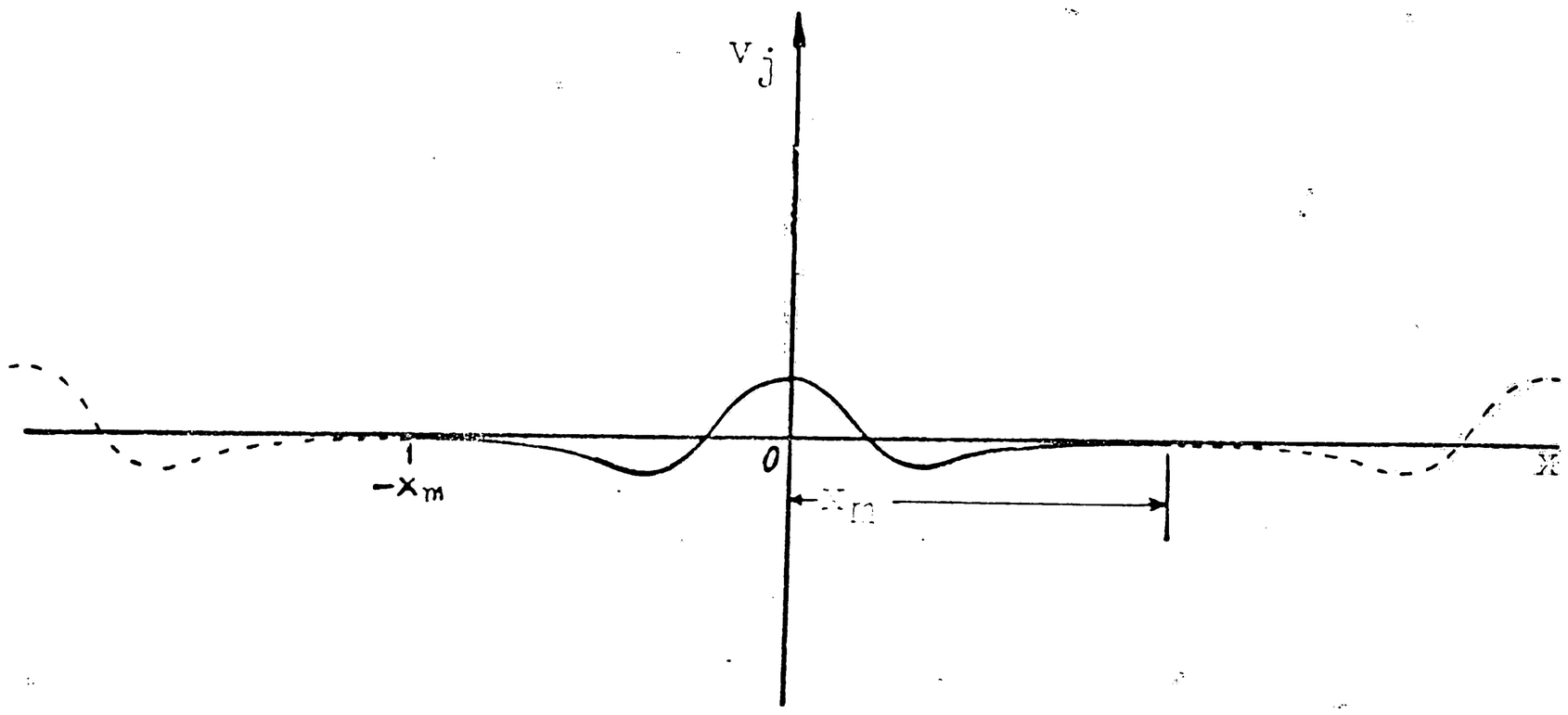

FIG. 46 THE FOURIER WAVE

TRANSVERSE VELOCITIES AT INSTANT 0 SECS.
(Inviscid Theory)

$\delta t = 0.0150$

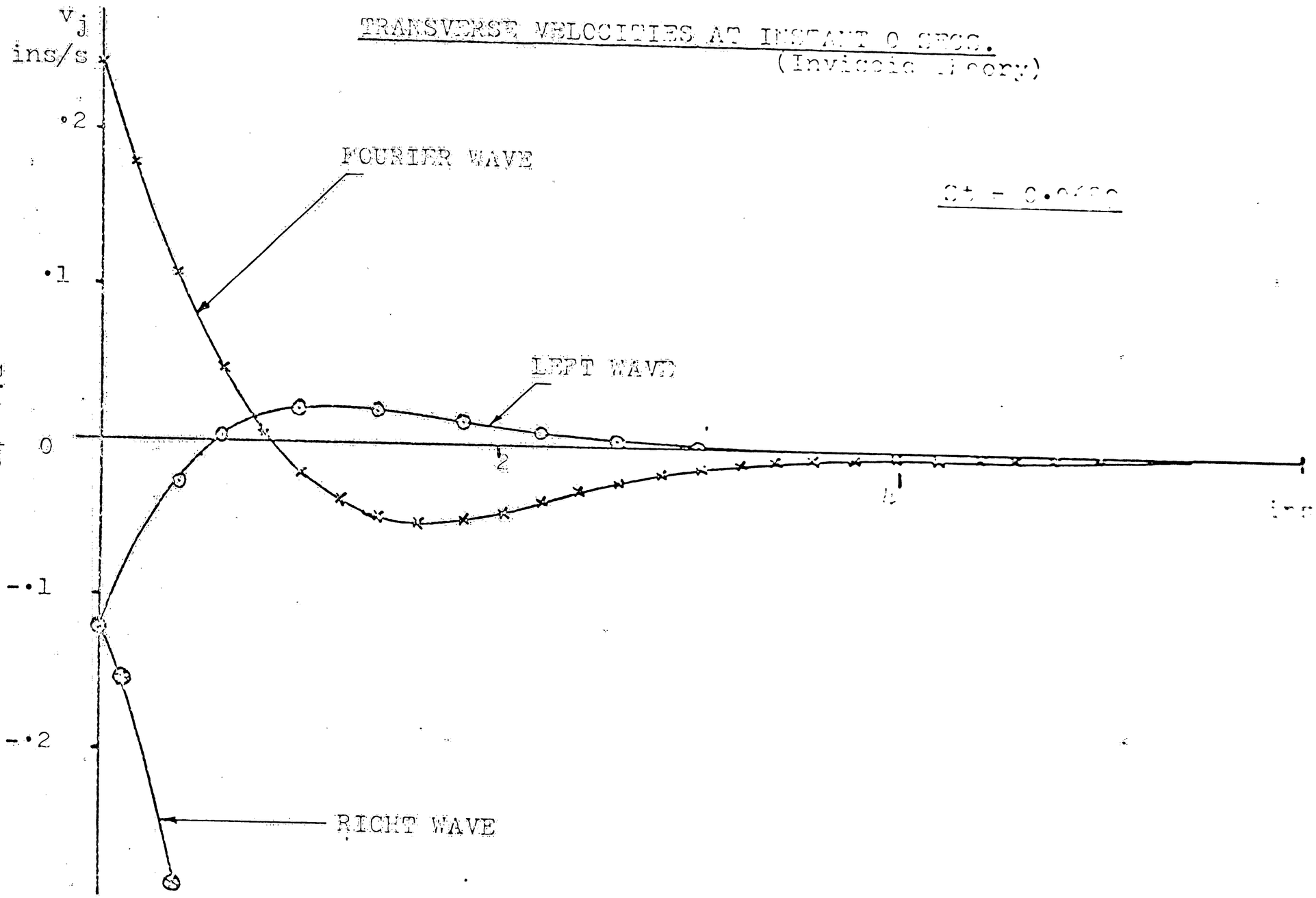

Fig. 47

91

TRANSVERSE VELOCITIES NEAR ORIGIN
(Inviscid theory)

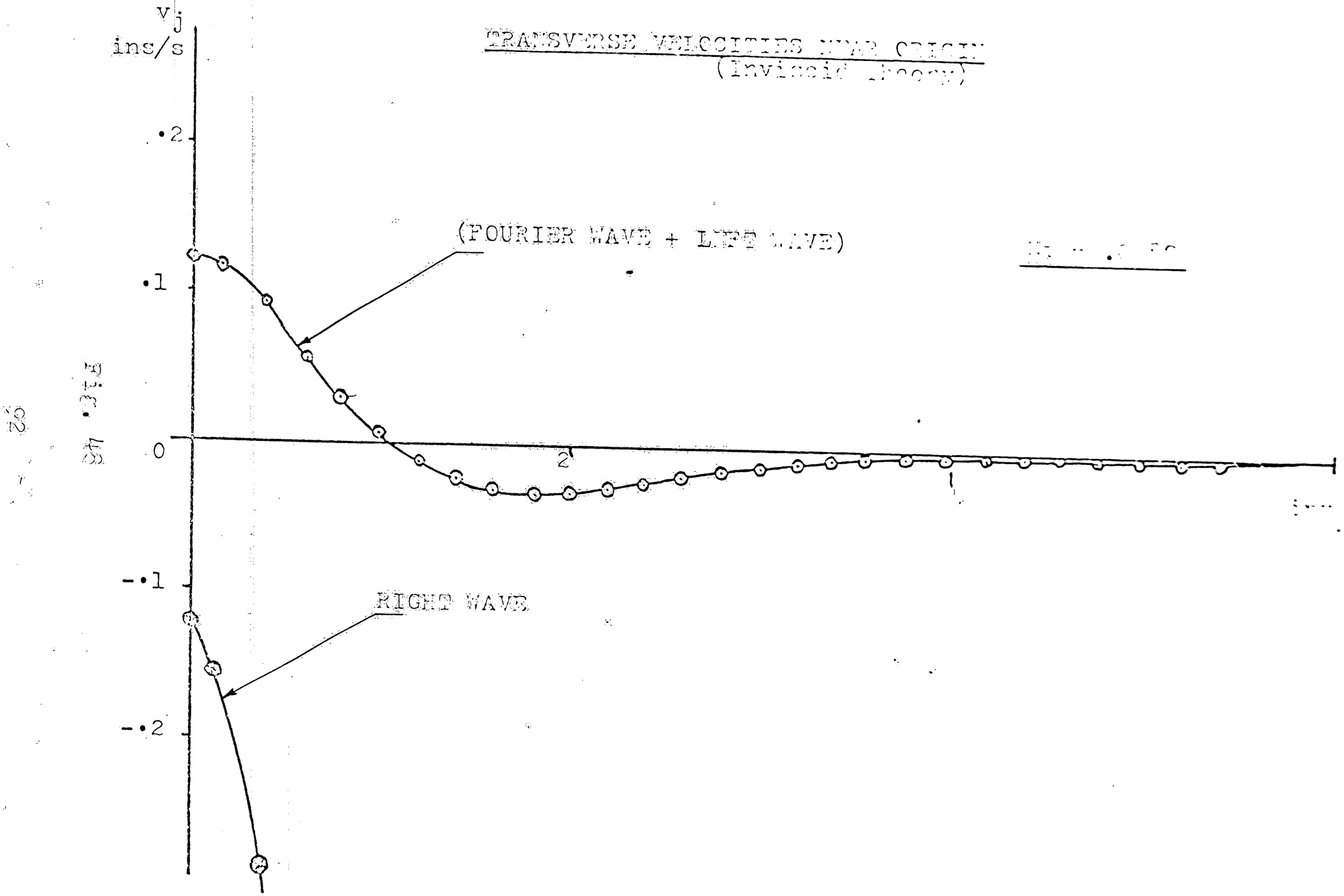

TRANSVERSE VELOCITIES AT INSTANT 1/4 TIME PERIOD.
(Inviscid Theory)

St = .0689

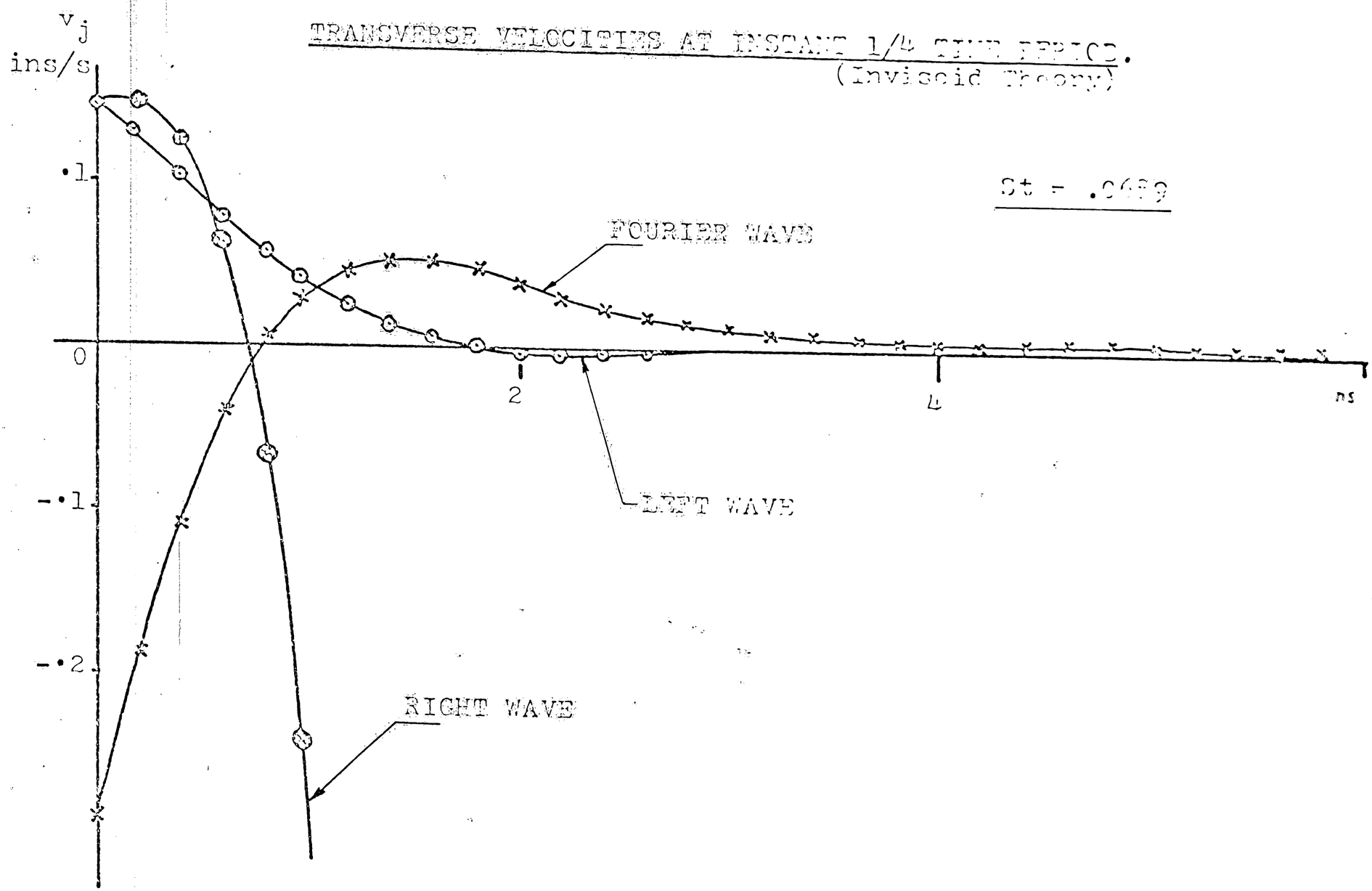

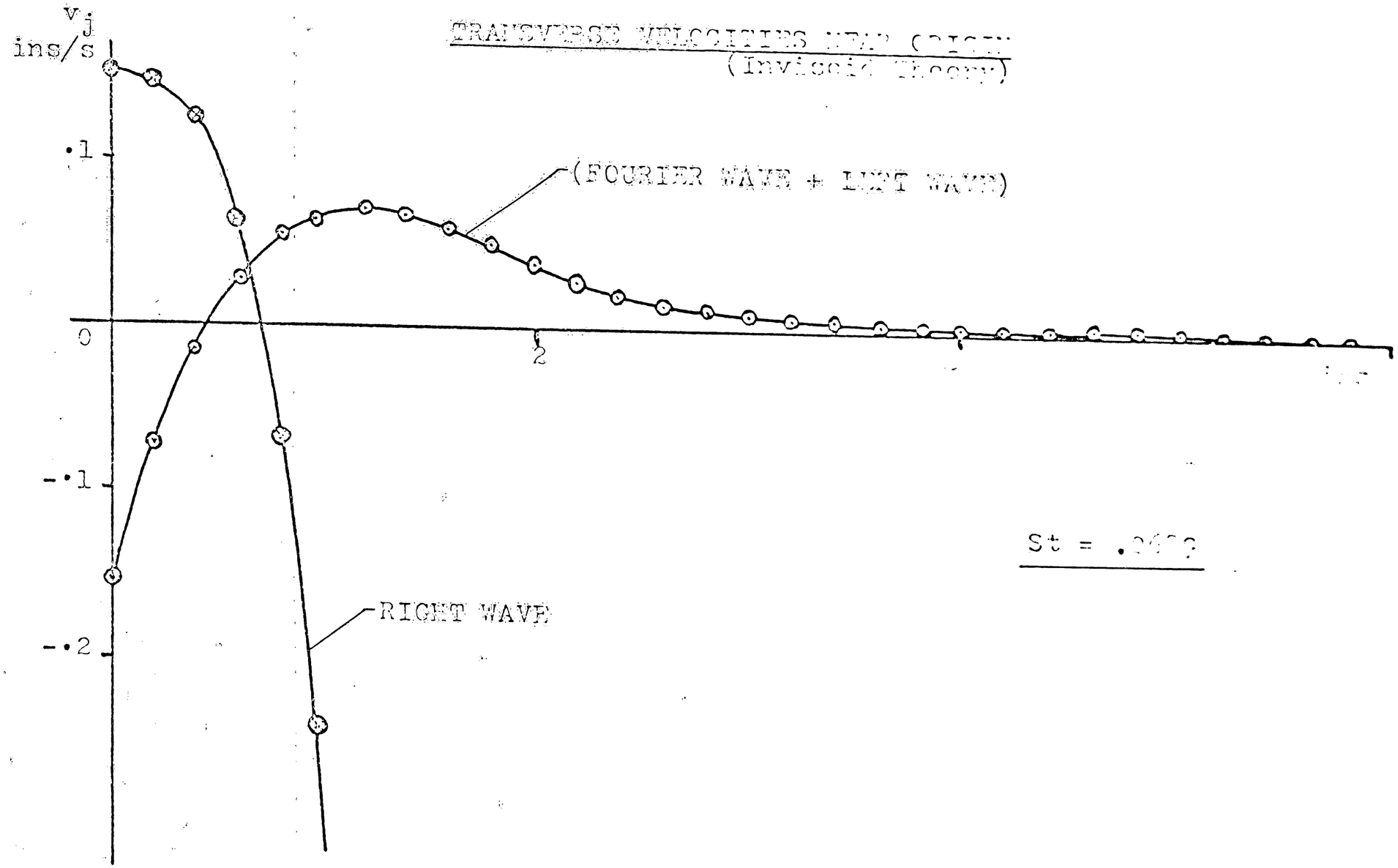

TRANSVERSE VELOCITIES HELD (RIGHT
(Inviscid Theory)

St = .2[illegible]?

45 .315

FIG. 51. LOCAL WAVE

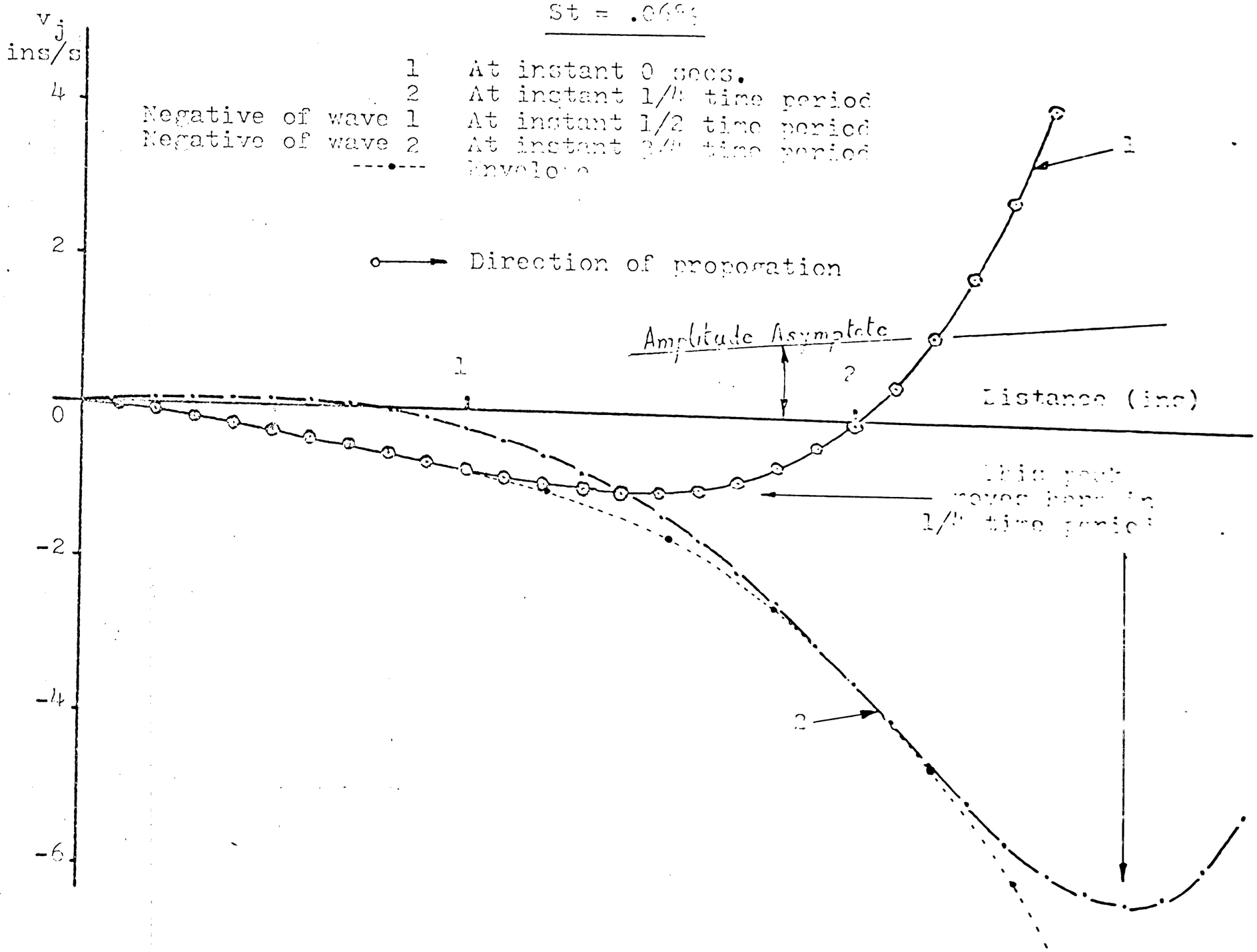

St = 0.9?1?

1 wave at initial time

2 wave at 1/4 time period

negative of 1 wave at 1/2 time period

negative of 2 wave at 3/4 time period

⊗ Fourier wave < 2% of origin magnitude

---•---- Envelope

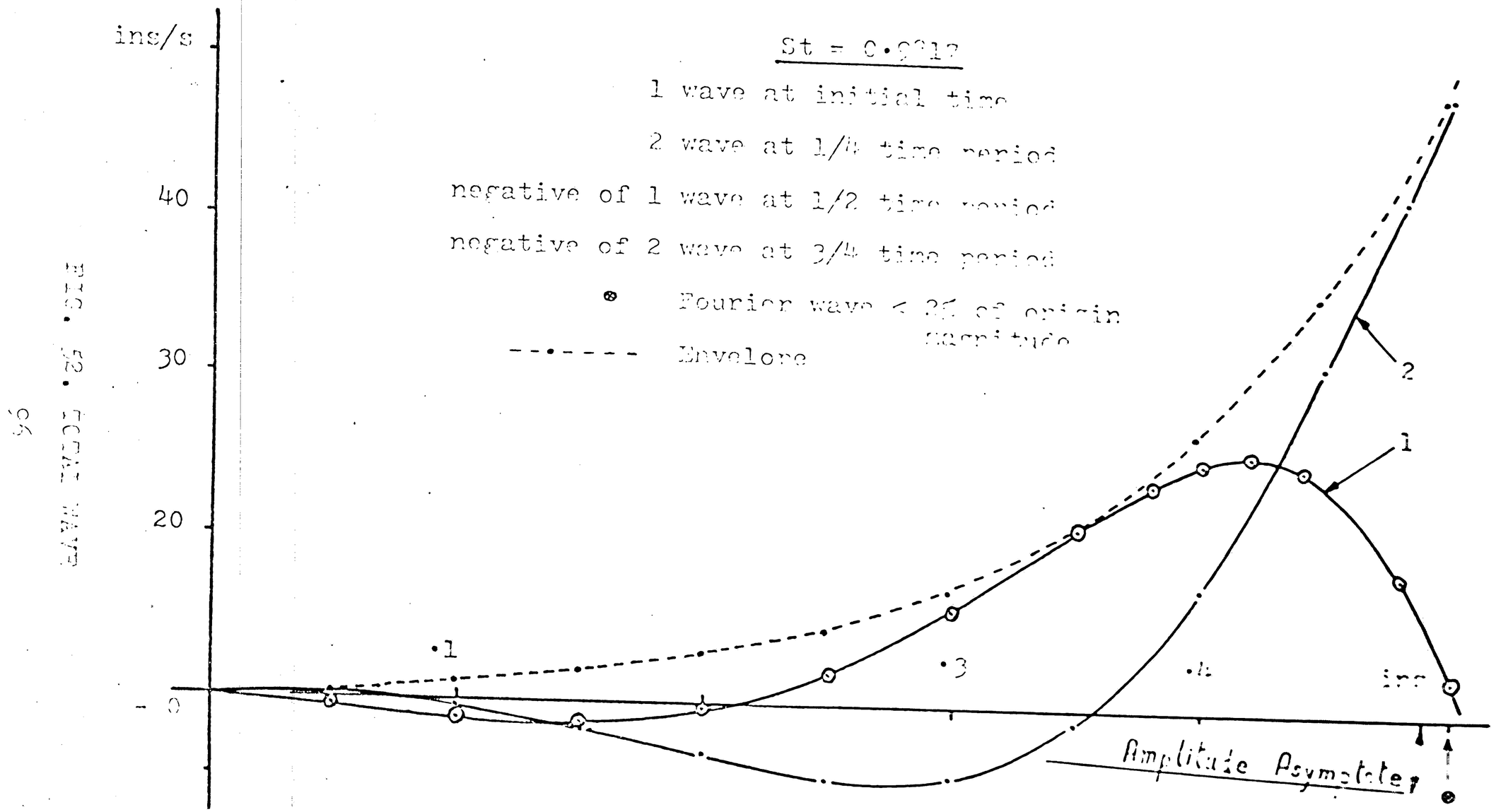

⟶ Direction of propagation

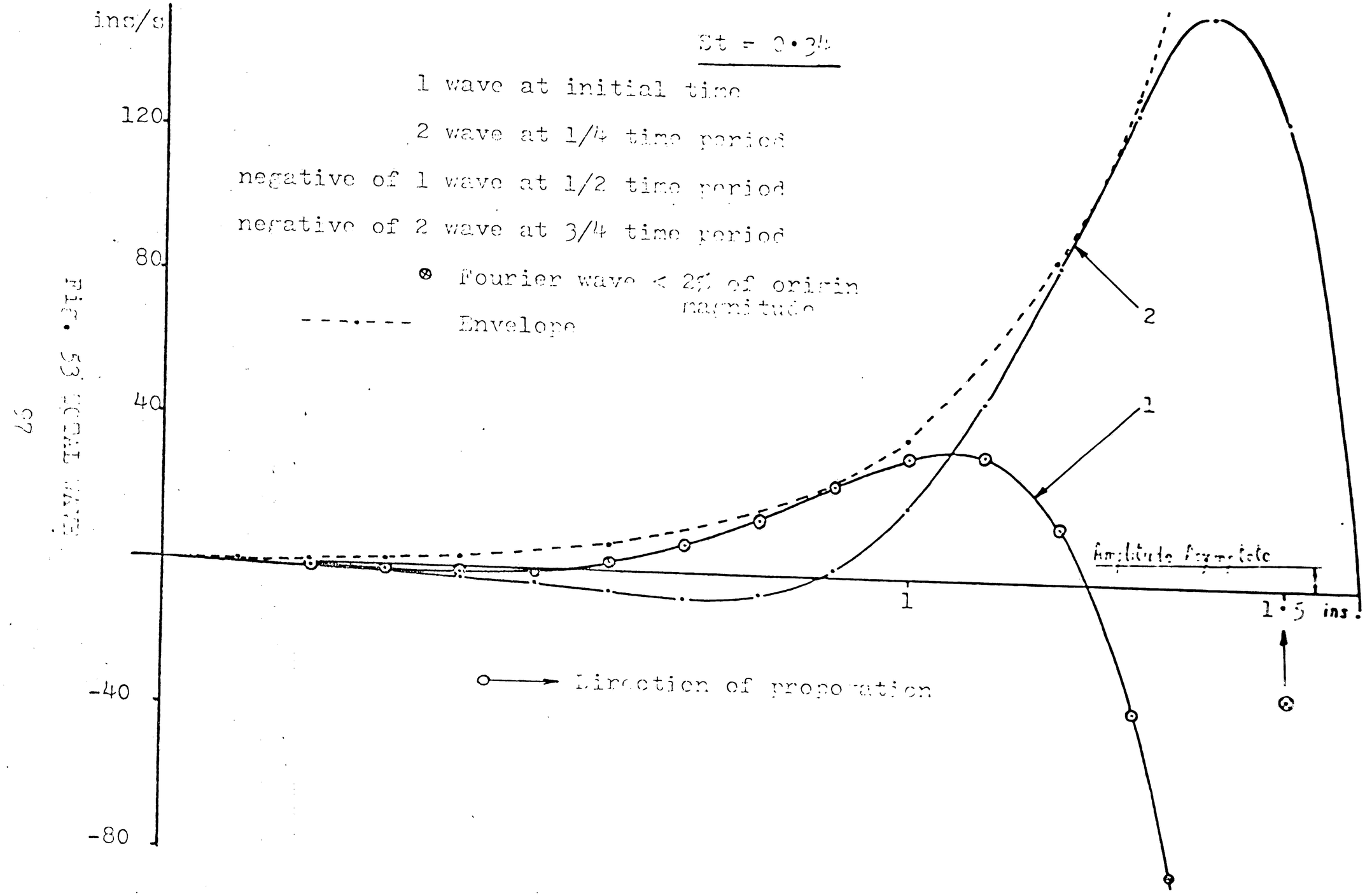

FIG. 3.3 (3) EXPL. TWOD. 3

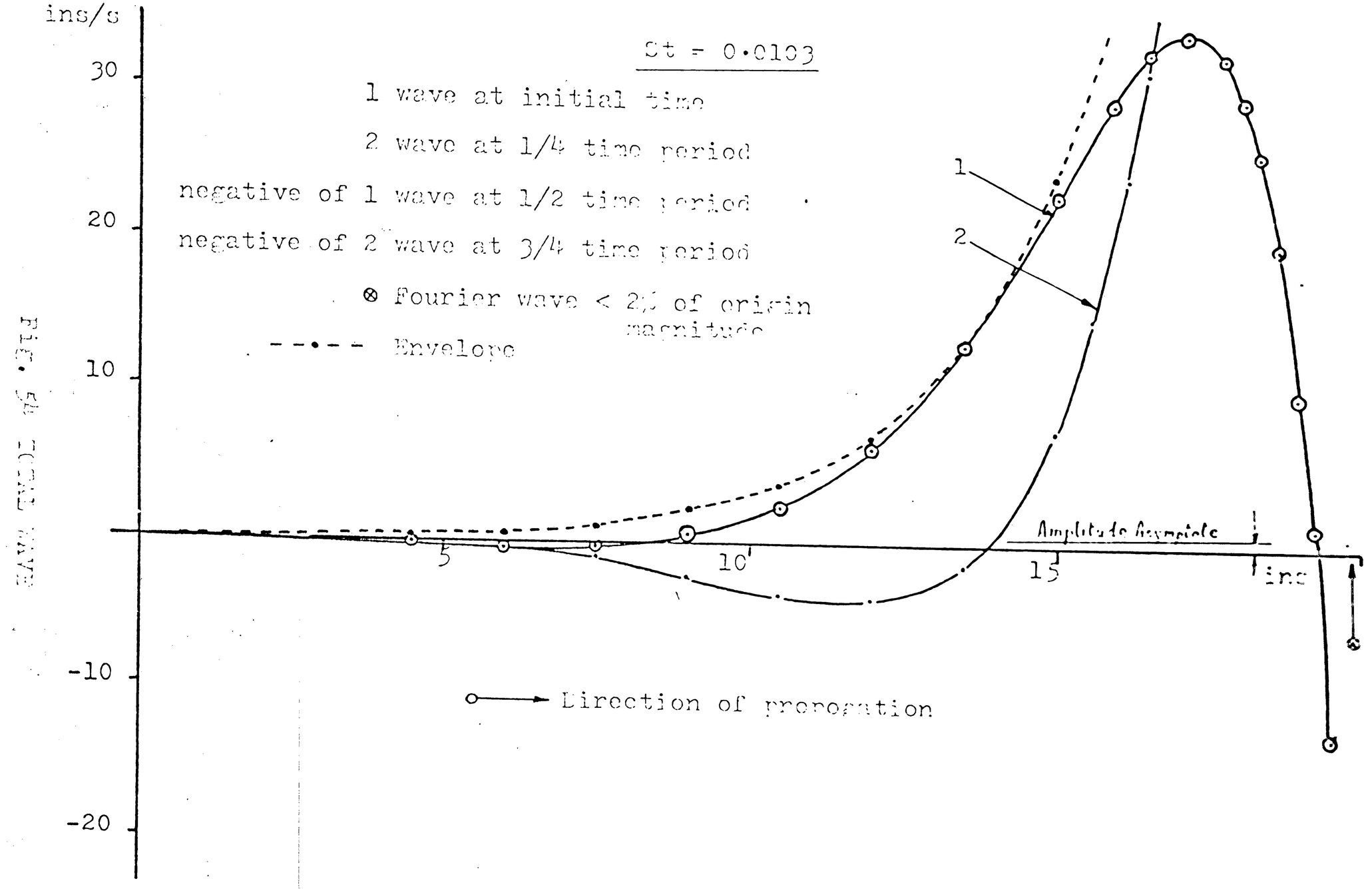
ins/s
30
20
10
-10
-20
EAM TYCE 45
St = 0·0103
1 wave at initial time
2 wave at 1/4 time period
negative of 1 wave at 1/2 time period
negative of 2 wave at 3/4 time period
⊗ Fourier wave < 2% of origin magnitude
Envelope
1
2
5
10
15
ins
Amplitude Asymptote
Direction of propagation

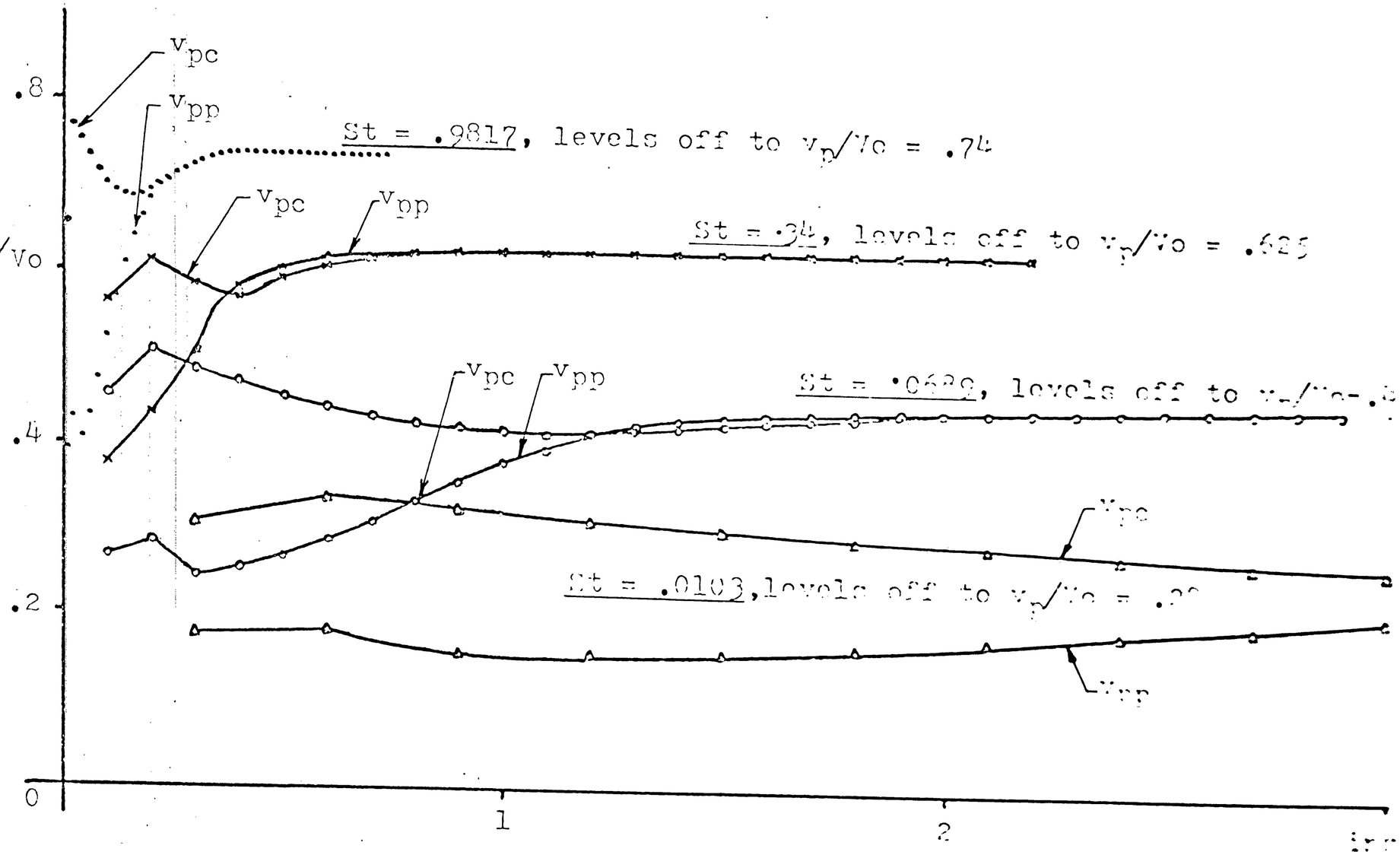

Fig. 55

PHASE VELOCITY vs DISTANCE FRO[illegible] INVISCID PLOTTING JET THEORY.

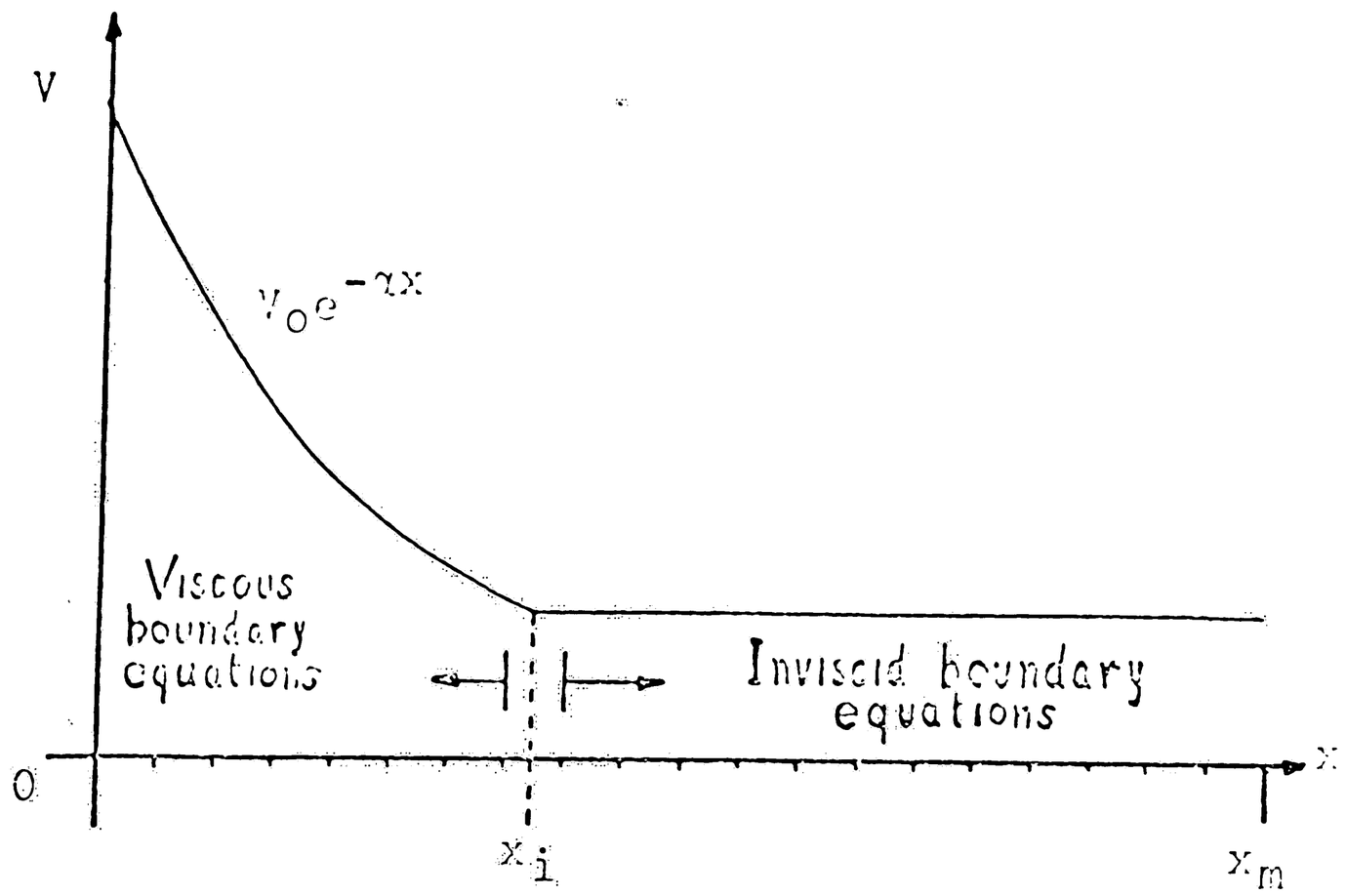

FIG. 56. THE EXPONENTIAL-VISCOUS JET

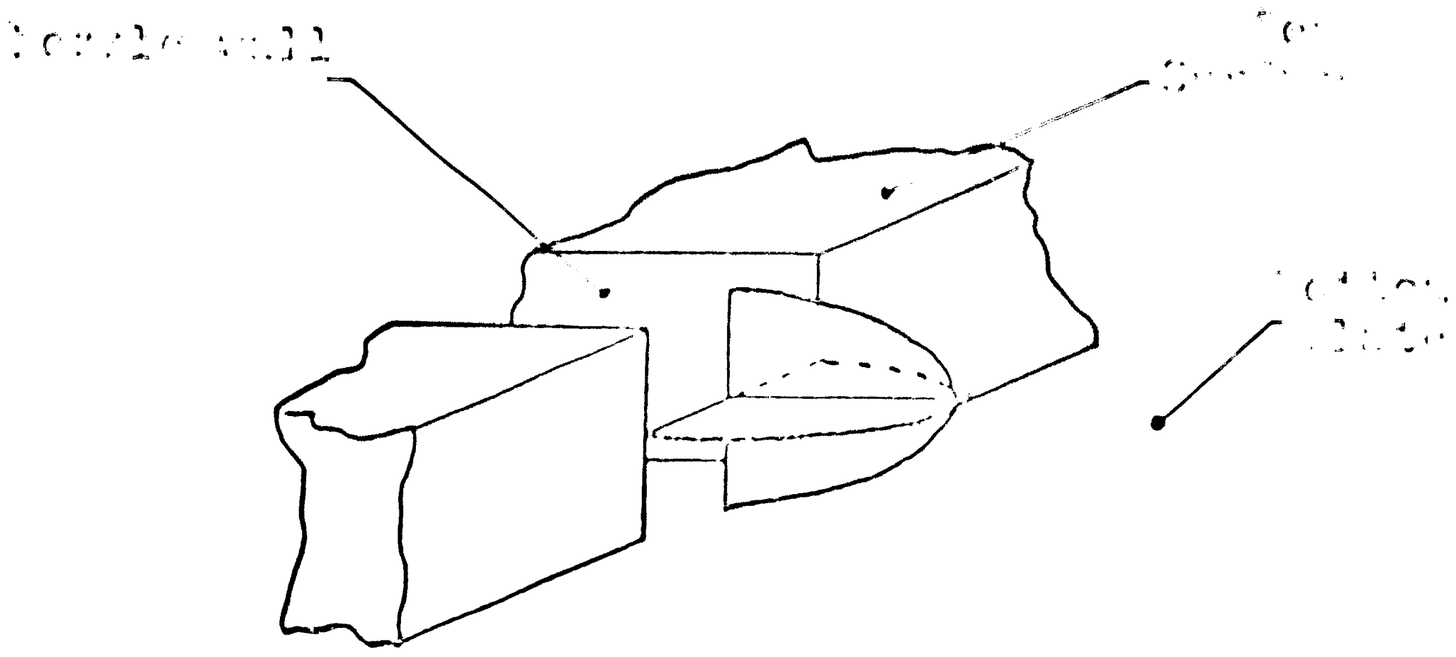

FIG. 57 DOUBLE PARABOLIC PROFILE

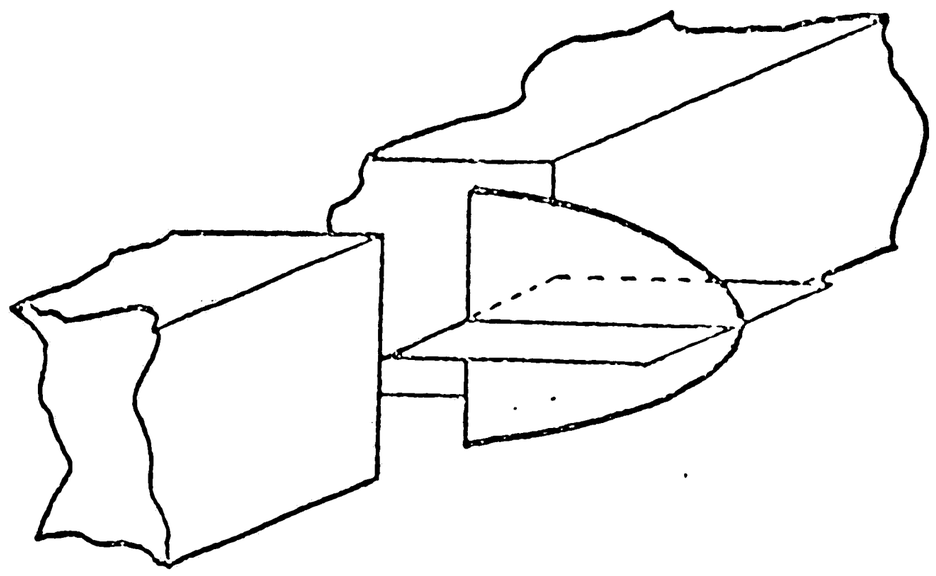

FIG. 58 SINGLE PARABOLIC PROFILE

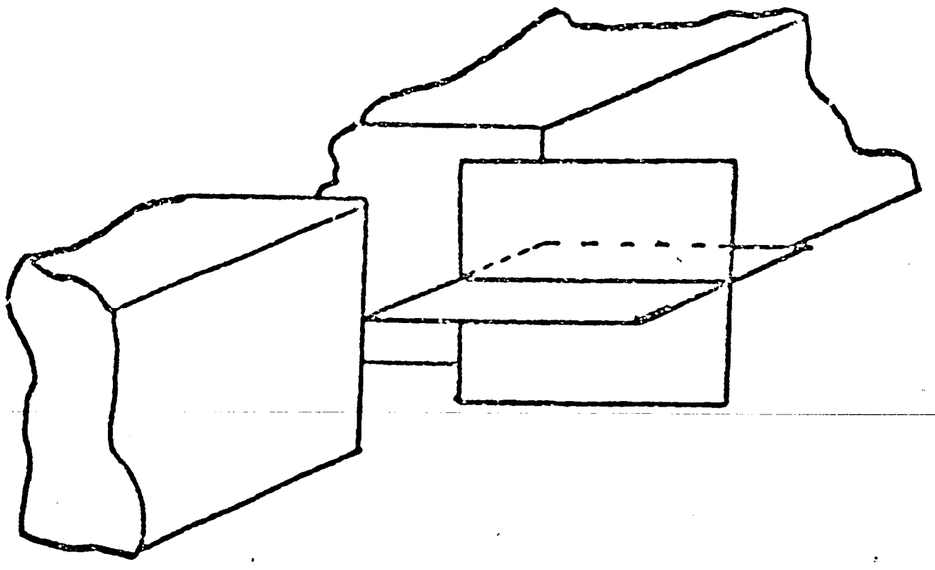

FIG. 59 COMPLETE BEUG PROFILE

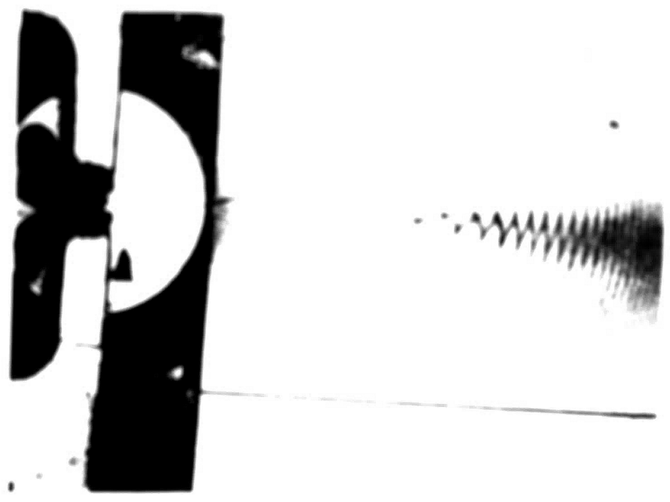

Re = 43.5

St = 0.154

Fig. 60 WAVE PATTERNS

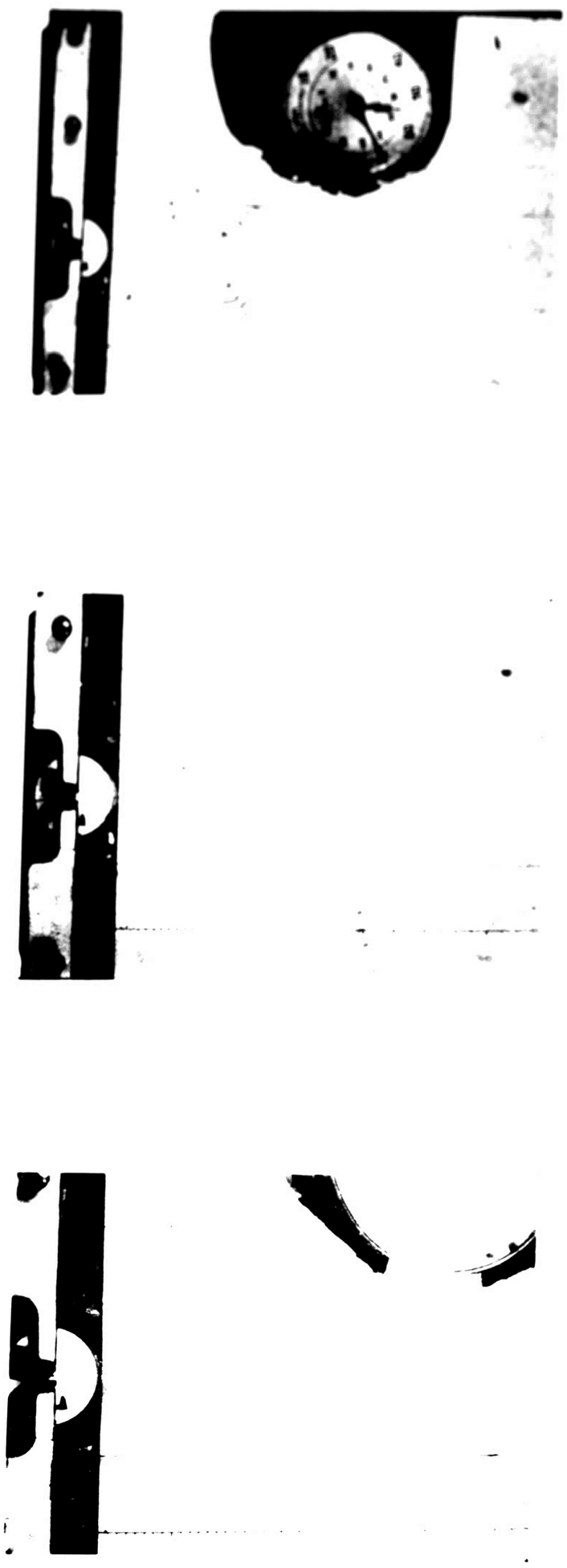

Fig. 61 WAVE PATTERNS

[illegible]

1. [illegible], "[illegible]," [illegible], 1968.

2. [illegible] Brown, "Fluid Amplifier [illegible]," [illegible] Projects Lab, Report [illegible] 72 [illegible]-1, M.I.T., Cambridge, Mass., September, 1970.

3. [illegible] and [illegible], "[illegible] -A [illegible] Matrix Package," [illegible] Lab., Dept. of Civil Eng., Lehigh University, Bethlehem, Pa., September, 1971.

4. H. Schlichting, "Boundary Layer Theory," McGraw Hill Book Company, New York, 1968.

5. W.E. Schiesser, "[illegible] - III, Introductory Programming Manual," Lehigh University Computing Center, Lehigh University, September, 1971.

APPENDIX

Results of the Exponential-viscous pivoting jet

[illegible]

[illegible] results for the theory of the inviscid oscillations of a jet with exponentially decaying stream velocity, as presented in section 3.3. Results of this theory were obtained for a Strouhal number of 0.01 at the origin. From experimental data for a Reynolds number of 223, the relaxation length x_r for the jet velocity decay was fixed at 4.5 ins. An initial computation was made for a completely inviscid region ($x_i = 0$). Then x_i was increased progressively to 8.39 ins. The spacing of the discrete locations at which the coupled boundary equation is satisfied was chosen so that at least 8 points were included in one wavelength of the rightward wave.

The highlights of the results are:

1. The Fourier wave decays to zero at the extreme right end, and the right wave predominates, as desired (Figs. A1 and A2).

2. Near the origin the Fourier wave compensates very strongly for the right wave plus the left wave resulting in a total wave pattern of a greater wave length than the right wave, as expected.

3. The discontinuity at x_i, where the jet is assumed to stop decaying, causes certain difficulties in this theory. This is seen in Fig. A3 in which the phase velocities

[illegible]

[illegible] (Fig. [illegible]).

In retrospect this behaviour should have been anticipated. The boundary condition suffers a discontinuity at x_0, producing reflected waves and a quasi standing-wave pattern. In fact the decay of the jet itself can be seen to produce <u>continuous</u> reflections, and the only real question is how they should be distributed in space. A discontinuity is unrealistic, and should be replaced, but no further work was actually done. One suggestion is the assumption that the jet velocity equals the exponential decay plus a constant; hopefully the Fourier wave could be computed, within computer storage limitations, far enough to the right so it would decay sufficiently. Other decay models could be proposed which better match the actual characteristics of the jet decay and spreading.

4. A tentative qualitative conclusion can be based on the amplitude growth curve shown in Fig. A4. It can be seen that up to a distance of 4 ins. the growth rate of the decaying jet wave is less than that of the wave with the inviscid jet. Despite the fact that Strouhal number increases towards the right due to decay of the jet its growth has been suppressed in the region within 4 ins. Beyond 4 ins. where the decay rate and the velocity of the viscous jet is much less the amplitude assumes a much

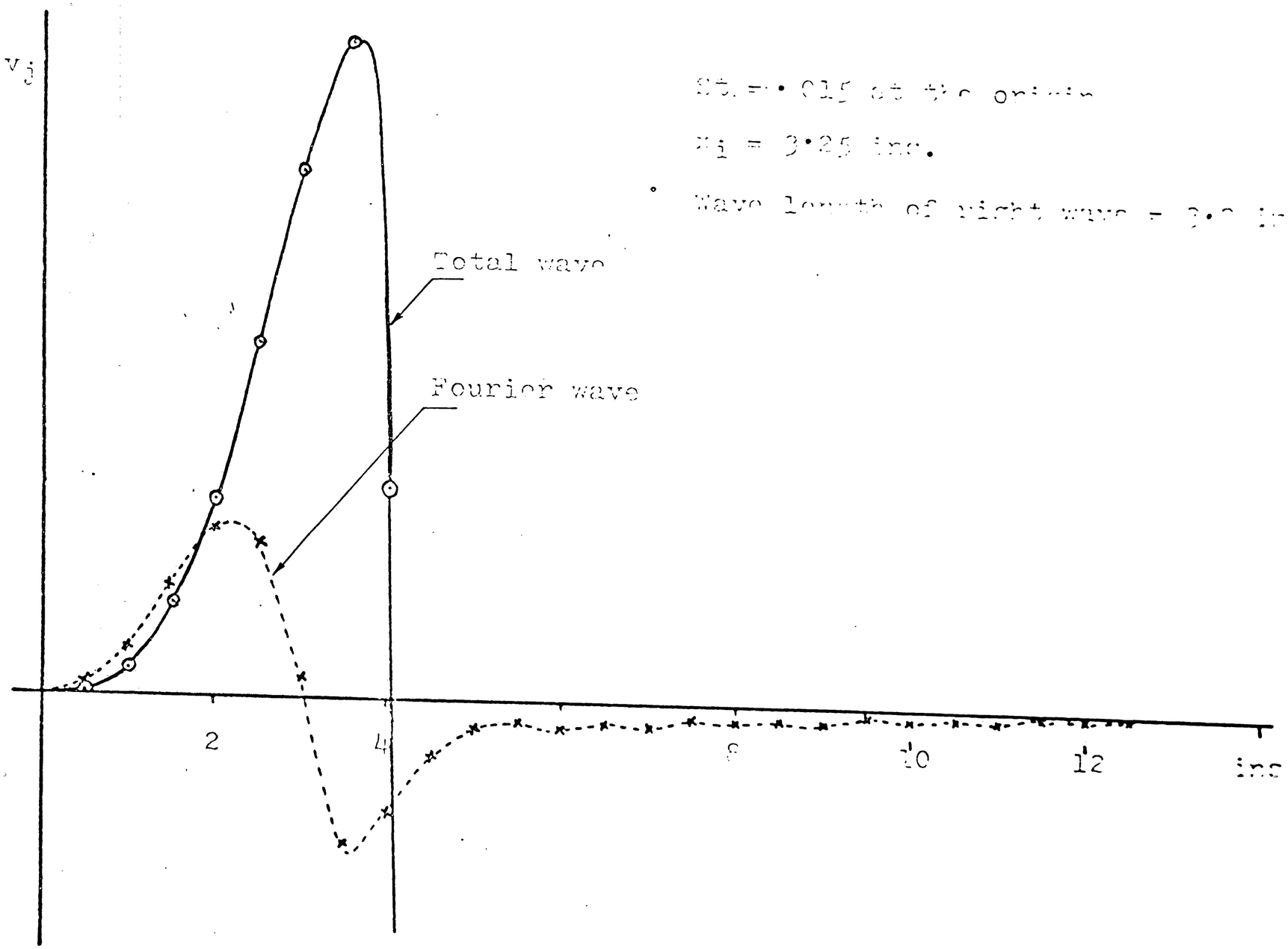

Fig. A1

$\delta t = 0.015$ at the origin

$x_i = 3.25$ ins.

Wave length of right wave = 3.0 ins.

V_j

Δt = ·015 at origin

Δ_i = ·125 ins.

Wave length of pitch wave = 1·75 ins.

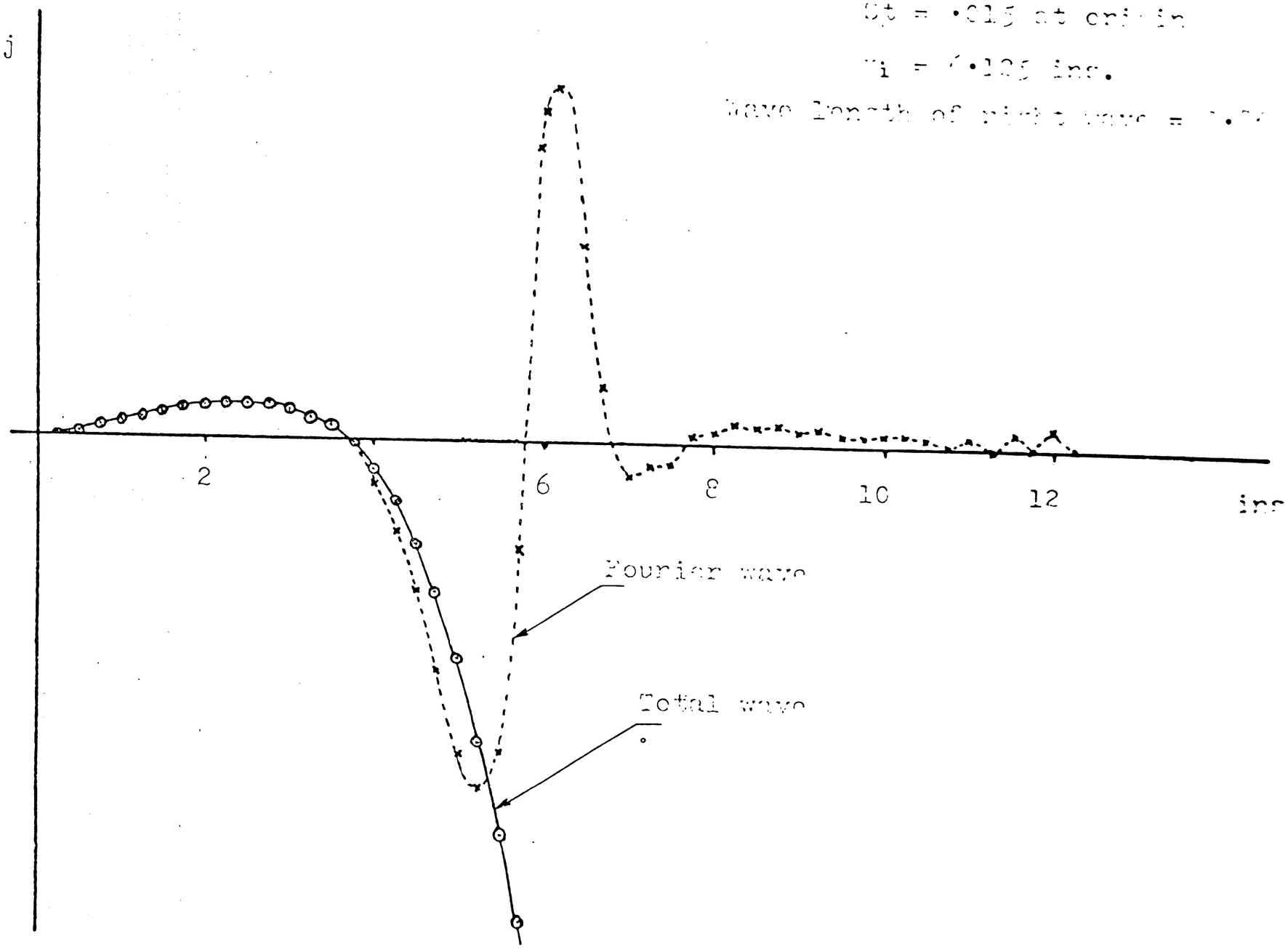

110

Fig. 42

δt = .015 at origin

⊙ Inviscid jet

× x_i = 3.25 ins.

◎ x_i = 2.20 ins.

△ x_i = 1.125 ins

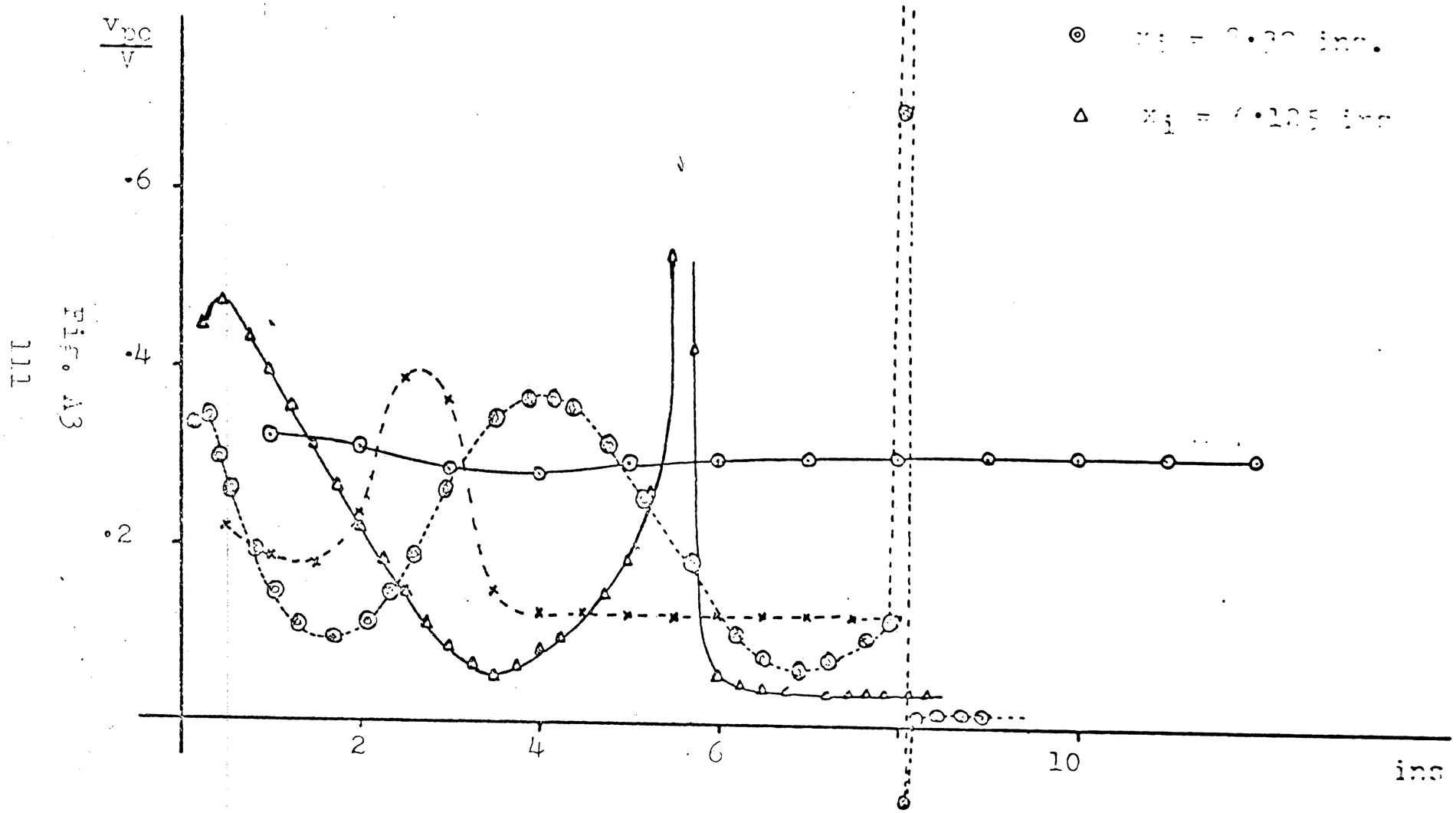

AMPLITUDE GROWTH VS DISTANCE

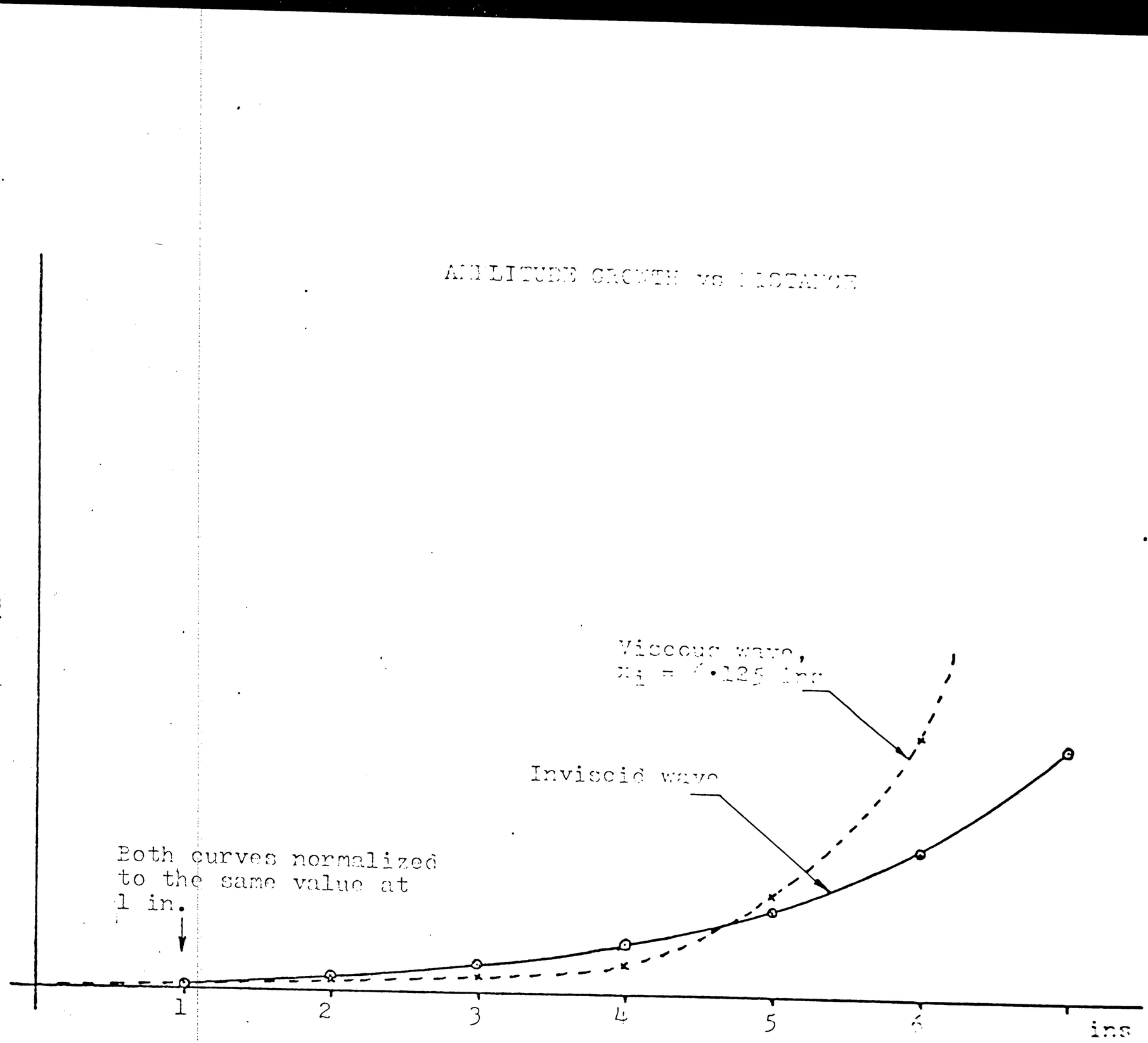

[illegible]

[illegible], [illegible] [illegible], [illegible] in India, the author [illegible] his schooling in [illegible] different [illegible] in India. [illegible] schooling was from [illegible] H. [illegible], New Delhi, while his undergraduate studies in Mechanical Engineering were completed at I.I.T. Madras in September, 19[illegible]. An enthusiastic engineer, the author has had practical training in the various engineering trades like machine-shop work, wood-work, smithy, etc., and also worked on an industrial engineering project at the workshops of Integral Coach Factory, Madras. It was in September, 1970, that the author came to the U.S.A. to do his graduate studies at Lehigh University where he worked as a research assistant with Dr. F.T. Brown in the area of fluid amplifiers.